Nano-Micro Letters

e-ISSN 2150-5551
CN 31-2103/TB

REVIEW

https://doi.org/10.1007/s40820-026-02197-6

Cite as
Nano-Micro Lett.
(2026) 18:351

Received: 30 December 2025
Accepted: 1 April 2026

Decoding the Oxygen Reduction Reaction: Mechanistic Insights from Transition Metal Heterostructures

Mingyu Sun[1], Xiayan Zhang[1], Jia Wang[1], Jialu Liu[1], Jinhai He[1], Wanmiao Ge[1], Shengwei Kong[1], Guoqing Zhang[1], Mai Gao[1], Jingqiang Wang[2], Zixu Sun[1] ✉, Yaping Yan[3] ✉, Xinjian Shi[1] ✉, Yao Xiao[4] ✉

HIGHLIGHTS

- This review presents a unified mechanistic framework for oxygen reduction reaction catalysis across diverse transition metal systems (Fe, Mn, Co, Ni, Cu), linking electronic structure, coordination environment, and interfacial effects to pathway selectivity.
- In situ/operando techniques and interfacial engineering are emphasized as critical tools for atomic-level active site probing and performance optimization.
- A cross-scale design paradigm bridges molecular-level insights with practical applications in fuel cells, metal-air batteries, and H_2O_2 electrosynthesis.

ABSTRACT The oxygen reduction reaction (ORR) plays a central role in determining the efficiency and durability of a broad range of electrochemical energy conversion technologies, while its intrinsically slow kinetics and multistep reaction nature remain key challenges. Transition metal-based heterogeneous electrocatalysts, particularly those incorporating Fe, Mn, Co, Ni, and Cu, have been extensively investigated as ORR active systems owing to their earth abundance, diverse coordination environments, and tunable electronic structures. Recent studies show that ORR on these catalysts can diverge into two-electron and four-electron pathways from a common O_2 reactant, with pathway selectivity governed by atomic-scale coordination and electronic effects. This review summarizes current understanding of ORR mechanisms on transition metal-based catalysts, with a focus on how atomic-scale structural features are related to reaction activity, selectivity, and stability under different electrolyte conditions. Representative applications in metal–air batteries, fuel cells, and electrochemical hydrogen peroxide production are also discussed to illustrate how mechanistic insights are reflected in practical electrochemical systems. By distilling shared mechanistic features across different systems, this review provides a coherent framework for understanding and guiding ORR catalyst design.

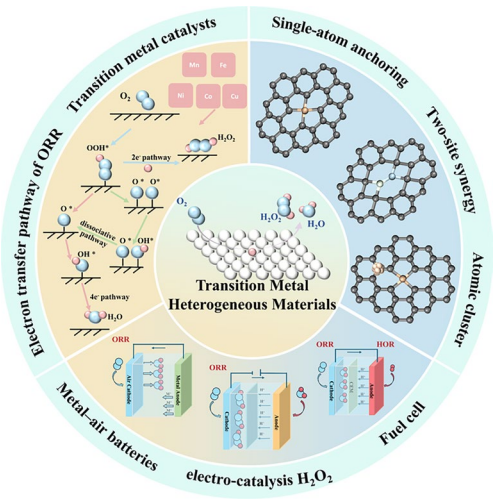

KEYWORDS Oxygen reduction reaction; Transition metal catalysts; Heterogeneous electrocatalysis

Mingyu Sun and Xiayan Zhang have contributed equally to this work.

✉ Zixu Sun, sunzixu@henu.edu.cn; Yaping Yan, yyp1990@haue.edu.cn; Xinjian Shi, shilx@henu.edu.cn; Yao Xiao, xiaoyao@wzu.edu.cn

[1] National & Local Joint Engineering Research Center for Applied Technology of Hybrid Nanomaterials, School of Nanoscience and Materials Engineering, Henan University, Kaifeng 475004, People's Republic of China

[2] College of Chemistry and Chemical Engineering, Inner Mongolia University, Hohhot 010021, Inner Mongolia, People's Republic of China

[3] Henan Engineering Technology Research Center for Fiber Preparation and Modification, Henan University of Engineering, Zhengzhou 451191, People's Republic of China

[4] College of Chemistry and Materials Engineering, Wenzhou University, Wenzhou 325035, People's Republic of China

Published online: 04 May 2026

Shanghai Jiao Tong University Press

Springer

1 Introduction

At a fundamental level, the oxygen reduction reaction (ORR) can be regarded as a highly coupled interfacial reaction network rather than a simple multielectron process proceeding along a single reaction coordinate. On electrode surfaces, the adsorption, activation, and reduction of molecular oxygen involve multiple near-degenerate intermediate states, including OOH*, O*, and OH*, whose formation, interconversion, and desorption compete with one another to determine the distribution of reaction flux among different pathways [1–3]. Because the free energy differences between these intermediates are often comparable in magnitude, the kinetic behavior of ORR exhibits pronounced sensitivity to local structural motifs, electrode potential, and interfacial environment, rendering the reaction system highly responsive to relatively small perturbations in both thermodynamic and kinetic terms [4–8]. As a prototypical proton-coupled electron transfer (PCET) reaction, the ORR reaction coordinate is not only governed by electronic structure but also modulated by interfacial electric fields, solvation structures, and proton donor configurations [9–12]. These factors can substantially alter charge distributions and reorganization energies at the transition states, thereby introducing strong potential dependence and environmental sensitivity. Consequently, the kinetic bottleneck of ORR is not confined to a single elementary step but can migrate among multiple steps under different operating conditions, manifesting as pathway competition, rearrangement of rate-determining steps, and environment-dependent shifts in reaction selectivity [13–15]. This intrinsic coupling of multiple pathways and length scales renders ORR difficult to describe adequately using a single energetic descriptor or static reaction model [16, 17].

Transition metal-based catalytic systems display distinct and complex behaviors in ORR studies, arising from the highly tunable coupling between the d electron structure of metal centers and their coordination environments. Metal–ligand interactions, mediated through crystal field splitting, orbital hybridization, and covalency modulation, reshape the bonding characteristics and charge transfer properties between metal centers and oxygen-containing intermediates, thereby influencing O–O bond activation, OOH* stability, and the preference of subsequent reaction pathways [18–20]. In contrast to the relatively rigid structures of noble metal surfaces, transition metal active sites are commonly embedded in heterogeneous coordination environments, where coordination number, ligand identity, and second coordination shell effects can modify the local electronic density of states at the atomic scale [21–24]. Under electrochemical operating conditions, applied potential, adsorbate coverage, and solvation collectively determine the effective oxidation state of the metal center, rendering both valence state and active site identity condition-dependent rather than static structural parameters [25–28]. In this context, ORR catalytic behavior no longer follows a single electronic structure descriptor but instead reflects the projection of multiple degrees of freedom onto the reaction coordinate. Additional complexity arises from the dynamic evolution of transition metal sites during operation, including coordination restructuring, ligand exchange, and localized hydration or redox processes, which cause the real reaction interface to adopt time- and potential-dependent state distributions. These dynamic characteristics imply that structure–activity relationships must be understood within the complete cycle of site formation, site stabilization, and site participation in catalysis, rather than inferred solely from idealized initial structures [29, 30].

In ORR catalysis, the concept of heterostructure extends beyond conventional bulk phase interfaces. At the atomic scale, heterogeneity in metal identity, coordination environment, and metal–support interactions can create localized junction-like regions with distinct electronic structures and adsorption behaviors [31–33]. From this perspective, single-atom and dual-atom catalysts may be regarded as atomic-scale heterostructures, in which asymmetric coordination or dissimilar neighboring atoms generate intrinsic electronic and chemical discontinuities analogous to classical interfacial effects. Such atomic-level heterogeneous motifs provide an effective platform for modulating intermediate stability, charge distribution, and reaction pathway branching in ORR [34–36].

With continued advances in in situ and quasi-in situ characterization techniques, first-principles calculations, and microkinetic modeling, experimental and theoretical information concerning local structural evolution, electronic state rearrangement, and intermediate behavior during ORR has accumulated rapidly, enabling mechanistic discussions to progress from empirical correlations toward more structured analyses [37–39]. Nevertheless, these advances remain

https://doi.org/10.1007/s40820-026-02197-6

largely fragmented at the field level: Most studies are conducted within specific material systems, narrowly defined electrolyte compositions [40–42], or limited potential windows, and their mechanistic interpretations are often embedded within particular model assumptions, making it difficult to maintain consistent reference standards across different systems or operating conditions [43–46]. As a result, descriptions of rate-determining steps, key intermediate stabilities, or electronic structure regulation frequently differ across studies and may even appear superficially inconsistent. Such discrepancies do not necessarily reflect contradictions in the conclusions themselves but rather underscore the high sensitivity of ORR, as a multipathway and strongly interfacial-coupled reaction network, to experimental and environmental parameters [47–49]. In the absence of a unified conceptual coordinate system, single-point or system-specific mechanistic interpretations provide limited support for broader extrapolation and constrain the extraction of transferable insights from existing results [50–52]. This limitation is particularly pronounced in transition metal-based catalytic systems, where strong coupling among coordination structure, electronic state distribution, interfacial environment, and reaction pathway branching is intrinsic. Many studies address only one of these dimensions, thereby obscuring the collective effects that shape the overall reaction network [53, 54]. Under these circumstances, a mechanism-oriented integrative analysis of transition metal-based ORR catalysis becomes essential. This review aims to study the results scattered under different material systems and experimental conditions from a multidimensional framework including coordinated structure, electronic modulation, interface effects and reaction networks, in order to identify common control factors, describe the key uncertainties in the current understanding of mechanisms, clarify the boundaries of descriptor applicability, and construct an extensible conceptual structure. To support reasonable model development, experimental design and strategy formulation in complex catalytic systems (Fig. 1).

2 Structure-Dependent Mechanisms of the ORR

Different transition metal-based ORR catalysts regulate reaction selectivity primarily by steering the divergence between the $2e^-$ and $4e^-$ pathways through distinct active site structures, oxygen adsorption configurations, intermediate evolution modes, and electron transfer characteristics [55–58]. Across diverse catalyst systems, the formation and subsequent fate of the OOH* intermediate constitute a universal mechanistic branching point that determines whether molecular oxygen undergoes partial reduction to H_2O_2 or complete reduction to H_2O. The relative preference for the $2e^-$ or $4e^-$ pathway is therefore governed not by a single descriptor, but by the coupled regulation of O_2 adsorption geometry, OOH* binding strength, O–O bond activation, and charge transfer capability at the active site [59–62].

In single-atom catalysts (SACs), isolated metal centers—typically coordinated by nitrogen or oxygen atoms—promote end-on O_2 adsorption and sequential proton–electron transfer at a single site [63–66]. In the absence of adjacent metal atoms, O–O bond cleavage depends entirely on the intrinsic ability of the metal center to stabilize and activate OOH*: weak OOH* binding favors direct desorption as H_2O_2 via the $2e^-$ pathway [67–69], whereas stronger OOH* adsorption enables O–O bond dissociation into O* and OH*, allowing the reaction to proceed through the $4e^-$ pathway toward H_2O formation. In contrast, metal nanoparticle catalysts provide contiguous multiatom active sites that enable side-on or bridging O_2 adsorption [70–72], significantly lowering the O–O bond dissociation barrier and favoring sustained multielectron transfer through the $4e^-$ pathway. For metal oxide catalysts, ORR proceeds via surface metal cations and lattice oxygen coordination, where limited electrical conductivity and metal–oxygen interaction strength critically influence pathway selection: Oxides with strong O_2 activation capability (e.g., cobalt-based spinels) can approach the $4e^-$ pathway in alkaline media [73–76], whereas oxides with weaker O_2 binding, such as TiO_2, preferentially follow the $2e^-$ pathway to H_2O_2 formation (Fig. 2).

Across transition metal-based ORR catalysts, the intrinsic electronic structure of the metal center plays a decisive role in governing the divergence between the two-electron and four-electron pathways. Fe-based active sites generally exhibit strong interactions with oxygenated intermediates, particularly OOH*, which facilitate O–O bond activation and stabilize dissociated O* and OH* species, thereby lowering the energetic barrier for O–O bond cleavage and favoring the $4e^-$ reduction pathway to H_2O [77–80]. Co-based catalysts often display intermediate and highly tunable behavior: their partially filled *d* orbitals enable effective O_2 activation and OOH* stabilization, while the extent of

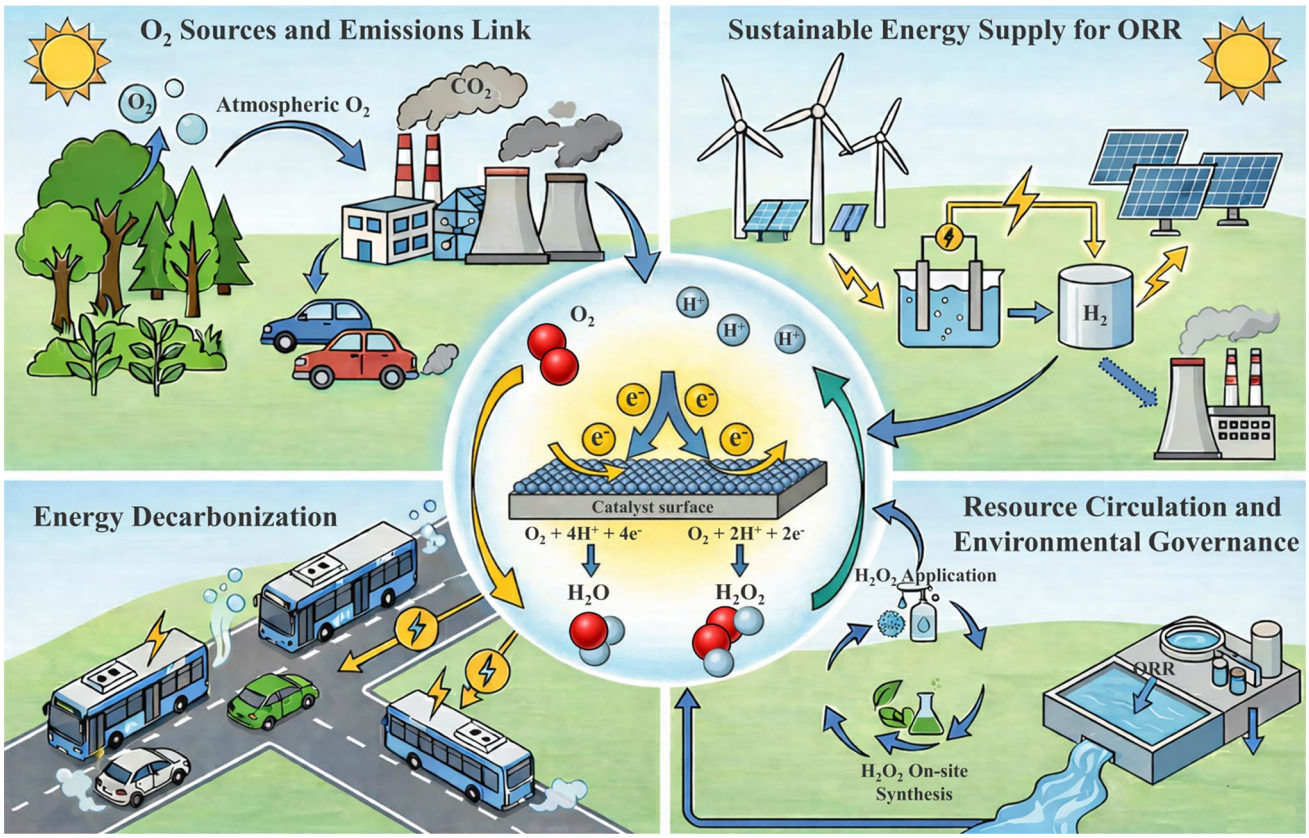

Fig. 1 Schematic illustration of the sustainable energy-driven ORR

O–O bond cleavage is strongly dependent on coordination environment and oxidation state, allowing Co sites to access either $4e^-$ or mixed pathways under different structural regulations. In contrast, Ni-based active sites typically bind OOH* more moderately and lack sufficient driving force for O–O bond dissociation, favoring OOH* desorption prior to bond cleavage and thus promoting selective $2e^-$ reduction to H_2O_2 [81–83]. Cu-based centers, characterized by more filled *d* orbitals and weaker interactions with oxygenated species, further suppress O–O bond activation and are intrinsically inclined toward end-on O_2 adsorption and OOH* release, reinforcing their preference for the $2e^-$ pathway [84–86]. Mn-based catalysts, on the other hand, exhibit pronounced sensitivity to spin configuration and spin-dependent electron transfer, as the multivalent and spin-flexible nature of Mn centers strongly couples oxygen activation with spin state transitions, leading to ORR activity and selectivity that are highly dependent on coordination symmetry, ligand field strength, and operating conditions.

Beyond individual elements, the distinct behaviors of Fe-, Co-, Ni-, Cu-, and Mn-based catalysts reflect a set of universally applicable mechanistic principles that extend across diverse ORR systems. At a fundamental level, ORR pathway selection is governed by the balance between OOH stabilization and O–O bond activation, which can be continuously tuned through electronic structure modulation, multicenter cooperation, and interfacial charge redistribution [87–90]. Catalyst architectures that enable cooperative adsorption—such as adjacent metal sites, metal–nonmetal bonded ensembles, or metal–oxide interfaces—effectively lower O–O bond dissociation barriers and favor sustained multielectron transfer, exhibiting Fe or Co-like characteristics associated with the $4e^-$ pathway [91–94]. In contrast, isolated or weakly interacting sites that stabilize OOH* without promoting bond cleavage emulate Ni or Cu-like behavior and preferentially yield H_2O_2 via the $2e^-$ pathway. Spin-sensitive centers, exemplified by Mn-based systems, further highlight the role of electronic degeneracy and dynamic state evolution in

https://doi.org/10.1007/s40820-026-02197-6

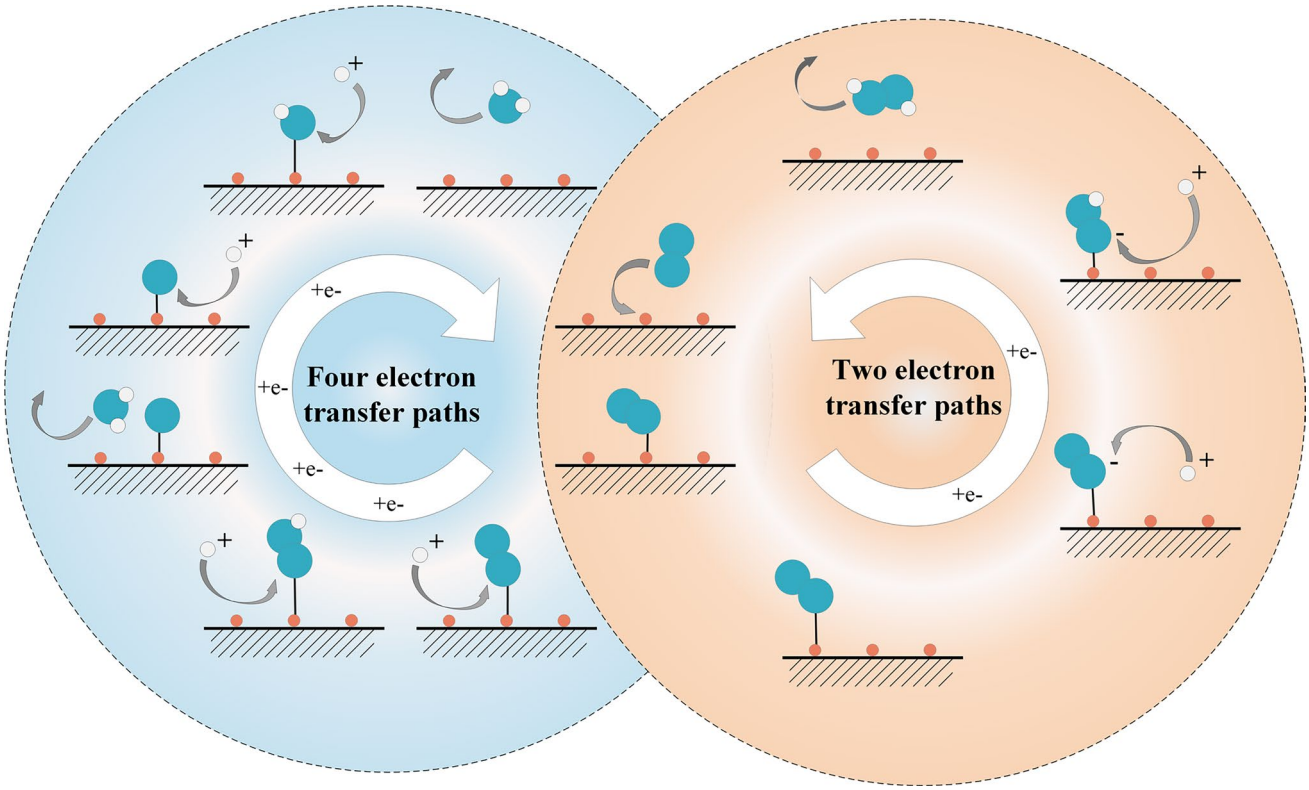

Fig. 2 ORR mechanism diagram (orange represents the active sites of the catalyst, blue represents oxygen atoms, and white represents hydrogen atoms)

shaping ORR kinetics. Collectively, these insights demonstrate that ORR selectivity across different materials is dictated not by catalyst class alone, but by shared and transferable mechanistic control factors, providing a unified framework for rational ORR catalyst design.

3 ORR Mechanism over Transition Metal Heterogeneous Catalysts

In addressing the catalytic requirements of the ORR, a diverse array of catalyst systems has been developed, encompassing precious metal-based, carbon-based, and transition metal-based catalysts (TMCs) [95–97]. Among these, heterogeneous electrocatalysis systems incorporating earth-abundant elements such as Fe, Mn, Co, Ni, and Cu have gained prominence as a primary research focus, owing to their compelling economic feasibility, environmental sustainability, and structural versatility [98, 99]. These TMCs have demonstrated notable advantages in electrocatalytic performance, positioning them as increasingly viable alternatives to precious metal-based benchmarks. To further optimize their performance, it is essential to develop a thorough comprehension of the structure–activity relationship, which not only elucidates the fundamental mechanisms of the ORR but also provides a critical theoretical and practical foundation for the rational design of novel, high-efficiency electrocatalysts (Fig. 3).

3.1 Fe-Based Catalysts

Fe-based catalysts are widely regarded as promising alternatives to precious metal catalysts due to their high O_2 activation capability and tunable electronic structure. Nevertheless, such systems face several challenges in the ORR [105–108]. Conventional Fe-based catalysts often exhibit

limited activity, largely attributable to their constrained electronic configuration, which complicates the optimization of intermediate adsorption without compromising stability. Under electrochemical conditions [109, 110], the active iron sites are susceptible to structural reconstruction or metal leaching, leading to gradual degradation of catalytic durability. Additionally, the poisoning of iron centers in certain reaction media remains a non-negligible issue. Furthermore, the structural simplicity of these catalytic sites restricts the regulation of electron transfer pathways, making precise control over ORR kinetics difficult to achieve [111–113].

Fe-based catalysts are a promising type of non-precious metal electrocatalysts for the ORR and show high activity in both acidic and alkaline environments because of high atomic utilization, clear Fe–N_x coordination structures, and adjustable electronic properties. Zhang et al. [114] developed a single-atom iron catalyst with a hierarchically porous structure using an embedding–pyrolysis–evaporation method (Fig. 4a). The porous and heterogeneous structure improved electronic regulation and oxygen adsorption at Fe active sites and also increased catalyst stability. In situ studies showed that Fe–N_4 sites change their structure under alkaline conditions and form Fe–N_4–OOH intermediates (Fig. 4b). This

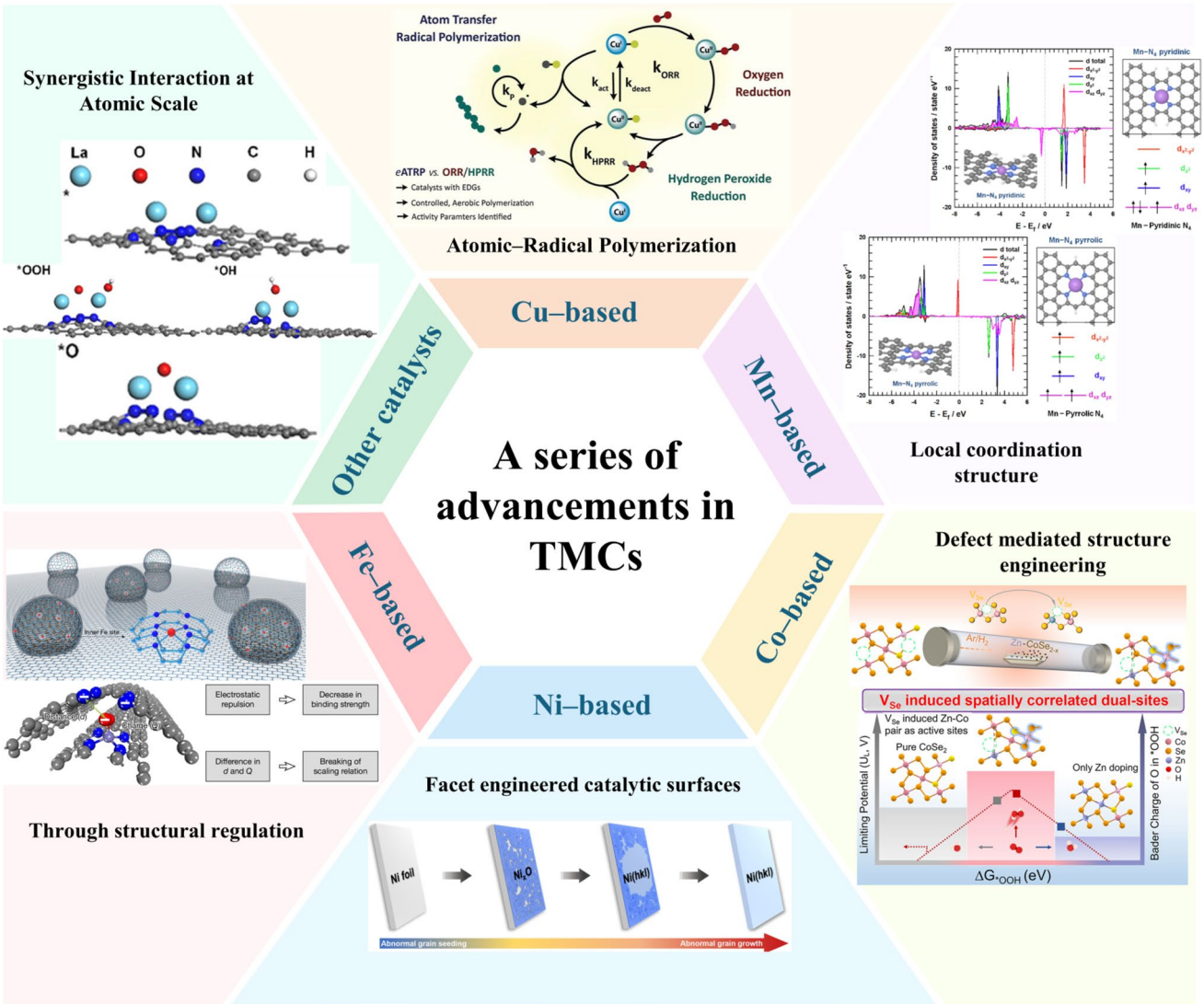

Fig. 3 Representative advances in TMCs enabled by atomic-scale regulation and structural engineering [100–104, 125]. Copyright 2025, Wiley–VCH; Copyright 2025, Elsevier; Copyright 2025, Springer Nature; Copyright 2025 American Chemical Society

https://doi.org/10.1007/s40820-026-02197-6

structural change improves the adsorption of oxygen species and supports O–O bond cleavage, which favors the 4e$^-$ ORR pathway. Attenuated total reflection surface-enhanced infrared absorption spectroscopy (ATR–SEIRAS) and Raman spectroscopy (Fig. 4c) showed gradual accumulation of OH* species at Fe sites with little desorption. This result indicates strong intermediate binding and local structural distortion at Fe centers. X-ray absorption near edge structure (XANES) and X-ray absorption fine structure (EXAFS) results showed a decrease in Fe coordination number and oxidation state and support a transition from Fe–N_4 to Fe–N_3. This dynamic coordination change helps maintain active Fe sites during operation and explains the stable high ORR activity. Overall, these results show that Fe-based single-atom catalysts favor the 4e$^-$ ORR pathway when strong OOH* binding is combined with flexible and stable Fe–N_x coordination structures.

In a complementary study, Ji et al. [115] constructed a single-atom Fe catalyst on a defect-rich N-doped carbon support using microenvironment engineering (Fig. 4d). The defect-induced Fe–N_4(OH)–A structure improves electron transfer and strengthens the interaction between Fe active sites and reaction intermediates, while in situ Raman spectroscopy confirms stable adsorption and efficient conversion of key species such as OOH* and O_2* at these sites. Free energy calculations show that the defect structure improves site anchoring and structural stability (Fig. 4e). These results indicate that defect engineering creates a more stable local environment for Fe single-atom sites and maintains strong intermediate binding during the ORR, which supports O–O bond cleavage and favors the 4e$^-$ ORR pathway. Engineering the local microenvironment and defect structure provides a powerful means to concurrently boost the activity and durability of Fe-based single-atom ORR catalysts, resulting in ORR performance superior to commercial Pt/C in acidic, alkaline, and neutral media and revealing substantial potential for practical applications.

To enhance the practical performance of Fe single-atom catalysts under complex electrolyte conditions, recent studies have shifted the focus from isolated active sites to multisite synergy and interfacial electronic regulation. Rao et al. [116] reported a Fe single-atom catalyst modified with Fe clusters by plasma treatment (Fig. 4f), forming a cooperative structure between atomic sites and metallic clusters. The catalyst showed high ORR activity and stable operation in alkaline seawater electrolyte. Fe clusters donate electrons to neighboring Fe–N_4 sites (Fig. 4g), adjusting local charge distribution and suppressing active site poisoning through preferential Cl^- adsorption, which improves durability in chlorine-rich environments. To increase the accessibility of Fe active centers and tune their coordination geometry, Liu et al. [117] used NH_4I-induced etching combined with iodine doping (Fig. 5a) to prepare Fe–N–C catalysts. The material showed elongated Fe–O bonds and a reduced ΔG_{OH^*}, which facilitates intermediate desorption and accelerates ORR kinetics. In zinc–air batteries, the catalyst delivered a peak power density of 249.1 mW cm^{-2} and long-term cycling stability (Fig. 5b, c), confirming its practical relevance. Qiao et al. [118] designed axial ligand-modified single-atom catalysts, Cl–FeN_4 and N–FeN_4, using chloride and pyridine nitrogen ligands (Fig. 5d). EXAFS analysis verified Fe–N_4Cl and Fe–N_5 coordination environments. Stronger ligand fields drive the Fe center from a high-spin to a medium-spin state (Fig. 5e). The shifted d band center in N–FeN_4 strengthens OH* adsorption and lowers the ORR energy barrier. The catalysts were applied in rechargeable zinc–air batteries (Fig. 5f), demonstrating the effectiveness of axial ligand-controlled spin regulation.

Sui's team reported a FeNb/C–SNC catalyst with asymmetric diatomic sites prepared by template-assisted pyrolysis [119]. Fe and Nb atoms are co-embedded in a porous carbon matrix, forming Fe–S_1N_3 and Nb–N_4 coordination structures at adjacent sites (Fig. 6a). This asymmetric diatomic configuration enables direct electronic interaction between Fe and Nb centers. Nb incorporation lowers the OH* adsorption energy on Fe sites and tunes the ORR pathway. Compared with single-metal catalysts, the bimetallic system shows improved intermediate stabilization and electron transfer (Fig. 6b). The free energy of OH* desorption decreases from + 0.78 to + 0.46 eV, reducing the reaction barrier. Zinc–air batteries assembled with this catalyst exhibit higher open-circuit voltage and power density (Fig. 6c) and stable operation for over 1000 h at 20 mA cm^{-2}, indicating good structural durability. Yang et al. [120] combined high-entropy alloy catalysts (HEACs) with Fe–N_4 sites to construct ORR catalysts with high activity and stability. In situ ATR–SEIRAS measurements show stronger OH* and OOH* signals during potential scanning (Fig. 6d), suggesting promoted formation and conversion of oxygen intermediates. Electronic structure analysis based on crystal field and molecular orbital models indicates that HEAC incorporation reorganizes the Fe *d* orbitals and weakens Fe–OH* bonding (Fig. 6e). Infrared and electrochemical results

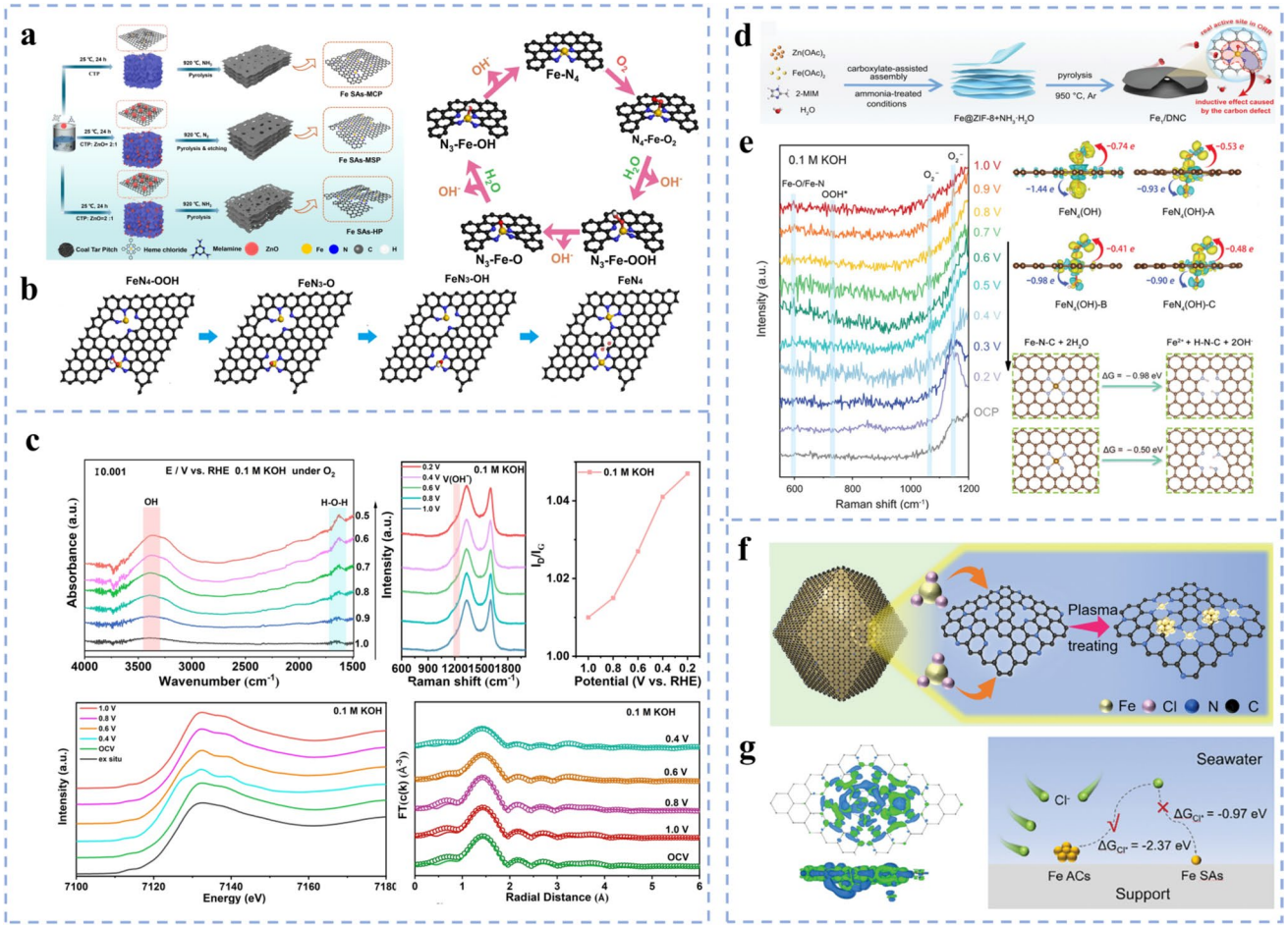

Fig. 4 **a** Preparation process of Fe SAs–HP and its dynamic evolution mechanism under alkaline conditions. **b** Stepwise reduction process of Fe–N_4 active center under alkaline conditions. **c** Fe SAs–HP was characterized in 0.1 M KOH using in situ ATR–SEIRAS, Raman spectroscopy, XANES, and FT–EXAFS [114]. Copyright 2024, Springer Nature. **d** Schematic diagram of the synthesis of Fe_1/DNC [115]. Copyright 2024, Wiley–VCH. **e** In situ Raman spectroscopy, charge distribution and Fe site stability analysis in O_2-saturated 0.1 M KOH. **f** Schematic diagram of the construction of Fe–N–C active sites by plasma treatment. **g** Differential charge density distribution between Fe_6 clusters and single-atom Fe and the comparative mechanism of their resistance to Cl^- in seawater [116]. Copyright 2024, Wiley–VCH

further confirm enhanced intermediate desorption, structural stability, and reaction kinetics in the HEAC/Fe–NC system (Fig. 6f), highlighting the role of high-entropy components in electronic modulation and ORR performance improvement.

With the advancement of research, the conventional Fe–N_4 configuration has revealed several critical limitations. Under complex practical conditions—such as chloride-rich environments, elevated temperatures, or prolonged operation—the active sites are prone to migration, structural reconstruction, and potential deactivation, which compromises their stability [121]. Additionally, challenges remain in achieving high Fe atom loading density, structural uniformity across sites, and controllable synthesis. To address these issues, current research prioritizes the dual objectives of "high activity" and "enhanced stability," and has developed multidimensional and complementary structural regulation strategies. At the synthesis level, in situ analysis of the pyrolysis process, the introduction of vapor deposition techniques, and the characterization of multiscale dynamic evolution mechanisms have collectively elucidated the intrinsic "synthesis–structure–performance" relationship within Fe/N/C systems [122]. From a holistic catalytic performance perspective, the "two-in-one" strategy—integrating high site density with high turnover frequency—is emerging as a key pathway to improve mass activity and

 https://doi.org/10.1007/s40820-026-02197-6

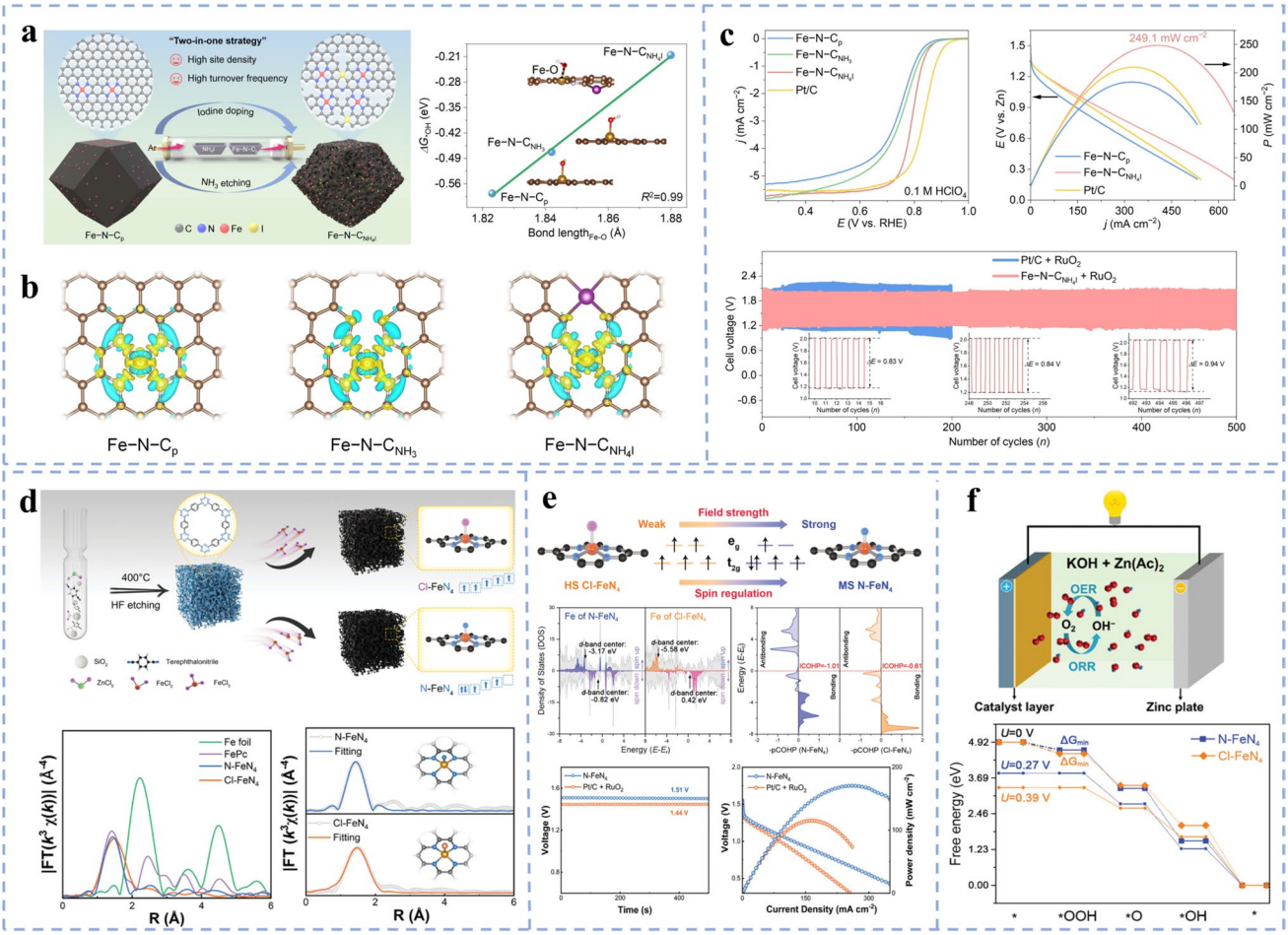

Fig. 5 **a** Construction strategy of Fe–N–C_{NH4I} catalyst and its correlation with Fe–O bond length and ΔG_{OH*}. **b** Charge density difference distribution under different coordination environments. **c** Comparison of ORR performance of each catalyst in acidic medium [117]. Copyright 2025, Wiley–VCH. **d** Synthesis schematic of N–FeN_4 and Cl–FeN_4 and comparison of their EXAFS characterization. **e** Differences between the two in atomic structure, electronic state density, Fe–OH bond strength and ORR reaction path. **f** Schematic diagram of liquid zinc–air battery [118]. Copyright 2024, Wiley–VCH

the practical output performance of devices. Fe-based catalysts are currently at a critical transition stage, moving from "single-active-site construction" toward "collaborative interface design and controllable modulation." Continuous performance enhancement relies not only on structural optimization but also on a comprehensive understanding of reaction mechanisms and site dynamic behavior. Future research should focus on strengthening in situ and quasi-in situ characterization methods, developing platforms that integrate multiscale simulation with experimental validation, and advancing the verification of long-term stable catalyst operation in real energy conversion devices.

3.2 Mn-Based Catalysts

The application of Mn-based catalysts in the ORR shows considerable potential, particularly in alkaline environments. These catalysts demonstrate high stability, environmental compatibility, excellent corrosion resistance, and low oxygen evolution tendency, rendering them suitable for electrochemical systems requiring long-term operational reliability [101]. However, the $3d^5$ high-spin electronic configuration of manganese leads to weak adsorption capacity for O_2 and key intermediates, often favoring the less efficient $2e^-$ pathway. This electronic structure presents challenges for achieving a highly selective $4e^-$ reduction process [123]. Furthermore,

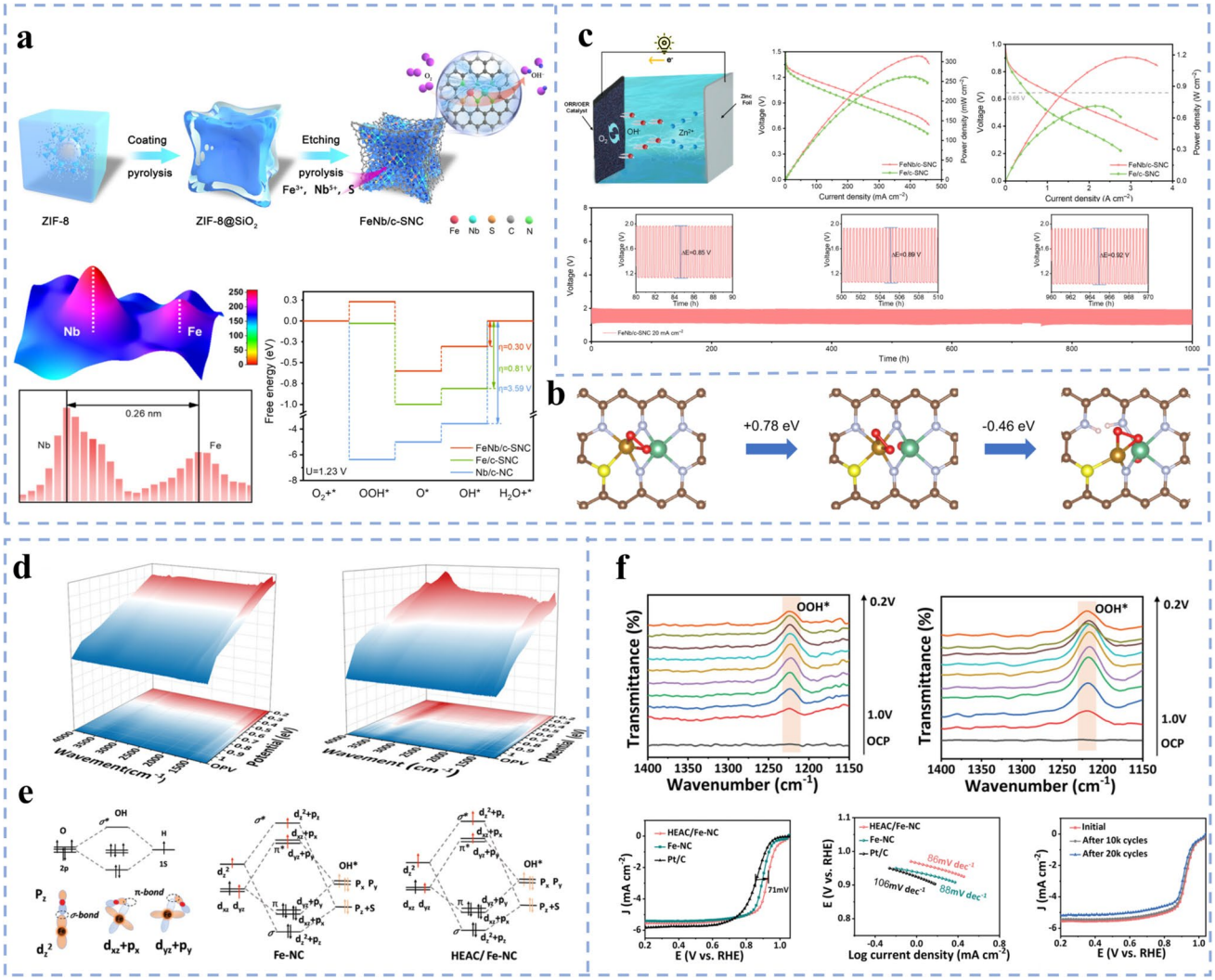

Fig. 6 **a** Synthesis process, atomic distribution and free energy diagram of FeNb/c–SNC. **b** Structural evolution during demetallization. **c** Zn–air battery and its polarization curve, power density and long cycle performance [119]. Copyright 2024, American Chemical Society. **d** 3D in situ ATR–SEIRAS spectra of HEAC/Fe–NC and Fe–NC. **e** Possible orbital interactions between Fe centers and OH intermediates and their regulation on adsorption behavior. **f** Comparison of OH and OOH* band intensities of HEAC/Fe–NC and Fe–NC, as well as electrochemical tests of different samples [120]. Copyright 2024, Wiley–VCH

the formation of inert Mn–O bonds on the carbon support surface can impede the construction and maintenance of efficient active sites, thereby limiting intrinsic activity and overall catalytic performance. Current research primarily focuses on enhancing O_2 adsorption and activation capabilities through electronic structure modulation and local coordination environment engineering. Key strategies include spin state regulation, construction of low-coordination structures, and introduction of heterogeneous interface synergy effects. These approaches aim to improve both the activity and stability of manganese-based ORR catalysts, advancing their development as high-performance non-precious metal electrocatalysts [124].

In the context of the ORR, the catalytic performance of Mn–N–C materials is often limited by the low-spin state of the manganese center and the overly strong adsorption of key reaction intermediates. Moreover, the ambiguous structure–activity relationship between ligand configuration and the true active site poses a fundamental challenge to rational catalyst design. To address these issues, researchers have developed strategies for precise electronic modulation of the Mn active center. Kim et al. systematically investigated the

 https://doi.org/10.1007/s40820-026-02197-6

influence of nitrogen ligand types on the electronic structure and ORR activity of Mn single-atom sites (Fig. 7a–d) [125]. Using aerosol spraying combined with ammonia-assisted pyrolysis, they constructed two distinct Mn–N_4 configurations on crumpled graphene carriers—one with pyrrole-type and the other with pyridine-type nitrogen coordination. Magnetic susceptibility tests and charge density difference analyses revealed that the pyrrole-type N coordination promotes a high-spin state in Mn, which facilitates intermediate desorption and enhances ORR activity, whereas the pyridine-type environment tends to passivate Mn sites. In situ infrared spectroscopy further verified that high-spin Mn serves as the active center for the reaction. In a separate study, Song's group introduced yttrium (Y) to prepare a MnY/NC catalyst containing both Mn clusters and unsaturated Mn–N_3 coordination motifs (Fig. 7e, f) [126]. It was found that Y preferentially binds oxygen during high-temperature carbonization, inhibiting Mn oxidation and promoting the formation of an unsaturated coordination structure. This "sacrificial protection mechanism" and the resulting "remote synergistic effect" effectively modulate the electronic state of Mn, significantly improving ORR performance. Additionally, Stracensky et al. adopted a chemical vapor deposition (CVD) approach to avoid the generation of MnO_x intermediates commonly encountered in conventional synthesis routes (Fig. 7g) [127]. By enabling direct reaction between Mn precursors and N-doped carbon substrates, the CVD method allows in situ formation of a stable Mn–N_4 structure, thereby enhancing both the structural integrity of the active sites and the efficiency of the ORR pathway.

Based on the previously discussed advances in ligand regulation and electronic structure engineering, research on Mn-based catalysts has expanded to structural-level modifications and interface coupling strategies, enabling more precise control over the Mn center's spin state and reaction pathway. Luo et al. [128] demonstrated a synergistic enhancement in spin state regulation and intermediate adsorption through the construction of a Mn-based heterostructure with

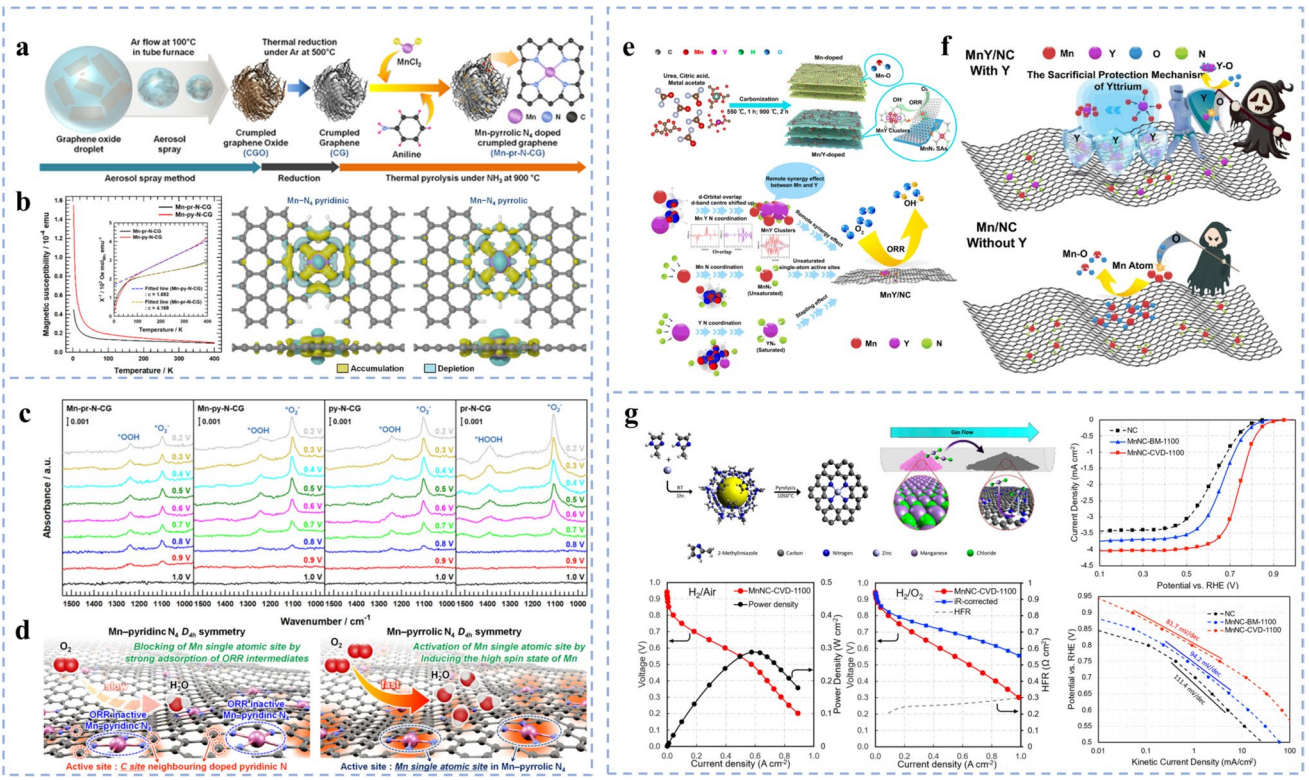

Fig. 7 **a** Synthesis route of Mn–pr–N–CG. **b** Magnetization behavior and charge density difference of Mn–N_4 (pyridine-type and pyrrole-type) coordination environment. **c** ATR–SEIRAS spectrum. **d** Different mechanism of activity source between Mn–py–N–CG and Mn–pr–N–CG in ORR [125]. Copyright 2024, American Chemical Society. **e** Schematic diagram of the synthesis of MnY/NC and the long-range synergistic effect mechanism of the catalyst. **f** Sacrificial protection mechanism of Y [126]. Copyright 2025, Elsevier. **g** Schematic diagram of the synthesis of MnNC–CVD–1100 and its electrochemical oxygen reduction performance [127]. Copyright 2023, American Chemical Society

strong interfacial interactions (Fig. 8a–c). Using ZIF-8 as a precursor, the team incorporated Mn and Mo precursors along with red phosphorus through a pyrolysis process to form a composite catalytic material. In this configuration, MoP nanocrystals induce an electronic rearrangement with $Mn–N_4$ sites, driving the transition of Mn centers from low-spin to high-spin states. This electronic modulation significantly enhances O_2 adsorption and activation capabilities. In situ spectroscopic analysis further revealed that this heterostructure exhibits stronger adsorption capacity and accelerated reaction kinetics for O_2^- and OOH* intermediates across multiple working potentials, leading to substantially improved ORR performance. In a complementary approach, Li et al. [129] developed a three-dimensional sea urchin-like hollow structure containing both Mn single atoms and sub-nanoclusters (Fig. 8d, e). This unique architecture enables effective electronic structure modulation through synergistic interactions between the atomic and cluster sites. The incorporation of sub-nanoclusters significantly enhance the electronic state density of $Mn–N_4$ sites near the Fermi level, thereby facilitating O_2 adsorption, promoting O–O bond cleavage, and substantially reducing the reaction energy barrier for the ORR.

Manganese-based catalysts still face several critical challenges, including poor stability in acidic media, incomplete understanding of the synergistic mechanisms between single atoms and clusters, limitations in real-time in situ characterization of electronic structure evolution, and insufficient quantitative studies on multifactor coupling mechanisms [130]. To advance Mn-based ORR catalysts, future research should focus on elucidating the intricate coupling relationships among atomic structure, electronic dynamics, and reaction pathways. This requires precise regulation of manganese active sites through atomic-level control of coordination environments and electronic states, combined with enhanced integration of in situ characterization and theoretical simulations to reveal dynamic structural evolution and catalytic mechanisms during operation [131]. The development of multimetal synergistic systems—such as composite structures incorporating manganese with other 3 d transition metals or rare earth elements—represents a promising direction for enhancing ORR performance. Through these strategies, manganese-based catalysts are expected to evolve from merely demonstrating high activity to achieving balanced performance in stability and practical applicability, thereby establishing a foundation for a new generation of environmentally friendly and efficient ORR catalytic systems [132].

3.3 Ni-Based Catalysts

Ni-based catalysts demonstrate outstanding catalytic activity and pathway selectivity in the ORR, stemming from their distinctive electronic structure, tunable coordination environment, and favorable oxygen affinity [133]. Their structural diversity further provides significant advantages in enhancing reaction selectivity, reducing energy barriers, and improving catalytic durability, making them a key candidate for high-performance ORR electrocatalysts. Recent research has developed a range of effective strategies to achieve precise control over interfacial electron distribution and band structure. These approaches include constructing heterojunction interfaces to promote O_2 dissociation and OH* desorption, introducing high-entropy atoms to induce strong electric dipole transitions and orbital hybridization, and designing low-valence nickel sites to enhance reaction activity and electron transfer efficiency [134]. The combined application of these strategies has consistently driven performance breakthroughs in Ni-based ORR catalysts, paving the way for their practical implementation in advanced energy conversion devices [135, 136].

Sun et al. [137] successfully synthesized a Ni-doped carbon nanosheet (Ni–CNS) material containing both Ni nanoparticles and single-atom Ni sites through pyrolysis and acid washing of MA-intercalated NiAl-LDH precursors (Fig. 9a). By selectively removing the particulate Ni species, they further obtained a purely single-atom Ni catalyst (Ni–SAC). A systematic electrochemical comparison among the three materials (Fig. 9b) revealed that Ni–SAC exhibited the highest onset potential, current density, Faradaic efficiency, and H_2O_2 yield under oxygen-rich alkaline conditions, demonstrating superior $2e^-$ ORR activity and selectivity over both Ni–CNS and the bare carbon nanosheet (CNS). Further mechanistic analysis (Fig. 9c) indicated that the single-atom Ni sites in Ni–SAC promote selective O_2 adsorption, while the CNS framework facilitates the generation of active hydrogen species (H*). The synergy between these components significantly enhances H_2O_2 production efficiency. In contrast, the presence of Ni nanoparticles in Ni–CNS favors O–O bond cleavage, leading to different reaction selectivity. These results collectively highlight the

 https://doi.org/10.1007/s40820-026-02197-6

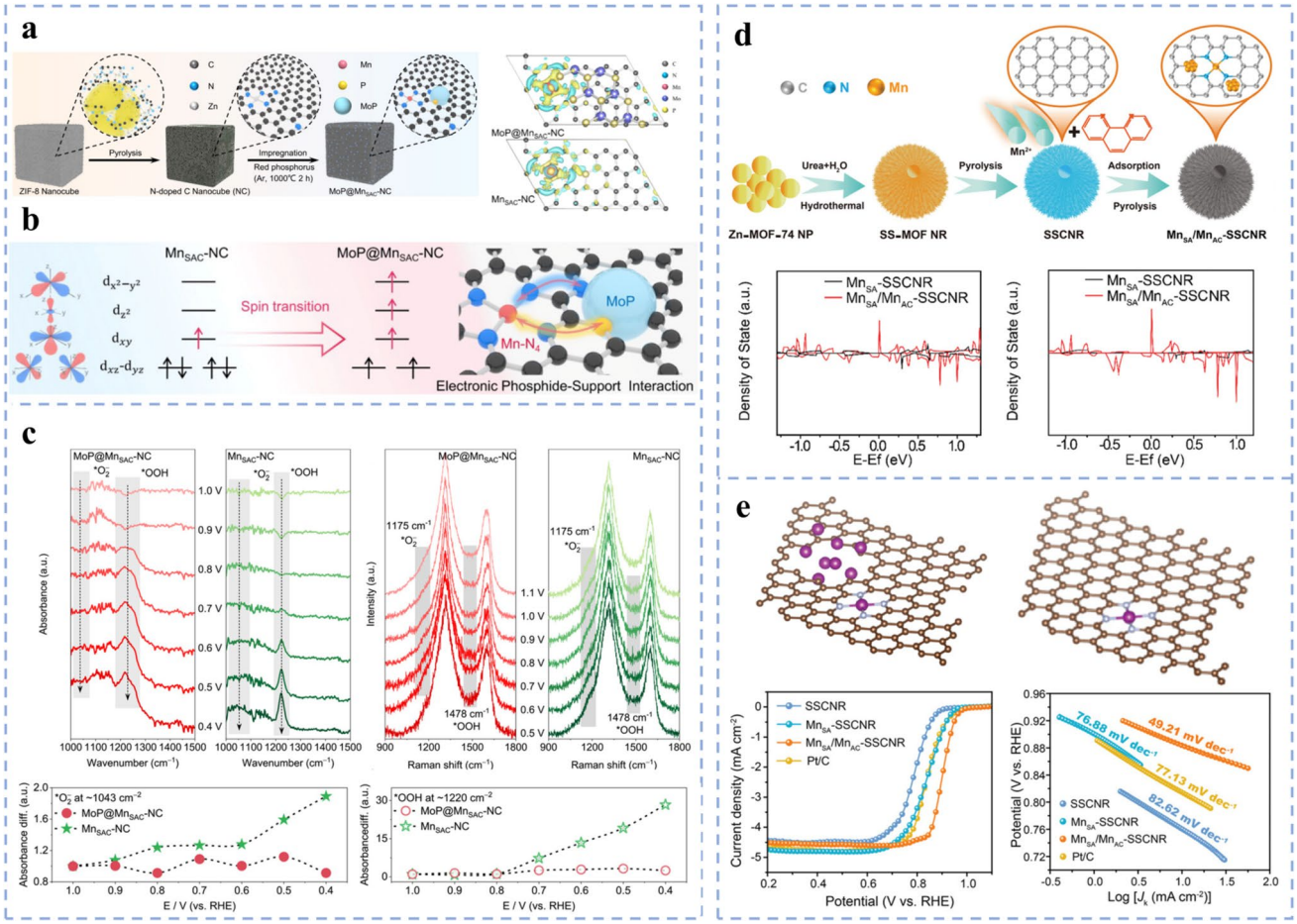

Fig. 8 **a** Preparation process of MoP@MnSAC–NC catalyst and its charge density difference distribution. **b** Mechanism of Mn atomic d orbital spin state transition induced by catalyst. **c** In situ FTIR and Raman spectra of MoP@MnSAC–NC and MnSAC–NC at different potentials [128]. Copyright 2025, Wiley–VCH **d** Synthesis process of MnSA/MnAC–SSCNR and its electrocatalytic test. **e** Calculation model of MnSA–SSCNR and MnSA/MnAC–SSCNR and their total density of states (TDOS) and local density of states (PDOS) [129]. Copyright 2024, Wiley–VCH

critical role of atomically dispersed Ni in modulating the ORR pathway for selective H_2O_2 synthesis.

In a separate study, Zhang's group proposed a high-entropy-induced electric dipole transition strategy to construct a spinel oxide (FeCoNiMnCrO) with bipolar dual-active sites for multiscale regulation of the ORR pathway [138]. As illustrated in Fig. 9d, the incorporation of multiple metal elements in FeCoNiMnCrO creates a highly distorted lattice, where Co and Ni serve as the main active centers, while Mn and Cr enhance lattice entropy and structural distortion. This high-entropy configuration significantly outperforms low-entropy Fe_3O_4 in bifunctional ORR/OER activity. The study further elucidated the electronic structure evolution at octahedral and tetrahedral sites (Fig. 9e). The high-entropy-induced lattice distortion activates originally inert tetrahedral sites, turning them into novel ORR active centers. Moreover, the electric dipole transition promoted by the high-entropy environment enhances the hybridization between the Co t_{2g} and O 2*p* orbitals (Fig. 9f), resulting in the formation of low-valence tetrahedral Co and high-valence octahedral Ni. This work identifies the "unpaired t_{2g} electron number" as a key electronic descriptor for ORR activity. Combined experimental and theoretical analyses confirm the effectiveness of the high-entropy strategy in regulating electronic structure and enhancing catalytic performance.

The Pan team developed an electrocatalytic system based on Ni–N_3S single-atom sites, achieving efficient electrochemical synthesis of H_2O_2 through precise electronic structure modulation via first coordination sphere engineering

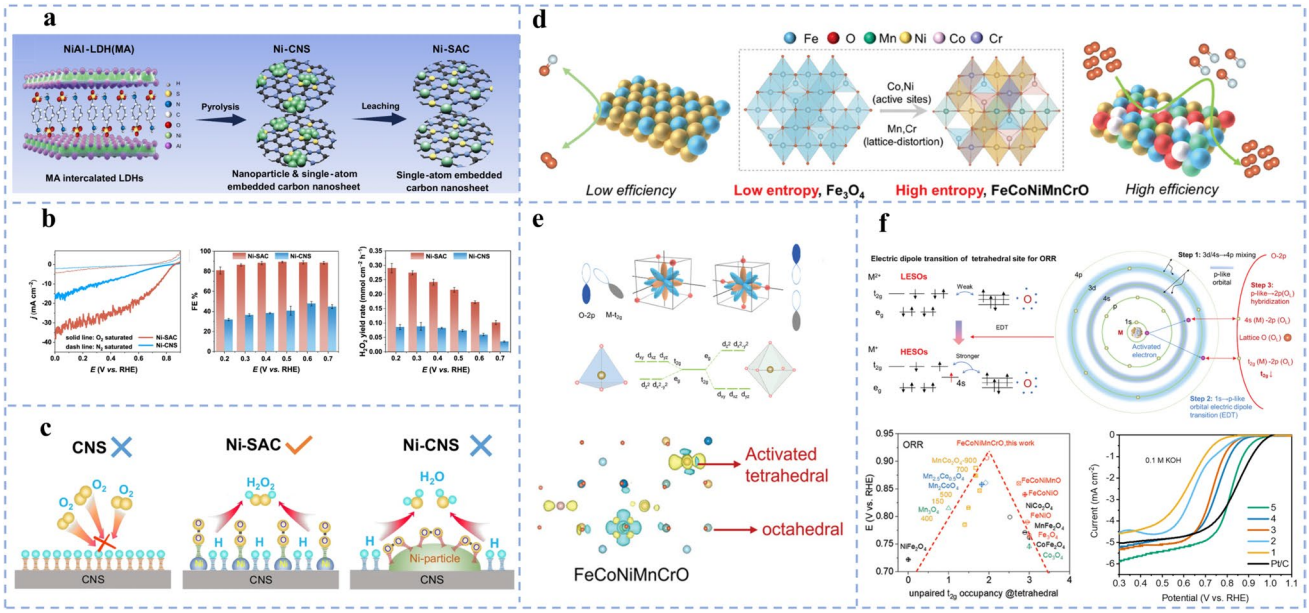

Fig. 9 **a** Flowchart of the preparation of Ni–SAC. **b** LSV curves, Faradaic efficiency (FE) and H_2O_2 yield of Ni–SAC and Ni–CNS at different potentials. **c** Reaction mechanism of Ni–SAC and Ni–CNS [137]. Copyright 2024, Springer Nature. **d** Characteristics of low-entropy spinel oxides with integrated single octahedral sites and high-entropy spinel oxides with bipolar dual-active sites. **e** Electronic structures of tetrahedron and octahedron in LESO. Differential charge density diagram of Fe_3O_4 and FeCoNiMnCrO, density of states projection. **f** High-entropy-induced robust electric dipole transitions enhance ORR activity on tetrahedral sites, volcano diagram of zircon oxides [138]. Copyright 2024, Wiley–VCH

(Fig. 10a) [139]. The adsorption strength of the key OOH* intermediate was found to positively correlate with the metal–oxygen bond length across different coordination structures (Fig. 10b). Both Co–N_3O and Ni–N_3S configurations fall within the optimal adsorption range, characterized by moderate binding capacity and low reaction free energy barriers, theoretically favoring selective H_2O_2 generation. While Co–N_3O resides in the strong adsorption region of the ΔG_{OOH*} diagram (Fig. 10c) with higher selectivity, Ni–N_3S positioned on the weak adsorption side demonstrates superior catalytic activity. Both coordination environments enable high current density and H_2O_2 selectivity over a wide potential range, significantly outperforming conventional M–N_4 structures. The introduction of heteroatoms with varying electronegativities into the first coordination shell effectively tunes the electronic structure of metal centers, enabling precise control over catalytic performance. Liu's group further demonstrated dynamic manipulation of Pt-based catalyst electronic states through construction of a heterogeneous a–c interface structure (Fig. 10d) [140]. In situ X-ray absorption fine structure (XAFS) analysis (Fig. 10e) revealed potential-dependent electron redistribution between Pt and Ni sites, where Ni initially accepts electrons to activate Pt sites before transferring electrons back to Pt, thereby accelerating oxygen protonation and enhancing reaction kinetics. Synchrotron radiation experiments (Fig. 10f) confirmed that this electron redistribution promotes OH* intermediate formation, facilitating the efficient $4e^-$ ORR pathway. The interfacial structure between a and c phases achieves synergistic enhancement of both activity and stability through electronic state modulation and intermediate adsorption behavior regulation. Chen's group elucidated the synthesis process of $Ni(OH)_2$–C_2O_4 electrocatalysts and their structural evolution during the $2e^-$ ORR process (Fig. 10g) [141]. In alkaline environments, NiC_2O_4 spontaneously transforms into $Ni(OH)_2$–C_2O_4, where oxalate self-assembles and adsorbs onto the $Ni(OH)_2$ surface, forming a stable functional layered structure. In situ infrared spectroscopy revealed enhanced O–O stretching vibrations and intensified OOH* adsorption signals with potential variation, indicating that oxalate modification promotes the adsorption and activation of key intermediates. In situ Raman spectroscopy demonstrated reversible formation and disappearance of NiOOH characteristic peaks during the

https://doi.org/10.1007/s40820-026-02197-6

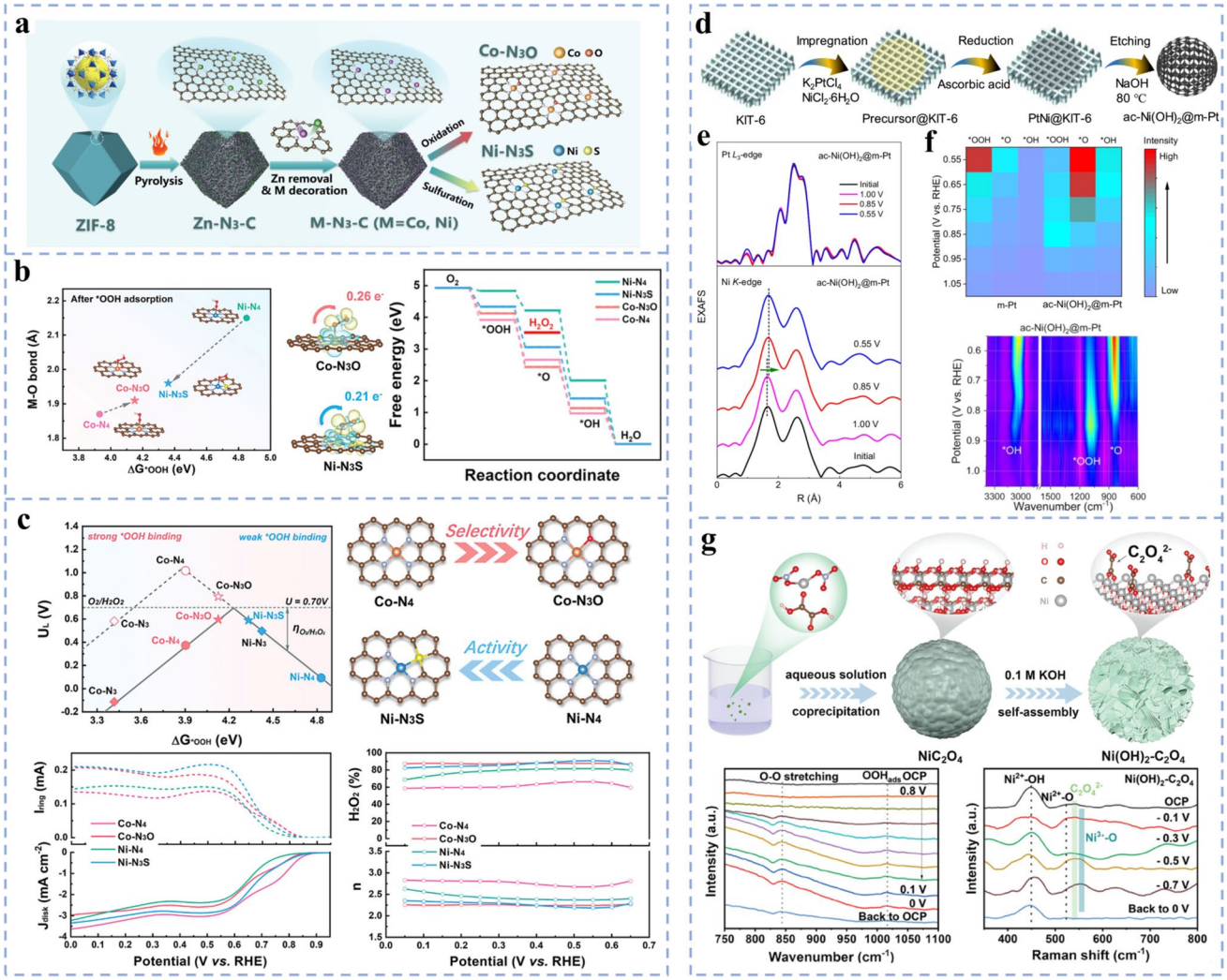

Fig. 10 **a** Synthesis process of Co–N_3O and Ni–N_3S. **b** Change of metal–oxygen bond length and charge difference density after OOH* adsorption and catalyst ORR free energy path. **c** Volcano plot of potential and free energy, RRDE experimental curve and H_2O_2 selectivity and electron transfer number [139]. Copyright 2024, Wiley–VCH. **d** Schematic diagram of the synthesis of the catalyst. **e** Changes in the in situ EXAFS spectrum at different potentials. **f** Differences in the adsorption strength of key intermediates between ac–$Ni(OH)_2$@m–Pt and m–Pt in the ORR process [140]. Copyright 2025, Springer Nature. **g** Synthesis path of NiC_2O_4 nanoparticles and $Ni(OH)_2$–C_2O_4 nanoflowers and their in situ spectral characterization in ORR [141]. Copyright 2024, Wiley–VCH

ORR process, confirming the remarkable reversibility and stability of nickel active sites. The persistent oxalate signals throughout the reaction suggest its structural integrity, indicating that oxalate not only stabilizes the overall structure but also plays a crucial role in modulating the electronic structure to facilitate intermediate adsorption/desorption and enhance electrocatalytic activity.

Despite their potential in the ORR, Ni-based catalysts often exhibit limited electrocatalytic activity and face challenges in forming efficient active centers. These materials typically suffer from insufficient electrical conductivity and structural vulnerability, particularly in both alkaline and acidic environments where nickel species are prone to dissolution or migration, leading to progressive degradation of catalytic integrity and rapid activity decay [142]. Moreover, TMCs based on nickel generally demonstrate restricted capability for O_2 adsorption and activation, along with inadequate control over key intermediates such as OOH*, which collectively impair ORR pathway selectivity and electron transfer efficiency [143]. In light of these structural and performance constraints, advanced regulation of Ni-based systems remains a compelling research direction. Future studies

should prioritize the rational design of efficient nickel active sites with tunable electronic structures, the development of novel low-valent nickel centers, and the construction of stable composite materials through heterogeneous electrocatalysis strategies. Special emphasis should be placed on enhancing structural durability and dissolution resistance under both strongly basic and acidic conditions to facilitate practical implementation.

3.4 Co-Based Catalysts

Cobalt-based electrocatalysts have emerged as promising candidates for the ORR, owing to their tunable electronic structure, effective intermediate adsorption capability, and cost-efficient characteristics [144–146]. Recent studies indicate that strategic manipulation of local atomic configuration, spin states, and exposed crystal planes can significantly enhance their catalytic performance. However, as research advances toward more precise control of active site structure and electronic environments, Co-based TMCs face two major challenges in ORR applications: conventionally pyrolyzed Co–N–C structures often suffer from poorly controlled coordination geometry, non-uniform charge distribution, and electronic state heterogeneity at active centers, which collectively impede a systematic understanding of their catalytic behavior and spatial dynamics. Moreover, the typical Co–N_4 configuration shows limited ability to balance reaction selectivity and kinetic activity during the adsorption regulation of key intermediates such as OOH*, thereby restricting its practical utility in selective H_2O_2 production and the $4e^-$ ORR pathway. In response, researchers have pursued precise coordination design, electronic modulation, and orbital hybridization strategies to overcome the limitations of conventional Co–N_4 sites. By adjusting the electronegativity of the Co center, local spin configuration, and ligand field strength, they have realized directed ORR pathway control and enhanced catalytic performance [147–149].

Yu and colleagues developed a heterogeneous molecular electrocatalyst system featuring an integrated built-in magnetic field, constructing a hierarchical CoPc/CB–Mag catalyst (Fig. 11a) [150]. This catalyst was synthesized by depositing cobalt phthalocyanine onto carbon black and combining it with polydopamine-coated magnetic nanoparticles, forming an interface structure characterized by distinct Co–N_4 active sites and the synergistic effect of the built-in magnetic field. In the ORR, the CoPc/CB–Mag catalyst demonstrated superior onset potential and current density, along with a lower Tafel slope and charge transfer resistance (Fig. 11b). Its catalytic activity and electron transport performance were significantly enhanced compared to the control group. Subsequent X-ray photoelectron spectroscopy (XPS) analysis, flux simulation, and *d* orbital energy level investigations (Fig. 11c) revealed that the built-in magnetic field induces a transition of the cobalt center from a low-spin to a high-spin state, elevating the d_{22} orbital energy level and thereby enhancing the adsorption and activation capabilities for O_2 and OOH* intermediates. This synergy effectively improves ORR performance and introduces a novel strategy for modulating the electronic structure of single-atom catalytic sites via magnetic field induction. In a separate study, Sun et al. [151] developed a morphology-controlled $Co(CN)_3$ microcrystalline catalyst through structural regulation of the cobalt coordination environment (Fig. 11d). By adjusting reaction temperature and ligand concentration, three distinct crystal morphologies—cube, truncated cube, and octahedron—were successfully synthesized. The systematic exposure of different crystal facets effectively modulated the local coordination structure of cobalt. Among these, the five-coordinate Co–C_2N_3 site, together with the corresponding free energy profile (Fig. 11e), exhibited the lowest overpotential and reaction free energy barrier. The $Co(CN)_3$–Cub variant demonstrated a higher onset potential and half-wave potential, as well as a lower Tafel slope (Fig. 11f), achieving peak power density of 1.67 W cm^{-2} in fuel cells while maintaining excellent cycling stability.

While Co-based catalysts have demonstrated considerable progress in the ORR, they continue to face critical scientific and engineering challenges that impede their practical implementation, necessitating further fundamental research and technological breakthroughs [152]. Currently, the inability to systematically detect the in situ dynamic behavior of key reaction intermediates (e.g., OOH* and OH*) at operating potentials hinders the precise identification of rate-determining steps and actual active sites. Furthermore, enhancing H_2O_2 selectivity often occurs at the expense of intrinsic catalytic activity, making the coordinated regulation of both high activity and high selectivity a central bottleneck [153]. Additionally, the long-term stability and environmental adaptability of these TMCs in practical devices—particularly under harsh conditions such as strongly acidic or basic electrolytes—require significant improvement. Future

https://doi.org/10.1007/s40820-026-02197-6

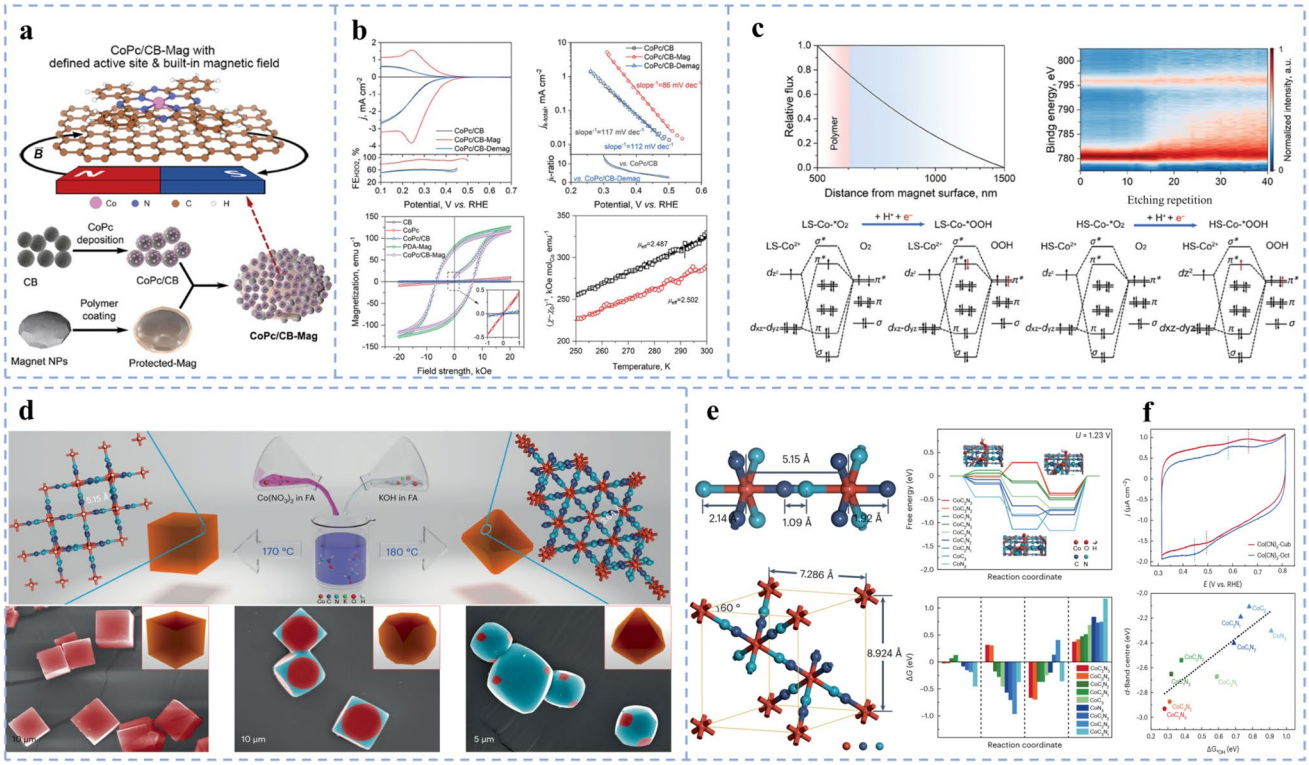

Fig. 11 **a** Schematic diagram of the synthesis of CoPc/CB–Mag composites and the catalytic system of active sites and built-in magnetic fields. **b** Performance in ORR as well as magnetic susceptibility and hysteresis loops. **c** Simulation of the effect of the polymer layer on the surface of magnetic particles on the spatial distribution of magnetic flux density and Co 2*p* XPS depth profile and orbital energy level diagram [150]. Copyright 2024, Wiley–VCH. **d** Three types of $Co(CN)_3$ microcrystals, namely, cube (Cub), truncated cube and octahedron (Oct), were synthesized. **e** Local atomic structure and unit cell model and free energy diagram of $Co(CN)_3$–Cub were revealed. **f** Relationship between the CV curve and the OH* adsorption energy and the *d* band center of the Co site [151]. Copyright 2023, Springer Nature

research should prioritize the design of novel coordination structures and the development of advanced electronic state control strategies, including interface polarization, spin state manipulation, and local strain engineering. The integration of in situ and quasi-in situ multiscale characterization techniques with first-principles simulations will be essential to elucidate the underlying catalytic mechanisms. Such integrated efforts are expected to accelerate the practical application of cobalt-based heterogeneous electrocatalysis systems in sustainable energy conversion and green chemical synthesis.

3.5 Cu-Based Catalysts

While Cu-based catalysts have demonstrated significant potential in electrochemical applications—particularly in the carbon dioxide reduction reaction where they exhibit notable electrocatalytic performance their role in the ORR is also attracting growing interest [154–157]. Although platinum-based catalysts generally remain more active for the ORR, Cu-based catalysts are increasingly regarded as promising alternative materials for energy conversion systems such as fuel cells and metal–air batteries, owing to their cost-effectiveness, natural abundance, and considerable stability [158, 159].

SACs represent a fundamental strategy for achieving efficient metal atom anchoring and precise regulation of active sites, owing to their atomic-level dispersion and structural tunability. The development of Cu–SACs holds particular significance for understanding structure–performance relationships in ORR catalysts. To systematically investigate these relationships, the Zong team engineered a structurally defined Cu–SAC with tailored defects and comprehensively studied its ORR activity (Fig. 12a) [160]. Their analysis of intermediate adsorption behavior and

reaction pathways across various Cu–N_4 coordination structures revealed that the Cu–$(N–C_2)_3$(N–C) configuration exhibited the lowest OOH* adsorption free energy (Fig. 12b), indicating superior reaction kinetics and intrinsic activity. These findings underscore the critical role of defect engineering in modulating electronic structure and enhancing the catalytic performance of single-atom systems. In a complementary approach, Zhou et al. [161] developed an efficient ORR catalyst based on copper nanocomposites (Fig. 12c), constructing a CuO_x/Cu nanostructure with tunable valence states. The combination of Cu^{2+} and zero-valent copper created a versatile valence electron reservoir that enabled dynamic regulation of the electronic state of supported single-atom platinum, ultimately optimizing catalytic performance. This strategy demonstrated excellent $4e^-$ ORR selectivity and remarkable electrocatalytic stability (Fig. 12d). Addressing key challenges such as SAC instability, unmodifiable electronic structures, and inefficient intermediate adsorption, Jiang et al. [158] developed a single-atom copper catalyst leveraging atomic interface effects for enhanced ORR performance (Fig. 12e). Through a strategy combining acid etching with sulfur–nitrogen synergistic doping, they effectively modulated the electronic structure and coordination environment of Cu single atoms. This approach maintained copper in a low-valence state, optimizing the adsorption and dissociation of key intermediates (OOH* and O*), thereby significantly improving overall ORR performance.

Through the implementation of defect engineering, valence state regulation, and interface doping strategies, researchers have successfully developed a series of structurally optimized Cu–SACs. These advances have enabled effective optimization of electronic structures and intermediate adsorption behaviors, addressing key limitations of Cu-based catalysts such as insufficient activity, inflexible electronic states, and poor stability. However, copper active sites typically exist in + 1 or + 2 valence states, where the limited number of *d* orbital electron impedes efficient O–O bond cleavage, consequently favoring the $2e^-$ pathway for H_2O_2 formation [162]. Furthermore, single-atom copper systems exhibit constrained electron transfer capability and reaction kinetics due to their rigid valence states and challenging coordination environments, making them susceptible to migration or dissolution under electrochemical conditions, which compromises active site stability. Future research on Cu-based ORR catalysts should prioritize several key directions: dynamic modulation of the copper center's electronic structure; in situ analysis of valence state evolution and coordination environment reconstruction; and mechanistic investigation of the copper site's behavior throughout the ORR cycle. Additional efforts should focus on constructing interface structures with electronic regulation capability to enable reversible electronic coupling at copper centers, enhancing active site stability and accessibility through defect engineering and hierarchical pore structure design. The integration of first-principles calculations with in situ spectroscopic techniques will be crucial for identifying rate-determining steps in intermediate adsorption and reaction pathways, thereby establishing a theoretical foundation for the rational design of high-performance Cu-based ORR catalysts.

3.6 Other Transition Metal Catalysts

Beyond the transition metals previously discussed, rare earth materials demonstrate distinctive advantages for electrocatalytic applications due to their unique electronic configurations, tunable valence states, and flexible coordination characteristics. These properties enable precise regulation of reaction intermediate adsorption strength, optimization of electron and proton transfer pathways, and enhanced stabilization of active site structures. Such capabilities make rare earth materials particularly promising for accelerating reaction kinetics, improving catalytic selectivity, and ensuring electrochemical stability—especially under demanding operational conditions requiring long-term durability. The unique 4*f* orbital configuration and multielectron characteristics of rare earth elements provide exceptional electronic regulation capabilities in the ORR. Through *f–p–d* orbital hybridization or asymmetric coordination with ligands such as oxygen, nitrogen, and chlorine, these materials can effectively modulate the electronic structure of transition metal active centers. This electronic optimization improves intermediate adsorption behavior, reduces reaction energy barriers, and accelerates overall reaction kinetics. Simultaneously, certain non-rare earth metal materials contribute significantly to enhancing catalytic performance by inhibiting competing reaction pathways and extending catalyst service life. Their exceptional chemical stability, resistance to oxidative damage, and structural controllability make them valuable complementary components in the development of

https://doi.org/10.1007/s40820-026-02197-6

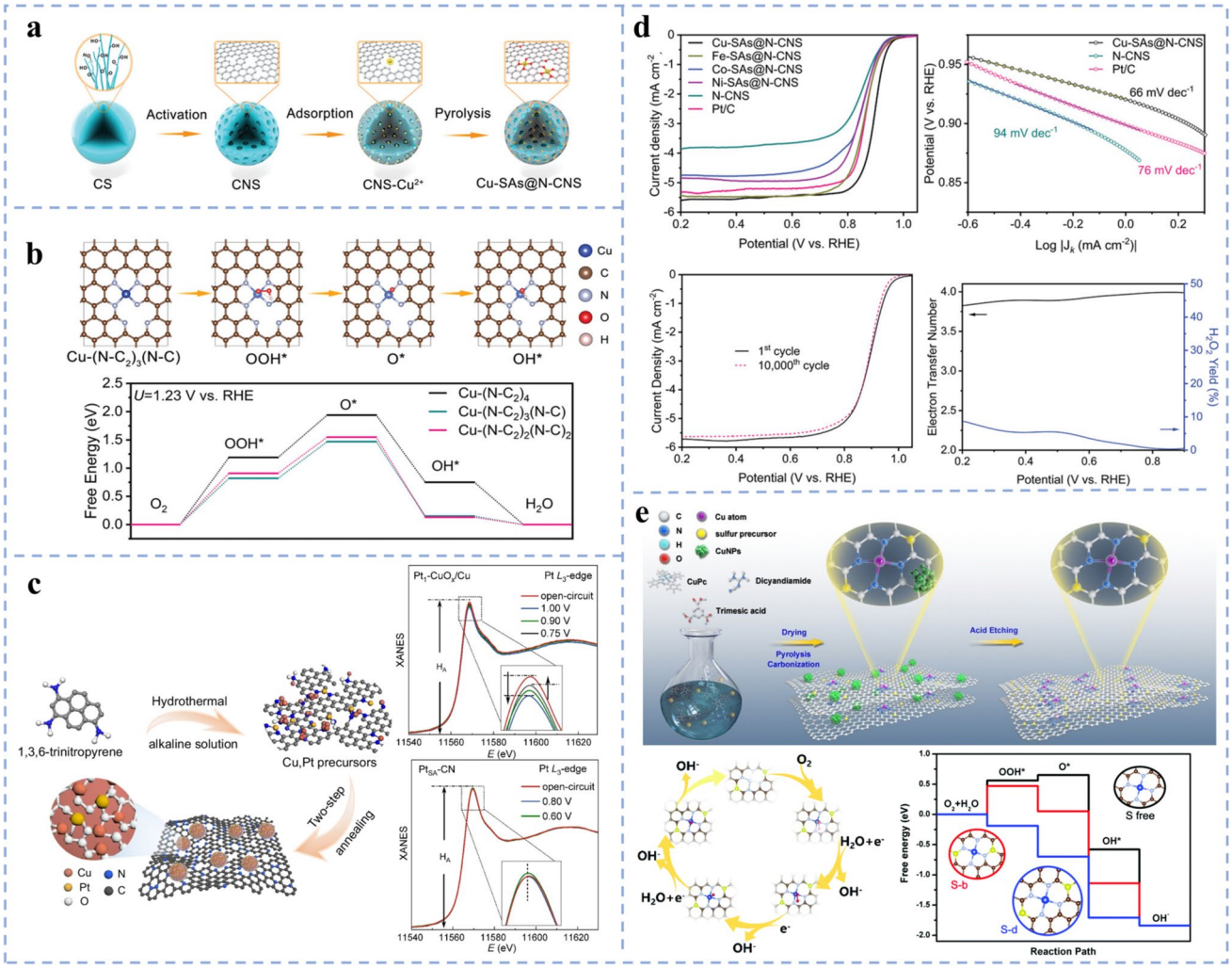

Fig. 12 **a** Schematic diagram of the synthesis process of Cu–SAs@N–CNS. **b** Adsorption configurations of intermediates (OOH*, O*, OH*) and free energy diagrams of $4e^-$ ORR paths in three different coordination environments [160]. Copyright 2021, Wiley–VCH. **c** Synthesis process of Pt_1–CuOx/Cu single-atom catalyst and its in situ structural evolution and in situ XAFS characterization during electrochemical reaction, as well as XANES of comparative samples [161]. Copyright 2024, Springer Nature. **d** Electrocatalytic performance of various transition metal single-atom catalysts in ORR as well as H_2O_2 yield and electron transfer number. **e** Synthesis process of sulfur-modified copper single-atom catalyst and its theoretical study in ORR [158]. Copyright 2019, Royal Society of Chemistry

high-performance, durable ORR catalysts. The synergistic integration of rare earth elements with these stable non-rare earth materials represent a promising direction for advancing next-generation electrocatalytic systems with both enhanced activity and prolonged operational lifetime [163–165].

In recent years, rare earth-based catalysts have attracted considerable research attention owing to their distinctive structural characteristics and unique electronic properties. Liu et al. reported an efficient two-electron ORR catalyst utilizing rare earth phosphate materials (Fig. 13a) [163]. Their study systematically investigated the intrinsic mechanism of H_2O_2 production, with particular focus on the adsorption and dissociation behavior of the key OOH* intermediate. By integrating theoretical calculations with in situ Raman spectroscopy, they elucidated the variation in OOH* adsorption free energy across different crystal planes (Fig. 13b). The Sm site was identified as the primary active center, exhibiting exceptional capability for intermediate adsorption and release. Electrochemical evaluation using a rotating ring disk electrode (RRDE) demonstrated outstanding $2e^-$ ORR performance (Fig. 13c), achieving over 93% H_2O_2 selectivity with remarkable stability under alkaline conditions. The layered $SmPO_4$

hollow structure, characterized by open channels, optimal metal spacing, and abundant proton transport pathways, contributes to its superior catalytic activity, selectivity, and structural stability. In a separate study, Yin et al. synthesized a La–SAC through chlorine axial coordination activation and systematically investigated its electronic structure regulation and catalytic mechanism [164]. Compared to conventional La–SACs, this modified catalyst exhibits a lower reaction energy barrier and increased density of exposed active sites. Figure 13d, e illustrates the distribution and coordination structure of La atoms within the carbon substrate. The energy barrier for the key intermediate transition from OOH* to OH* was merely 0.39 eV (Fig. 13f), significantly lower than that of conventional La–SACs, indicating substantially enhanced ORR kinetics. When applied as an air cathode in both liquid and flexible solid-state zinc–air batteries, this catalyst demonstrated superior discharge voltage, power density, and flexibility, outperforming the 20% Pt/C control group (Fig. 13g).

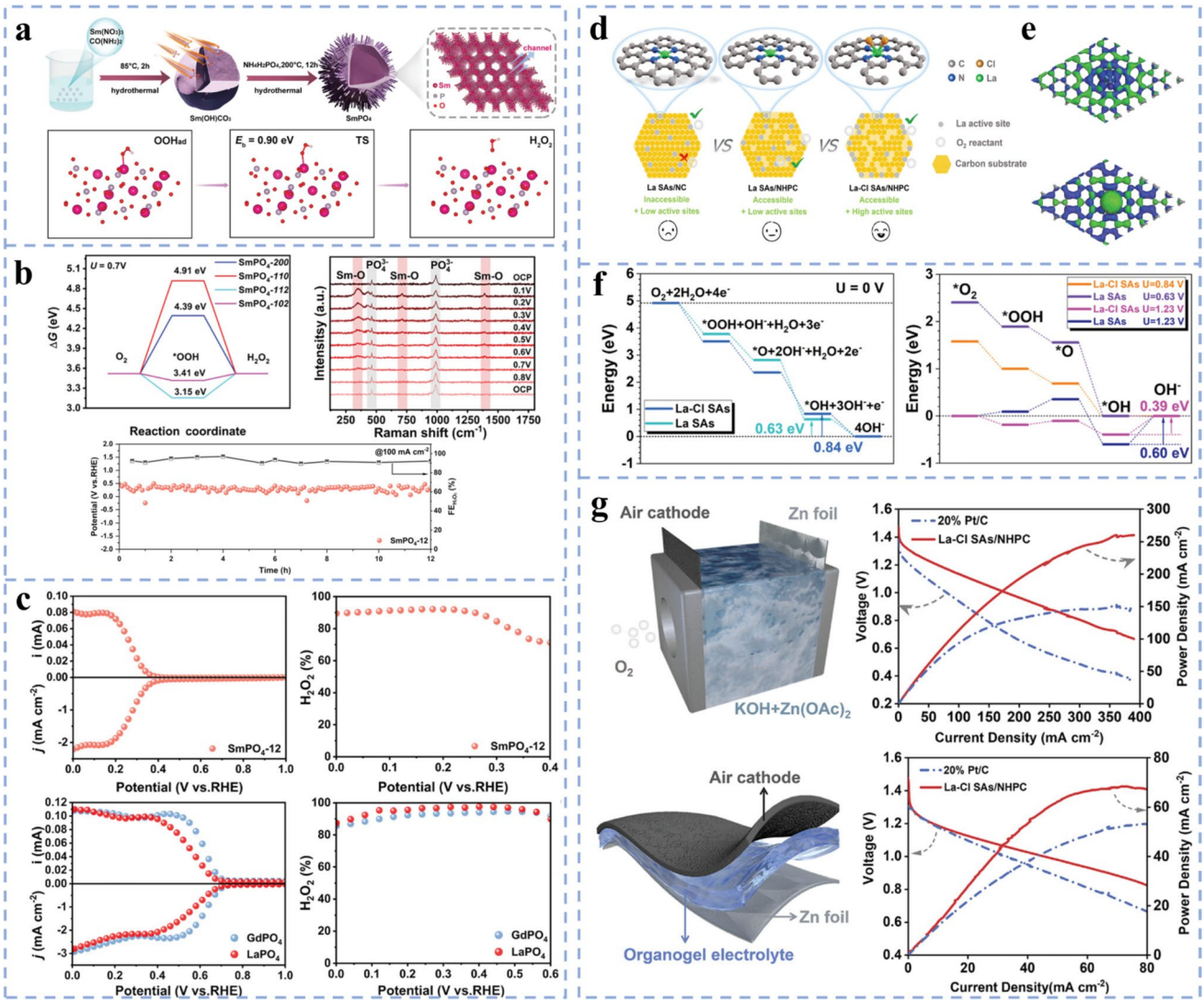

Fig. 13 **a** Schematic diagram of the synthesis of $SmPO_4$ nanospheres and the atomic model of the initial state, transition state and final state of the OOH* to H_2O_2 path. **b** Different crystal planes have different reaction barriers for the $2e^-$ ORR path at U = 0.70 V and in situ Raman spectra and stability tests under gas diffusion electrode configuration [163]. Copyright 2025, Wiley–VCH. **c** LSV curve of catalyst and H_2O_2 yield. **d** Schematic diagram of the structures of three different configurations of La single-atom catalysts. **e** Comparison of the electron orbital distribution of La–Cl SAs and La SAs near the Fermi level: blue is the bonding orbital, green is the antibonding orbital, **f** ORR free energy path of La–Cl SAs and La SAs at U = 0 V and different applied potentials. **g** Actual performance of La–Cl SAs/NHPC in aqueous and flexible zinc–air batteries is introduced [164]. Copyright 2025, Wiley–VCH

https://doi.org/10.1007/s40820-026-02197-6

Furthermore, Cheng et al. developed a FePc/Eu_2O_3 composite catalyst based on f–p–d (Eu–O–Fe) gradient orbital coupling (Fig. 14a) [165]. Through the construction of a heterostructure comprising FePc and Eu_2O_3, atomic Fe site modification was successfully achieved on the carrier. The Eu–O–Fe bridging structure significantly enhances the adsorption behavior of critical intermediates (OOH*, O*, and OH*), thereby reducing the reaction energy barrier. Differential charge density and electronic state distribution analyses (Fig. 14b) revealed that electron redistribution within the FePc/Eu_2O_3 system facilitates improved electron transfer. Quantitative comparison of *d* orbital electronic states and unpaired electron numbers between this system and FePc provided detailed insight into the *f–p–d* gradient orbital coupling mechanism. The coupling of the Eu f orbital with the O *p* orbital stimulates *d* orbital transitions in Fe, increasing e_g orbital occupancy and transforming the Fe center from a low-spin to a medium-spin state. This electronic reorganization enhances the cooperative adsorption and desorption capabilities for reaction intermediates. Additionally, the incorporated f band functions as an electron buffer layer, effectively mitigating electron loss and maintaining structural stability (Fig. 14c). These studies collectively demonstrate that rare earth elements, through their unique 4*f* electronic configurations and flexible coordination characteristics, provide powerful strategies for designing advanced ORR catalysts with tailored activity, selectivity, and stability.

During the investigation, researchers have discovered that various TMCs demonstrate significant anti-Fenton reaction characteristics. Yue et al. [166] systematically studied a Re–SAC, thoroughly examining its exceptional anti-Fenton performance and underlying mechanism. The Re–SAC effectively suppresses the formation of OH* radicals in the presence of H_2O_2, which is attributed to its stable Re–N_4 coordination structure that prevents oxidative degradation of the carbon support. Analysis of charge density distribution and electronic structure revealed pronounced electron localization and enhanced oxidative resistance at the Re active sites (Fig. 14d). Subsequent Fenton reaction tests using ABTS probes (Fig. 14e) confirmed the remarkable anti-Fenton capability of the Re–SAC system. When implemented in zinc–air batteries (Fig. 14f), the Re–SAC demonstrated outstanding practical performance, including a high open-circuit voltage, substantial maximum power density, and stable charge–discharge cycling over 300 h, surpassing the performance of commercial Pt/C + RuO_2 benchmarks.

Despite these advantages, the broader adoption of Re–SACs in ORR catalysis remains limited. Compared with Fe–SACs, Re–SACs suffer from higher material cost, lower elemental abundance, and a narrower optimal operating window, which restrict their scalability and general applicability. Moreover, the strong oxidative resistance and moderated *OOH binding at isolated Re sites, while beneficial for suppressing radical-induced degradation, may compromise catalytic activity or pathway flexibility under certain ORR conditions. Consequently, Re–SACs are currently better suited for stability-critical or radical-sensitive applications, rather than serving as a universal replacement for Fe-based single-atom catalysts.

Rare earth-based supports demonstrate exceptional structural stability and dissolution resistance, maintaining remarkable electrochemical durability particularly under alkaline conditions. Future investigations should prioritize elucidating the orbital hybridization mechanisms between rare earth elements and transition metals, developing precise single-atom regulation strategies, and constructing enhanced architectures with optimal coordination in conductive matrices. Concurrently, research should address the optimization of their stability in acidic media to expand their applicability in energy conversion devices such as fuel cells and metal–air batteries. Complementarily, TMCs exhibit significant activity in the ORR due to their tunable *d* orbital electronic structures and variable oxidation states. Future research directions should focus on precise modulation of d band center positioning and intermediate adsorption behavior, along with constructing multimetal synergistic systems or heteroatom coordination environments to enhance catalytic selectivity and electron transfer efficiency. Substantial efforts should also be directed toward developing effective anti-dissolution strategies—including interface engineering and protective carbon layer coating—to address stability challenges in acidic environments. These coordinated advances will establish a robust foundation for practical device applications across diverse energy conversion systems.

4 Application of Transition Metal Heterogeneous Catalysts in ORR

Transition metal-based heterogeneous electrocatalysis demonstrates significant potential across diverse applications in the ORR. In energy conversion and storage technologies

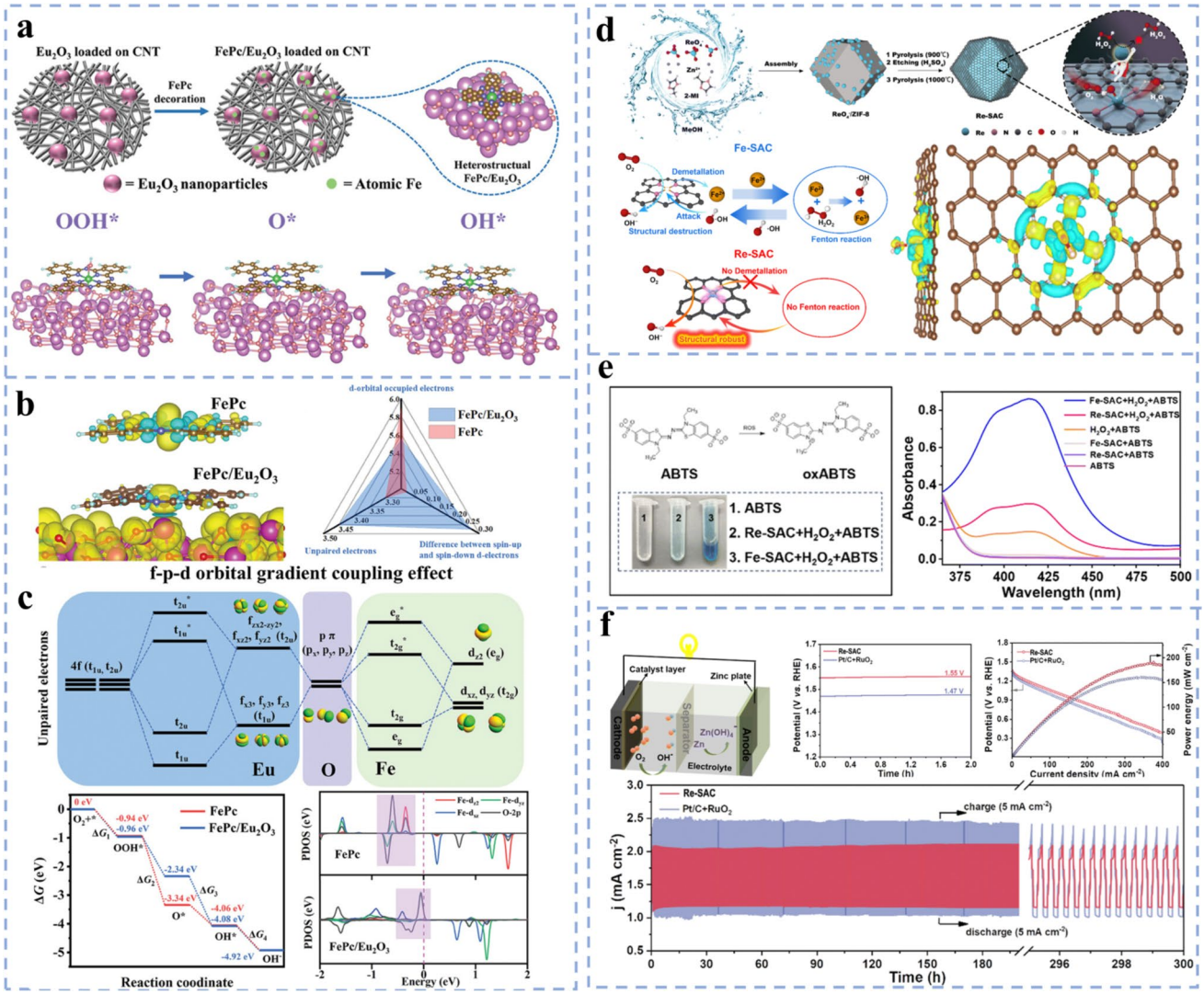

Fig. 14 **a** Synthesis path of FePc/Eu_2O_3/CNT and the optimized configuration after OOH*, O*, and OH* adsorption. **b** Comparison of the electron spin density distribution of FePc and FePc/Eu_2O_3 and the degenerate diagram of the d orbital occupation of Fe atoms. **c** Comparison of the *f–p–d* orbital gradient coupling effect and free energy diagram as well as the density of states after OOH* adsorption [165]. Copyright 2025, Wiley–VCH. **d** Synthesis route of Re–SAC and its inherent anti-Fenton reaction characteristics and the differential charge density diagram showing the redistribution of electrons in Re–SAC (light yellow for charge accumulation and cyan for charge depletion). **e** Schematic diagram of the reaction of ROS with ABTS and the color map and UV–Vis absorption spectrum of the solution after the reaction. **f** Schematic diagram of the zinc–air battery device and performance test results [166]. Copyright 2024, Royal Society of Chemistry

such as fuel cells and metal–air batteries, these TMCs serve as critical components for enhancing device efficiency and prolonging cycle life, owing to their exceptional catalytic activity, remarkable durability, and cost-effectiveness [167]. Furthermore, through precise regulation of the electronic structure and local coordination environment of the metal centers, these catalysts can achieve highly selective $2e^-$ reduction pathways, enabling efficient synthesis of H_2O_2. This capability provides innovative and sustainable solutions for environmental remediation, green chemical production, and medical disinfection. A central challenge in advancing the design and optimization of these catalytic systems lies in the precise control between $2e^-$ and $4e^-$ ORR pathways to meet distinct application requirements [168]. This section systematically reviews recent progress and future prospects of transition metal-based heterogeneous catalysts, with a focus on two key directions: electrocatalytic synthesis of H_2O_2 and their implementation in energy devices.

https://doi.org/10.1007/s40820-026-02197-6

4.1 Metal–Air Batteries

The ORR serves as a fundamental process governing the performance of metal–air batteries, where its catalytic efficiency directly determines key operational parameters including energy density, power output, and cycling stability. Owing to their high theoretical energy density and environmental sustainability, metal–air battery systems represent a primary application domain for advanced ORR catalyst development [169, 170]. In recent years, TMCs and their derived materials have demonstrated remarkable advantages in enhancing ORR kinetics and selectivity. This is attributed to their multivalent characteristics and highly tunable electronic structures, which enable precise regulation of intermediate adsorption/desorption behavior. Consequently, these materials have emerged as a crucial category of electrocatalysts for developing next-generation metal–air batteries with superior performance.

Among numerous studies exploring the regulation of Fe-based catalysts for zinc–air batteries, Ji et al. reported a Fe, Mn–HCNS catalyst where Mn atoms modulate the electronic structure of FeN_4 sites on hollow carbon nanospheres (Fig. 15a) [171]. Their findings demonstrate that Mn incorporation effectively modifies the electronic configuration of FeN_4 centers (Fig. 15b), reducing reaction free energy barriers and enhancing kinetic processes. Electrochemical characterization revealed that Fe, Mn–HCNS exhibits a more positive half-wave potential and lower Tafel slope in the ORR, ultimately enabling superior performance in practical rechargeable zinc–air battery tests (Fig. 15c). These results comprehensively confirm the crucial role of Mn-induced synergistic regulation in enhancing bifunctional electrocatalytic performance, validating the catalyst's effectiveness for advanced zinc–air batteries. In a complementary multivalent synergistic strategy, Qiu's research group engineered a Mn-doped γ-Fe_2O_3/CNT composite catalyst (Mn–Fe_2O_3/CNT) as high-performance air electrode material for metal–air batteries [172]. Selective incorporation of Mn atoms into octahedral vacancies of the γ-Fe_2O_3 lattice enables precise modulation of Fe active sites' electronic structure. This catalyst demonstrated exceptional discharge performance, high open-circuit voltage, and prolonged operational stability in both Mg–air and Al–air battery systems (Fig. 15d), highlighting its broad applicability in practical devices. Structural modeling and d band density of states analysis (Fig. 15e) reveal that Mn doping not only enhances O_2 molecule adsorption but also establishes synergistic interactions with Fe sites, effectively regulating the ORR pathway. Subsequent free energy calculations and charge density difference analysis (Fig. 15f) demonstrate that Mn incorporation reduces reaction energy barriers while enhancing OH* intermediate adsorption capacity, significantly improving catalytic reaction kinetics. This integrated theoretical and experimental investigation elucidates the critical role of octahedral Mn doping in enhancing the ORR performance of Fe-based catalysts, providing valuable insights for developing efficient non-precious metal catalysts for metal–air battery applications.

The Li research team has developed an advanced catalytic system for metal–air batteries by strategically engineering a Cu–N–C catalyst through elemental regulation [173]. By incorporating sodium functional groups into the carbon framework to modify conventional $Cu–N_4$ sites (Fig. 16a), they constructed a unique $C_2–Cu–N_4–COONa$ coordination structure that synergistically enhances both catalytic activity and structural stability. This innovative configuration effectively modulates the electronic structure of $Cu–N_4$ centers, optimizes the ORR pathway, and significantly mitigates carbon framework corrosion along with copper center migration and dissolution. When applied as an air cathode in zinc–air batteries (designated as CuNa–CF), the catalyst demonstrates exceptional overall performance (Fig. 16b), matching or even surpassing the ORR activity of commercial Pt/C catalysts while substantially improving battery longevity. The system maintains stable operation for over 5000 h at low current density and approximately 950 h at high current density. Atomic structure analysis and charge density difference mapping (Fig. 16c) further reveal that the $Na–COO^-$ functional group induces electron redistribution around the $Cu–N_4$ site, thereby optimizing O_2 adsorption and intermediate conversion processes—a crucial factor in enhancing catalytic performance. Remarkably, the catalyst exhibits high power density and outstanding discharge characteristics in both flexible solid-state and button-type all-solid-state zinc–air batteries, indicating substantial potential for broad applications in wearable energy devices and micropower sources.

In the design of TMCs, the modulation of active center electronic structures through main group elements has proved to be an effective strategy for enhancing catalytic performance and stability. Building on this approach, Zhang's group developed a nitrogen-doped mesoporous

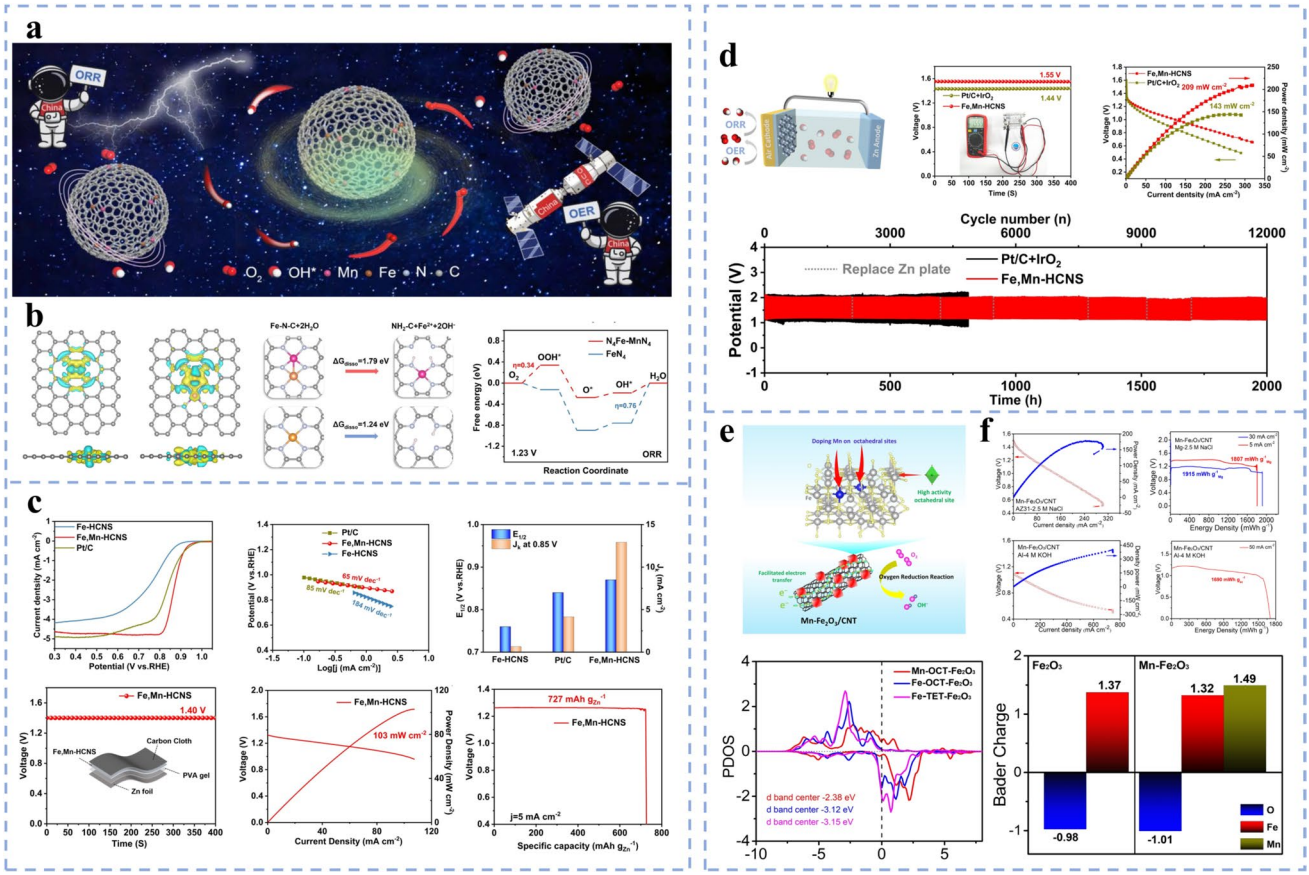

Fig. 15 **a** Synergistic mechanism of Fe and Mn promoting ORR and OER respectively in the catalytic cycle. **b** Differential charge density and free energy change of FeN_4 and Fe–MnN_4 and state density analysis. **c** Fe–Mn–HCNS electrocatalytic performance test and constructed flexible zinc–air battery [171]. Copyright 2024, Elsevier. **d** Schematic diagram of the battery structure of Fe, Mn–HCNS and the performance of alkaline zinc–air batteries in practical applications. **e** Octahedral sites, state density analysis and Bader charge and charge density difference diagram in Mn-doped activated Fe_2O_3. **f** Polarization performance and power density of zinc–air batteries and aluminum–air batteries constructed with Mn–Fe_2O_3/CNT [172]. Copyright 2025, Wiley–VCH

carbon catalyst featuring well-defined Fe–N_4 and Cu–N_4 diatomic sites, synthesized via molten salt-assisted pyrolysis to achieve uniform metal distribution within the carbon matrix (Fig. 16d). In the resulting FeCu–N_7 structure, Cu introduction induces asymmetric electron distribution around the Fe center, lowering O_2 adsorption energy and preventing excessive OH* intermediate adsorption, thereby optimizing the rate-determining step of the ORR (Fig. 16e). Electronic structure analysis further reveals that Cu synergistically shifts the Fe d band center downward, weakening OH* binding strength and modulating the reaction pathway to enhance both activity and stability. Electrochemical tests (Fig. 16f) demonstrate that this diatomic catalyst significantly surpasses commercial Pt/C in magnesium–air and zinc–air batteries, robustly confirming the synergistic advantages of dual metal sites in improving electrocatalytic performance and durability for advanced energy storage systems.

The development of transition metal-based heterogeneous electrocatalysis systems for metal–air batteries has achieved remarkable progress, demonstrating significant enhancements in ORR activity, cycling stability, and energy conversion efficiency [175]. Through precise engineering of metal coordination environments, optimization of *d* orbital electronic configurations, and strategic implementation of defect engineering and interface coupling, substantial improvements have been realized in intermediate adsorption behavior and electron transfer kinetics. The synergistic integration of in situ characterization techniques with computational modeling has further illuminated the dynamic evolution of key intermediates and energy-determining steps, establishing

 https://doi.org/10.1007/s40820-026-02197-6

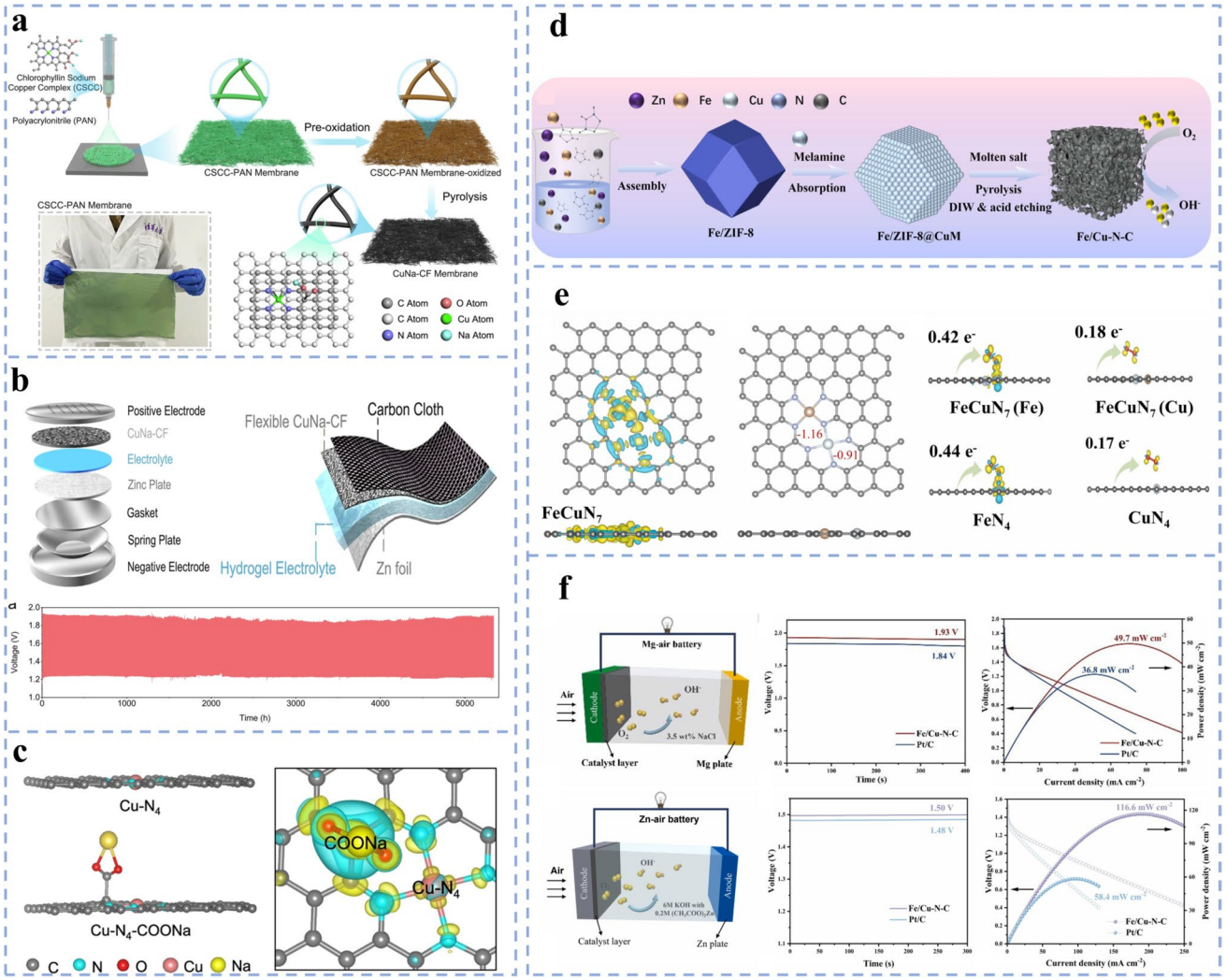

Fig. 16 **a** Catalyst synthesis method. **b** Application of CuNa–CF in liquid and flexible all-solid-state zinc–air batteries. **c** Charge density difference analysis. **d** Schematic diagram of catalyst synthesis [173]. Copyright 2024, Springer Nature. **e** Charge density difference diagram and Bader charge analysis and state density of $FeCuN_7$. **f** Application effect in Mg–air and Zn–air batteries [174]. Copyright 2024, Elsevier

a robust framework for understanding structure–activity relationships [176]. Despite these advances, fundamental challenges remain regarding the dynamic evolution of electrode–electrolyte interfaces, electrolyte-induced structural degradation, and the delicate balance between activity and durability. Future research directions should emphasize the regulation of interfacial charge distribution, investigation of active site dynamics under operational conditions, and development of well-defined catalytic architectures for stable integration into diverse device configurations. These developments represent crucial steps toward realizing high-energy–density, long-cycle-life metal–air battery systems for sustainable energy applications.

4.2 Fuel Cells

The high cost and scarcity of platinum-based catalysts have substantially hindered the large-scale commercialization of proton exchange membrane fuel cells, making the development of alternative TMCs a central focus in current fuel cell research. Addressing this challenge, Li et al. reported a proton exchange membrane fuel cell incorporating a highly dispersed manganese-based catalyst with exceptional stability (Fig. 17a) [177]. Through comprehensive characterization using in situ XPS, XANES, and EXAFS analyses, the researchers confirmed that manganese predominantly exists in the + 2 oxidation state with a well-defined $Mn–N_4$

coordination structure, without detectable metal clusters (Fig. 17b, c). This Mn–N–C catalyst demonstrates superior performance in acidic electrolytes compared to conventional carbon-based nonmetallic catalysts, effectively facilitating the four-electron ORR pathway with a H_2O_2 yield below 2%, thereby minimizing the detrimental impact of by-products on fuel cell operation. Practical evaluation in membrane electrode assemblies reveals outstanding performance under reduced precious metal loading conditions and exceptional operational durability. The remarkable stability of the Mn–N–C catalyst in fuel cell applications is primarily attributed to the antioxidant properties of the MnN_4 structure and its ability to suppress carbon support corrosion. Compared to iron and cobalt-based counterparts, manganese demonstrates superior resistance to Fenton reaction-induced catalyst degradation due to its lower reactivity with H_2O_2, thereby significantly enhancing fuel cell stability and operational lifetime.

Zhang's research group successfully developed a bimetallic catalyst featuring adjacent Fe-based and Mn-based active sites for fuel cell applications (Fig. 17d) [178]. Electronic structure analysis revealed that Mn incorporation effectively modulates the electronic distribution of Fe centers, lowering the d band center position. This electronic optimization enhances OH* desorption capability and increases the reaction limiting potential, thereby significantly improving both the activity and stability of the ORR. When employed as a cathode material in fuel cells, the catalyst demonstrates exceptional performance—achieving high power density in both anion exchange membrane and proton exchange membrane fuel cells while surpassing commercial Pt/C catalysts in durability and methanol tolerance (Fig. 17e), highlighting its strong potential for practical energy conversion devices. In a complementary approach, Bai et al. achieved substantial improvements in Fe–N–C catalyst stability through chemical vapor modification (Fig. 17f) [179]. This process transformed conventional FeN_4 sites into symmetric coordination structures containing both pyridinic and pyrrolic nitrogen atoms, while simultaneously enhancing carbon support graphitization, reducing structural defects, and establishing a more stable microenvironment that effectively suppresses Fe center displacement and structural collapse. Electrochemical evaluations (Fig. 17g) demonstrated that the modified catalyst exhibits accelerated reaction kinetics, reduced H_2O_2 yield ($< 2\%$), and higher electron transfer number, along with remarkable durability—showing only 10% performance decay over 250 h at 0.67 V compared to > 70% decay within 43 h for unmodified counterparts. Furthermore, it achieved a peak power density of 450 mW cm^{-2} in proton exchange membrane fuel cells, representing a significant advancement toward practical implementation.

Shi's research group developed an innovative acid–base coupled flow fuel cell (CF–FC) system that utilizes synergistic acidic ORR and alkaline hydrogen oxidation to harness additional electrical neutralization energy (Fig. 18a) [180]. Unlike conventional fuel cell configurations (Fig. 18b), this system employs acidic ORR at the cathode and alkaline hydrogen oxidation at the anode, separated by cation and anion exchange membranes to prevent direct neutralization while converting electrical neutralization energy into additional voltage output. This design increases the theoretical open-circuit voltage from 1.229 to 2.057 V. The team also designed a single-atom Fe–N–C catalyst with $Fe–N_4$ sites as the cathode material, demonstrating exceptional ORR activity and four-electron pathway selectivity. In practical CF–FC operation (Fig. 18c), the catalyst achieved an output voltage of 1.16 V at 50 mA cm^{-2} with 91% voltage retention over 110 h and a minimal decay rate of 0.9 mV h^{-1}, outperforming conventional membrane electrode assembly fuel cells and commercial Pt/C systems. The system maintained 83.5% of its initial performance through multiple charge–discharge cycles, with negligible Fe leaching, demonstrating excellent stability and practical potential. The battery module allows flexible power expansion through series, parallel, and hybrid configurations. In a separate development, Chen's team created a Mn–N–C ORR catalyst with high-density atomically dispersed Mn active sites using a combined ball milling and dual high-temperature pyrolysis approach (Fig. 18d) [181]. This method promotes the formation of MnN_4-rich sites and creates a distinctive axisymmetric dual MnN_4 structure. The resulting material features well-defined mesoporosity, high graphitization, and uniform manganese–nitrogen distribution, exhibiting the lowest reaction energy barrier and enhanced dissolution resistance crucial for ORR activity and durability. XPS analysis revealed the evolution of elemental chemical states during synthesis (Fig. 18e), confirming that the three-step strategy effectively establishes $Mn–N_x$ active sites while regulating carbon framework graphitization. The catalyst demonstrated exceptional ORR performance in both alkaline and acidic environments, achieving peak power densities of 649 mW cm^{-2} in proton exchange membrane fuel cells and 770 mW cm^{-2} in anion exchange membrane fuel

https://doi.org/10.1007/s40820-026-02197-6

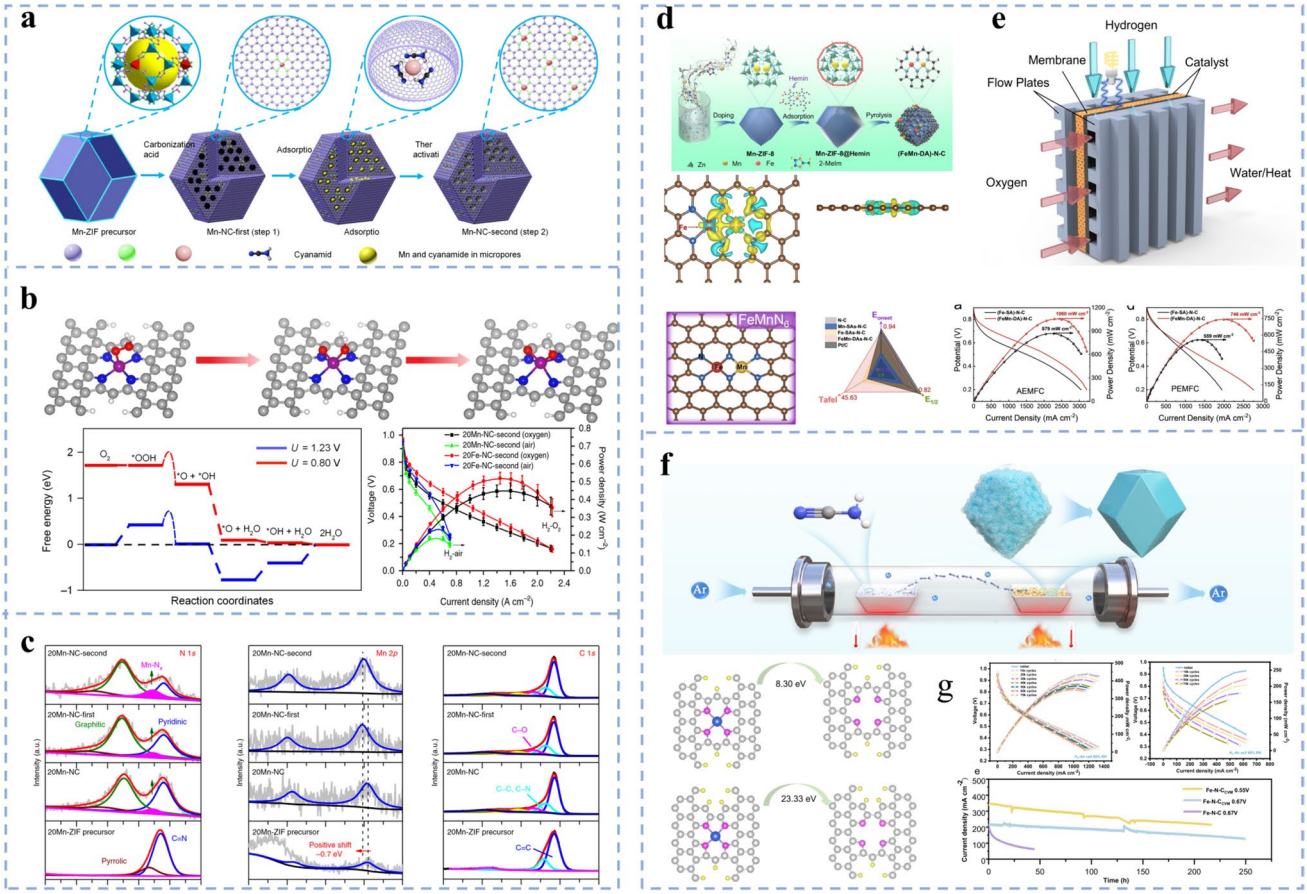

Fig. 17 **a** Flowchart of the construction of the MnN_4 active site catalyst with atomic-level distribution. **b** ORR free energy path of the MnN_4–Cl_2 site. **c** High-resolution XPS spectra of materials at different synthesis stages [177]. Copyright 2018, Springer Nature. **d** Synthesis path, electronic structure and three-dimensional radar map of FeMn co-doped N–C catalyst. **e** Schematic diagram of the application of the catalyst in proton exchange membrane fuel cells and anion exchange membrane fuel cells [178]. Copyright 2024, Springer Nature. **f** Schematic diagram of the synthesis of the Fe–N–CCVM catalyst and the S1-type FeN_4 site can be converted into a N_4C_{12} structure, while the FeN_2+N'$_2$ site evolves into a N_4C_{11} coordination environment. **g** Electrochemical test diagram of Fe–N–CCVM and the comparative material Fe–N–C [179]. Copyright 2024, Springer Nature

cells. Accelerated aging tests showed only 18.4% performance degradation after 30,000 cycles, significantly outperforming Fe–N–C materials prepared by the same method and demonstrating superior oxidative corrosion resistance and long-term stability.

In fuel cell systems, performance is primarily governed by three critical factors: the coordination structure of metal active centers, the microstructural configuration of carbon supports, and the overall stability of catalytic materials [182]. At the material design level, enhancing electron transfer kinetics, improving reaction selectivity, and strengthening corrosion resistance can be achieved through precise regulation of metal–ligand bonding environments, optimization of carbon support graphitization and conductivity, and rational design of pore structure distribution. From the perspective of atomic-level regulation, key strategies for achieving high catalytic efficiency and durability include constructing highly dispersed single-atom active sites, suppressing metal agglomeration and undesirable side reactions, and steering the ORR toward the efficient $4e^-$ pathway. On the device integration level, developing novel electrode architectures compatible with diverse electrolyte environments presents promising avenues for enhancing both power output and operational stability. The advancement of fuel cell technology fundamentally relies on continuous innovation in high-stability, cost-effective catalytic materials, coupled with coordinated optimization across multiple scales—including material synthesis, interface engineering,

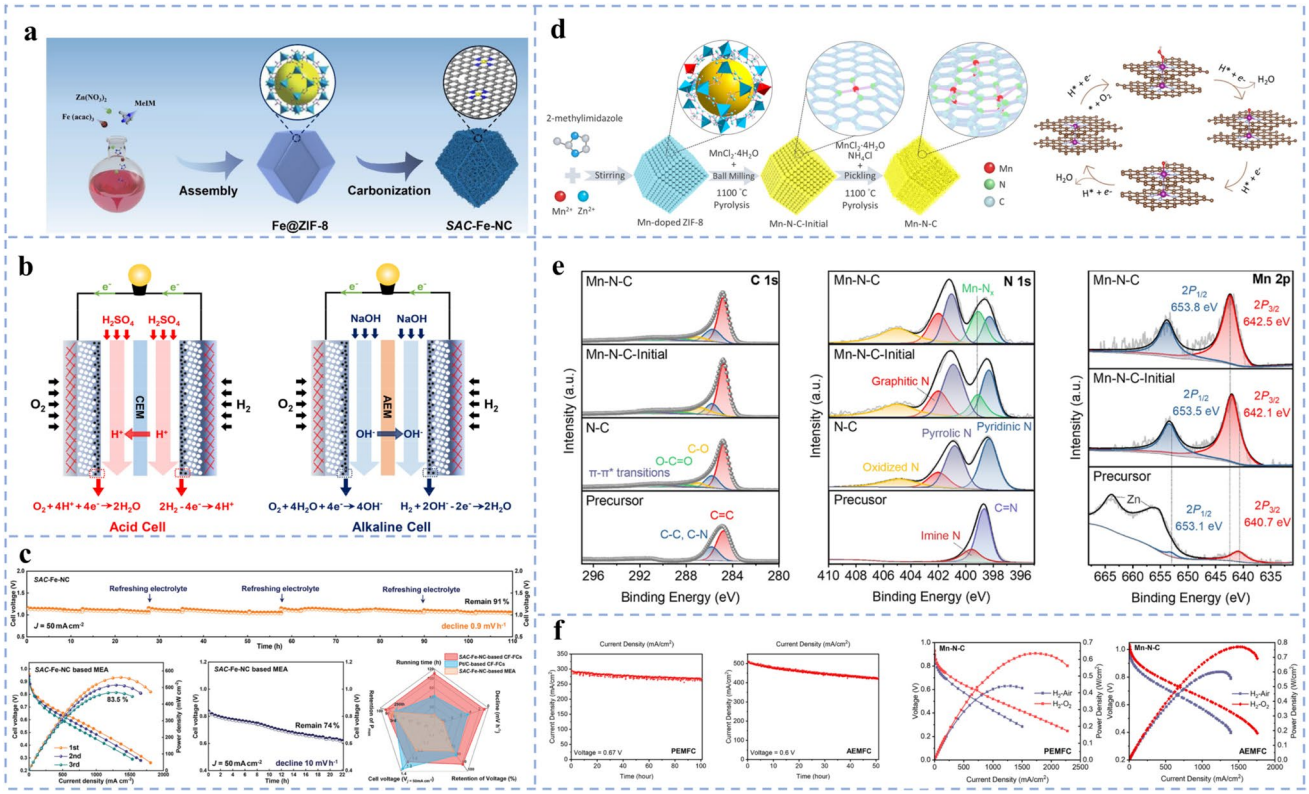

Fig. 18 **a** Schematic diagram of the synthesis of SAC–Fe–NC from Fe@ZIF-8 after carbonization. **b** Acidic and alkaline CF–FC battery structures. **c** Battery performance and comparison of SAC–Fe–NC catalysts [180]. Copyright 2024, Wiley–VCH. **d** Schematic diagram of the synthesis of Mn–N–C catalysts and the adsorption configuration of intermediates during the ORR process. **e** C 1*s*, N 1*s* and Mn 2*p* XPS spectra of samples at different stages. **f** Electrocatalytic performance of Mn–N–C–4.5 in proton exchange membrane fuel cells and anion exchange membrane fuel cells [181]. Copyright 2025, Wiley–VCH

and system integration—to ultimately realize efficient and sustainable energy conversion systems.

4.3 ORR Pathway Selectivity for Electrochemical H_2O_2 Production

In both fuel cells and metal–air batteries, the ORR ideally proceeds through the four-electron pathway to achieve complete reduction of O_2 to H_2O (or OH^-), ensuring high energy efficiency and device stability. However, the competing two-electron pathway that produces H_2O_2 is generally regarded as an undesired side reaction, as the generated peroxide species can lower energy output and corrode catalysts or carbon supports. Interestingly, this so-called undesired reaction in energy conversion devices can be advantageously harnessed in chemical synthesis [183]. The selective two-electron ORR pathway forms the electrochemical basis for sustainable H_2O_2 production, offering a green alternative to traditional anthraquinone processes. Therefore, transition metal-based heterogeneous catalysts that exhibit partial $2e^-$ selectivity in fuel cells or metal–air batteries can be repurposed as efficient catalysts for electrochemical H_2O_2 synthesis. This complementary relationship highlights how insights from energy conversion systems can guide the rational design of catalysts for selective oxygen reduction in chemical production.

Huang and colleagues successfully developed an efficient electrochemical system for synthesizing hydrogen peroxide in acidic media by constructing diatomic cobalt sites (Fig. 19a) [184]. The reaction mechanism was elucidated through schematic representation (Fig. 19b), demonstrating that the diatomic cobalt configuration significantly slows OOH* intermediate adsorption compared to conventional single-atom Co–N–C sites, thereby effectively inhibiting its further reduction to water. Electrochemical characterization (Fig. 19c) confirmed that the catalyst achieves over

 https://doi.org/10.1007/s40820-026-02197-6

95% H_2O_2 selectivity with a partial current density reaching 2.7 mA cm^{-2} in acidic electrolyte. When implemented in a flow electrolyzer, the system maintains high H_2O_2 production rate and stable operation over 100 h, substantially outperforming traditional Co–N–C catalysts. Subsequent investigations attribute this superior performance to the optimized electronic structure and reduced adsorption strength for oxygen intermediates enabled by the diatomic coordination environment.

Yang et al. [185] systematically investigated the photocatalytic synthesis of H_2O_2 using WO_3^-supported single-atom copper catalysts with controlled valence states. Their study compared the performance of WO_3, Cu(II)–SA/WO_3, and Cu(I)–SA/WO_3 under visible light irradiation, providing the first detailed mechanism of O_2 adsorption and activation at atomic Cu sites on WO_3 surfaces. The results demonstrate that Cu(I) sites formed under low loading conditions significantly enhance photocatalytic activity, achieving an H_2O_2 production rate of 102 μmol h^{-1}, 17.3 times higher than pristine WO_3 (Fig. 19d). The catalyst maintained stable performance over 7 h of continuous operation in a panel reactor with linear H_2O_2 accumulation, indicating promising scalability for practical applications. Through a series of in situ XANES and EXAFS analyses (Fig. 19e), the research elucidated the electronic structure evolution and local coordination environment changes of Cu(I) sites during the reaction. Under O_2 atmosphere with illumination, the average coordination bond length at Cu sites increased from 1.35 to 1.48 Å, confirming effective O_2 activation following photogenerated electron capture. At Cu(I) active centers, the hydrogenation process of the key OOH* intermediate transitioned from endothermic to exothermic, substantially reducing the reaction energy barrier and enhancing selectivity toward the $2e^-$ ORR pathway. This electronic optimization

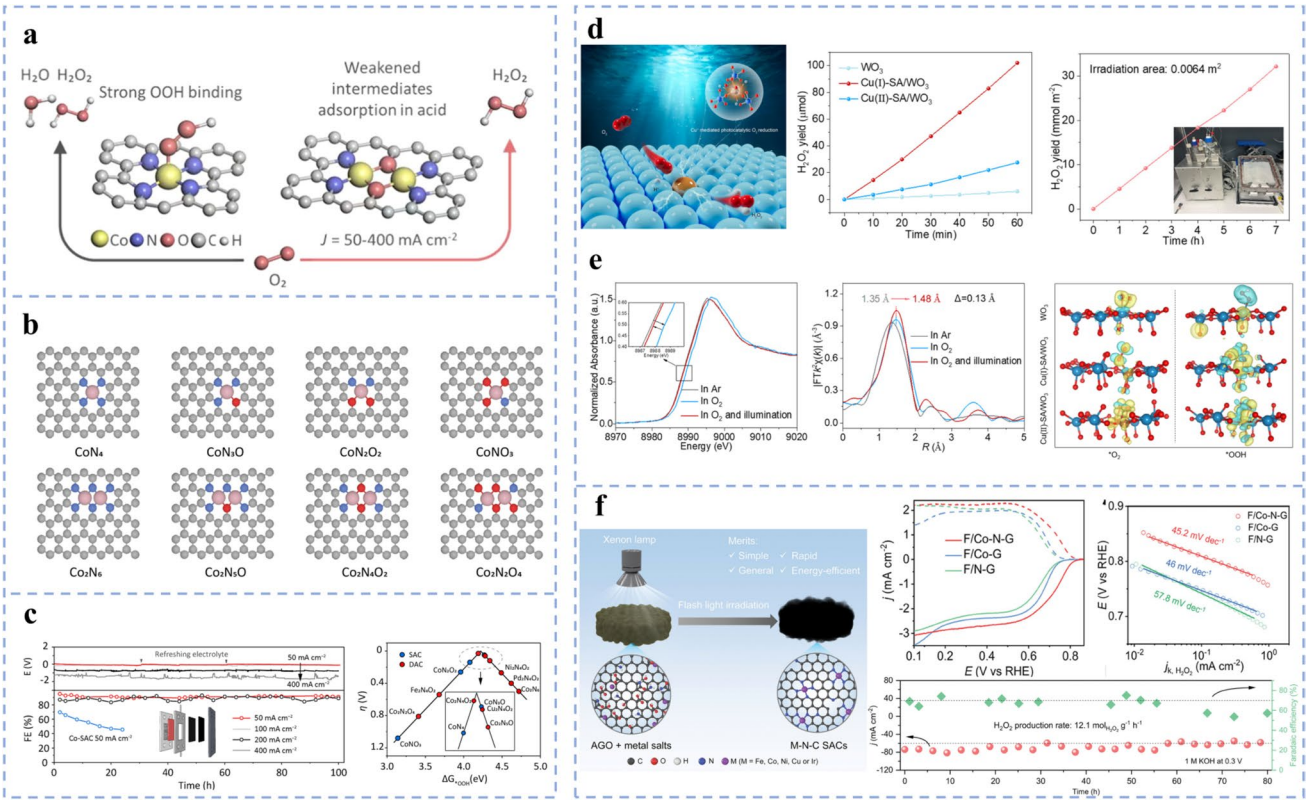

Fig. 19 **a** Co–N_x site achieves highly selective H_2O_2 reaction mechanism by regulating intermediate adsorption under acidic conditions. **b** Stability of the catalyst at different current densities and volcano plot analysis. **c** Various Co–N/O coordination structure models used for calculation [184]. Copyright 2024, American Chemical Society. **d** Schematic diagram of photocatalytic O_2 reduction promoted by Cu(I) single-atom and electrochemical test and actual reactor diagram. **e** In situ XANES and EXAFS spectra and the adsorption of intermediates on different catalyst surfaces and charge difference density maps during O_2 photoreduction [185]. Copyright 2025, American Chemical Society. **f** Schematic diagram of flash irradiation-assisted synthesis of F/M–N–G SACs and electrochemical tests [186]. Copyright 2024, Wiley–VCH

enabled an exceptional photon quantum efficiency of up to 30%, representing a significant advancement in overcoming the efficiency limitations of conventional catalytic H_2O_2 synthesis methods.

For fundamental metal–nitrogen–carbon (M–N–C) catalysts, extensive research has confirmed their significant catalytic activity and remarkable stability in the $2e^-$ ORR. These materials are typically synthesized by incorporating transition metal centers and coordinating nitrogen atoms within a carbon-based framework. Gong's team developed an efficient flash thermal-assisted strategy to rapidly achieve reduction, nitrogen doping, and metal atom anchoring at the atomic level, producing M–N–C single-atom catalysts such as Co–N_4 [186]. This method is simple, rapid, energy-efficient, and applicable to various metal precursors, demonstrating the versatility of different central metal atoms in the electrochemical synthesis of H_2O_2. Building on this foundation, the study further compared the polarization curves and Tafel slopes of different catalysts in O_2-saturated KOH electrolyte, all of which exhibited excellent ORR performance (Fig. 19f). This synthetic approach is equally applicable to the development of M–N–C single-atom catalysts based on other metals such as Fe, Ni, and Cu, demonstrating its universality and scalability while providing novel concepts and technical platforms for the green synthesis of H_2O_2 and the large-scale production of single-atom catalysts.

Transition metal-based heterogeneous electrocatalysis systems have demonstrated considerable potential for the electrocatalytic production of H_2O_2, though several challenges persist in achieving controlled selectivity, maintaining catalyst stability, and preventing compromised efficiency in industrial settings [187]. Recent research advances have addressed these limitations through innovative approaches including the construction of diatomic sites, introduction of π–d conjugated structures, and precise electronic structure optimization, collectively enhancing both catalytic activity and H_2O_2 selectivity. Concurrently, the adoption of rapid synthesis techniques such as photothermal methods has significantly improved preparation efficiency and material scalability. Future investigations should prioritize refined regulation of electronic structures and intermediate adsorption behaviors, enhancement of catalyst durability under acidic conditions and high current densities, and progression toward distributed, environmentally sustainable catalytic systems adaptable to diverse application scenarios (Table 1).

5 Summary and Outlook

5.1 Summary

This review systematically summarizes the research progress of transition metal-based heterogeneous catalysts in the ORR, with emphasis on structure-dependent reaction mechanisms, electronic structure regulation, and catalytic design strategies. By systematically comparing Fe, Mn, Ni, Co, Cu, and rare earth-based systems, it elucidates the crucial roles of different metal centers in coordination environments, *d* orbital modulation, adsorption energy matching, and reaction pathway selection ($2e^-/4e^-$). Furthermore, the review highlights the synergistic effects of single-atom, dual-atom, and heterogeneous interface structures in modulating charge distribution, enhancing electron transport, and optimizing intermediate adsorption. Integrating in situ characterization with theoretical simulations, it also summarizes the mechanistic advantages of emerging strategies such as multimetal synergistic regulation, defect engineering, and high-entropy structures for improving catalytic activity and structural stability, and outlines their application prospects in fuel cells, metal–air batteries, and electrochemical H_2O_2 synthesis.

Despite significant breakthroughs achieved by transition metal-based catalytic systems in ORR research, several critical challenges remain, including structural reconstruction and dissolution under strong acidic or alkaline conditions, unclear adsorption–desorption kinetics of key intermediates, and the difficulty in balancing high activity with long-term stability. Future research should focus on atomic-level electronic structure design and multimetal synergistic regulation to construct highly stable heterogeneous structures with interfacial charge coupling and strain modulation capabilities. Moreover, the integration of in situ/operando spectroscopy with multiscale simulations is essential to uncover real reaction pathways and the dynamic evolution of active sites. The synergistic advancement of material design, mechanistic understanding, and system optimization will provide theoretical foundations and technical guidance for developing the next generation of efficient, durable, and low-cost ORR electrocatalysts.

https://doi.org/10.1007/s40820-026-02197-6

Table 1 Performance comparison of representative ORR electrocatalysts

Types	Electrocatalyst	Electrolyte	Durability	Half-wave potential (vs. RHE) (V)	Tafel slope(m V dec^{-1})	H_2O_2 yield	References
Fe	Fe SAs–HP	0.1 M KOH	> 30k cycles; 97.3% (50k s)	0.94	84.0	< 5%	[114]
	Fe_1/DNC	0.1 M KOH	> 20 k cycles; 93% (50 h)	0.95	54.0	< 0.35%	[115]
	Fe_{SA}–Fe_{AC}/NC	0.1 M KOH	> 10 k cycles; 91% (10 h)	0.886	73	< 2%	[116]
	Fe–N–C_{NH4I}	0.1 M KOH	> 20 k cycles; 96.7% (11 h)	0.924	52.1	< 1%	[117]
	N–FeN_4	0.1 M KOH	100% (50 h)	0.91	64.9	< 1%	[118]
	FeNb/c-SNC	0.1 M KOH	> 5k cycles;	0.922	52	< 0.5%	[119]
	HEAC/Fe–NC	0.1 M KOH	> 20k cycles; 89% (40k s)	0.927	86	< 4%	[120]
	Fe–Mn DAC/N–C	0.1 M KOH	> 10k cycles; 93% (40 h)	0.91	58	< 3%	[178]
	Fe–N_4–CVM	0.1 M $HClO_4$	> 30k cycles; 92% (100 h)	0.82	75	< 2%	[179]
	SAC–Fe–NC	0.5 M H_2SO_4	91% (110 h)	0.794	57.5	< 2%	[180]
Mn	Mn–pr–N–CG	0.5 M H_2SO_4	95% (20 h)	0.896	43.6	< 5%	[125]
	MnY–NC	0.1 M KOH	> 10k cycles; 100% (30 h)	0.93	58	< 3%	[126]
	MoP@Mn_{SAC}–NC	0.1 M KOH	> 1000 cycles; 98% (10 h)	0.894	67.1	< 9%	[128]
	Mn_{SA}/Mn_{AC}–SSCNR	0.1 M KOH	> 5k cycles; 91% (42 h)	0.90	49.2	< 5%	[129]
	Mn, Fe–HCNS	0.1 M KOH	> 10k cycles; 91% (48k s)	0.87	65	< 6.6%	[171]
	Mn–γ-Fe_2O_3	0.1 M KOH	> 10k cycles; ~ 90% (40 h)	0.86	68	< 10%	[172]
	Mn–N–C	0.5 M H_2SO_4	> 30k cycles; 88% (100 h)	0.80	80	< 2%	[177]
Ni	FeCoNiMnCrO	1.0 M KOH	> 20k cycles;	0.87	62	< 5%	[138]
	$Ni(OH)_2$/Pt	0.1 M $HClO_4$	> 15k cycles;	0.912	65.8	< 4%	[140]
	$Ni(OH)_2$–C_2O_4	0.1 M KOH	> 5k cycles; ~ 100% (20 h)	–	–	≈ 93%	[141]
	Ni–SAC/CNS	0.1 M KOH	100% (20 h)	–	79.5	≈ 89%	[137]
Co	$Co(CN)_3$–Cub	0.1 M KOH	> 10k cycles	0.90	57	< 5%	[151]
	CoPc/CB–Mag	0.1 M $HClO_4$	90% (100 h)	–	86	≈ 93%	[150]
	Co_2–DAC	0.1 M $HClO_4$	85%(100 h)	–	124	≈95%	[184]
	F/Co–N–G	0.1 M KOH	90% (20 h)	–	45.2	≈90%	[186]
Cu	Pt_1–CuO_x/Cu	0.1 M KOH	100% (100 h)	0.92	65	< 3%	[161]
	Cu–SA/SNC	0.1 M KOH	> 10k cycles	0.893	–	< 5%	[158]
	Cu–N–C	0.1 M KOH	> 10k cycles; 100% (50k s)	0.89	63	< 5%	[173]
	Cu/Fe–N–C	0.1 M KOH	> 5k cycles; 95% (50k s)	0.89	69.4	< 1.77%	[174]
Other	$SmPO_4$	0.1 M KOH	> 5k cycles; 90% (12 h)	–	–	≈ 96%	[163]
	$LaPO_4$	0.1 M KOH	> 5k cycles; 90% (12 h)	–	–	≈ 94%	[163]
	$GdPO_4$	0.1 M KOH	> 5k cycles; 90% (12 h)	–	–	≈ 92%	[163]
	La–Cl SAs/NHPC	0.1 M KOH	> 6k cycles; 94.8% (30 h)	0.91	50.4·	< 4%	[164]
	FePc/Eu_2O_3	0.1 M KOH	> 20k cycles; 98.2% (100k s)	0.931	56.5·	< 3%	[165]
	Re–SAC	0.1 M KOH	> 10k cycles	0.89	72·	< 5%	[166]

5.2 Outlook

Future research on the oxygen reduction reaction is expected to progress from atomic-level regulation toward multidimensional, system-level engineering, in which activity, selectivity, and durability must be optimized simultaneously. Beyond static electronic structure descriptors, it is essential to elucidate how coordination environments, charge distribution, and intermediate adsorption evolve dynamically under operating conditions, particularly in acidic media and at high current densities. Under such extreme conditions, structural reconstruction, metal dissolution, and site aggregation remain critical challenges for transition metal heterostructures, especially those based on single-atom and dual-atom motifs. Addressing these issues requires mechanistic understanding of active site stability and adaptability under strong interfacial electric fields, continuous redox cycling,

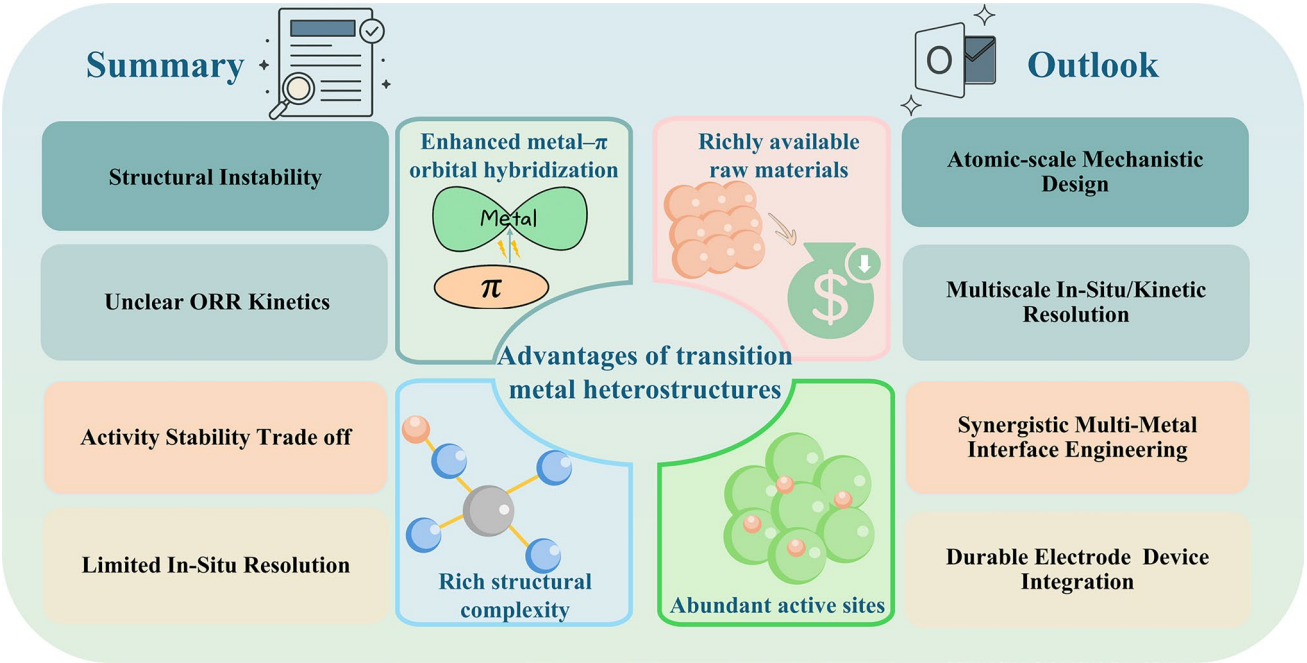

Fig. 20 Challenges and prospects of ORR in heterogeneous transition metal materials

and intense mass transport, rather than treating stability as an intrinsic materials property.

Selective regulation of two-electron versus four-electron ORR pathways represent another key frontier, especially for hydrogen peroxide electrosynthesis. Future advances will likely rely on multifield coupled control strategies, in which coordination asymmetry, interfacial electric fields, solvation structures, and spin-related effects collectively reshape reaction pathway branching. In this context, the increasing complexity of heterogeneous design highlights the need for data-driven and machine learning-assisted approaches to explore high-dimensional structure–property–kinetics relationships. From a translational perspective, bridging the gap between atomic-level precision and industrial implementation will further require synthesis strategies compatible with high-throughput processing, structural reproducibility, and cost constraints, together with electrode architectures that integrate catalyst stability with efficient mass and charge transport. Overall, future progress in ORR catalysis will depend on the co-development of mechanistic insight, scalable materials design, and device-level integration, enabling the transition from laboratory demonstrations to practical clean energy technologies (Fig. 20).

Acknowledgements This work was funded by the Henan Provincial Natural Science Fund for Outstanding Youth (252300421185); the International Postdoctoral Exchange Fellowship Program (YJ20220090); the Key Research Project Plan for Higher Education Institutions in Henan Province No.24A430011; the Natural Science Foundation of Henan (Grant No. 252300420424); and the Natural Science Foundation of Inner Mongolia Autonomous Region (2024QN02014).

Author Contributions Mingyu Sun and Xiayan Zhang contributed to the literature collection, initial draft writing, and figure preparation. Mingyu Sun participated in literature analysis and draft editing. Xiayan Zhang, Jinhai He, Shengwei Kong, Guoqing Zhang, and Mai Gao assisted with literature management and manuscript organization. Jialu Liu engaged in conceptual discussions and manuscript editing. Jia Wang contributed to conceptual development, project oversight, and substantive manuscript revisions. Jingqiang Wang, Zixu Sun, Yaping Yan, Xinjian Shi, and Yao Xiao were responsible for overall supervision, funding acquisition, project management, literature analysis, structural optimization, and key manuscript revisions.

Declarations

Conflicts of interest The authors declare no conflict of interest. They have no known competing financial interests or personal relationships that could have influenced the work reported in this paper.

References

1. D.M. Harraz, K.M. Lodaya, B.Y. Tang, Y Surendranath, Homogeneous-heterogeneous bifunctionality in Pd-catalyzed vinyl acetate synthesis. Science **388**(6742), eads7913 (2025). https://doi.org/10.1126/science.ads7913
2. M. Luo, Z. Zhao, Y. Zhang, Y. Sun, Y. Xing et al., PdMo bimetallene for oxygen reduction catalysis. Nature **574**(7776), 81–85 (2019). https://doi.org/10.1038/s41586-019-1603-7
3. Y. Yan, S. Xu, H. Li, N.C.S. Selvam, J.Y. Lee et al., Perpendicularly anchored $ReSe_2$ nanoflakes on reduced graphene oxide support for highly efficient hydrogen evolution reactions. Chem. Eng. J. **405**, 126728 (2021). https://doi.org/10.1016/j.cej.2020.126728
4. R. Chattot, O. Le Bacq, V. Beermann, S. Kühl, J. Herranz et al., Surface distortion as a unifying concept and descriptor in oxygen reduction reaction electrocatalysis. Nat. Mater. **17**(9), 827–833 (2018). https://doi.org/10.1038/s41563-018-0133-2
5. S. Dey, B. Mondal, S. Chatterjee, A. Rana, S. Amanullah et al., Molecular electrocatalysts for the oxygen reduction reaction. Nat. Rev. Chem. **1**(12), 98 (2017). https://doi.org/10.1038/s41570-017-0098
6. T. Fukushima, W. Drisdell, J. Yano, Y. Surendranath, Graphite-conjugated pyrazines as molecularly tunable heterogeneous electrocatalysts. J. Am. Chem. Soc. **137**(34), 10926–10929 (2015). https://doi.org/10.1021/jacs.5b06737
7. A.A. Gewirth, J.A. Varnell, A.M. DiAscro, Nonprecious metal catalysts for oxygen reduction in heterogeneous aqueous systems. Chem. Rev. **118**(5), 2313–2339 (2018). https://doi.org/10.1021/acs.chemrev.7b00335
8. J. Hong, L. Zhang, Q. Zhu, Z. Du, Y. Zhou et al., A macroporous carbon nanoframe for hosting Mott–Schottky Fe–Co/Mo_2C sites as an outstanding bi-functional oxygen electrocatalyst. Mater. Horiz. **10**(12), 5969–5982 (2023). https://doi.org/10.1039/D3MH01237A
9. J. Wang, M. Sun, X. Zhang, J. Liu, J. He et al., pH-dependent urea electrooxidation: from mechanism to catalysts and applications. Adv. Mater. **38**(4), e15043 (2026). https://doi.org/10.1002/adma.202515043
10. Z. Hou, C. Cui, Y. Yang, Z. Huang, Y. Zhuang et al., Strong metal-support interactions in heterogeneous oxygen electrocatalysis. Small **20**(52), 2407167 (2024). https://doi.org/10.1002/smll.202407167
11. C. Hu, G. Xing, W. Han, Y. Hao, C. Zhang et al., Inhibiting demetalation of Fe-N-C *via* Mn sites for efficient oxygen reduction reaction in zinc-air batteries. Adv. Mater. **36**(32), 2405763 (2024). https://doi.org/10.1002/adma.202405763
12. J.J. Huang, Y. Yang, D. Weinstock, C.R. Bundschu, Q. Li et al., Multimodal *in situ* X-ray mechanistic studies of a bimetallic oxide electrocatalyst in alkaline media. Nat. Catal. **8**(2), 116–125 (2025). https://doi.org/10.1038/s41929-025-01289-7
13. B. Ji, J. Gou, Y. Zheng, X. Pu, Y. Wang et al., Coordination chemistry of large-sized yttrium single-atom catalysts for oxygen reduction reaction. Adv. Mater. **35**(24), 2300381 (2023). https://doi.org/10.1002/adma.202300381
14. N. Kuwamura, T. Konno, Heterometallic coordination polymers as heterogeneous electrocatalysts. Inorg. Chem. Front. **8**(10), 2634–2649 (2021). https://doi.org/10.1039/d1qi00112d
15. Y. Li, H.-R. Wu, Y. Yu, M.-Y. Chen, K.-M. Zhao et al., High-shell sulfur doping enhances Mn-N4 spin states and boosts oxygen reduction reaction performance in both acidic and alkaline media. Small **21**(11), 2411678 (2025). https://doi.org/10.1002/smll.202411678
16. Y. Pei, D.P. Wilkinson, E. Gyenge, Insights into the electrochemical behavior of manganese oxides as catalysts for the oxygen reduction and evolution reactions: monometallic core-shell Mn/Mn_3O_4. Small **19**(19), 2204585 (2023). https://doi.org/10.1002/smll.202204585
17. S.C. Perry, D. Pangotra, L. Vieira, L.-I. Csepei, V. Sieber et al., Electrochemical synthesis of hydrogen peroxide from water and oxygen. Nat. Rev. Chem. **3**(7), 442–458 (2019). https://doi.org/10.1038/s41570-019-0110-6
18. F.N.I. Sari, Y.-C. Lai, Y.-J. Huang, X.-Y. Wei, H. Pourzolfaghar et al., Electronic structure engineering in NiFe sulfide *via* a third metal doping as efficient bifunctional OER/ORR electrocatalyst for rechargeable zinc-air battery. Adv. Funct. Mater. **34**(21), 2310181 (2024). https://doi.org/10.1002/adfm.202310181
19. T. Sharifi, E. Gracia-Espino, A. Chen, G. Hu, T. Wågberg, Oxygen reduction reactions on single-or few-atom discrete active sites for heterogeneous catalysis. Adv. Energy Mater. **10**(11), 1902084 (2020). https://doi.org/10.1002/aenm.201902084
20. J. Song, Z.-X. Qian, J. Yang, X.-M. Lin, Q. Xu et al., In situ/operando investigation for heterogeneous electro-catalysts: from model catalysts to state-of-the-art catalysts. ACS Energy Lett. **9**(9), 4414–4440 (2024). https://doi.org/10.1021/acsenergylett.4c01488
21. D.-W. Wang, D. Su, Heterogeneous nanocarbon materials for oxygen reduction reaction. Energy Environ. Sci. **7**(2), 576 (2014). https://doi.org/10.1039/c3ee43463j
22. X. Wang, N. Zhang, H. Shang, H. Duan, Z. Sun et al., Precisely designing asymmetrical selenium-based dual-atom sites for efficient oxygen reduction. Nat. Commun. **16**(1), 470 (2025). https://doi.org/10.1038/s41467-025-55862-6
23. H. Tian, A. Song, H. Tian, J. Liu, G. Shao et al., Single-atom catalysts for high-energy rechargeable batteries. Chem. Sci. **12**(22), 7656–7676 (2021). https://doi.org/10.1039/d1sc00716e
24. Y. Wang, G.I.N. Waterhouse, L. Shang, T. Zhang, Electrocatalytic oxygen reduction to hydrogen peroxide: from

homogeneous to heterogeneous electrocatalysis. Adv. Energy Mater. **11**(15), 2003323 (2021). https://doi.org/10.1002/aenm.202003323

25. L.-H. Xu, Q. Wang, L. Hu, D. Shen, S. Chu et al., Engineering asymmetric bimetallic CoM (M = Ni, Fe, Mn, Cu) nanoparticles encapsulated in freestanding wood-derived carbon electrodes for enhanced ORR kinetics in zinc-air batteries. Small **21**(5), e2410290 (2025). https://doi.org/10.1002/smll.202410290
26. Y. Yan, R. Yu, M. Liu, Z. Qu, J. Yang et al., General synthesis of neighboring dual-atomic sites with a specific pre-designed distance *via* an interfacial-fixing strategy. Nat. Commun. **16**(1), 334 (2025). https://doi.org/10.1038/s41467-024-55630-y
27. H. Yang, N. An, Z. Kang, P.W. Menezes, Z. Chen, Understanding advanced transition metal-based two electron oxygen reduction electrocatalysts from the perspective of phase engineering. Adv. Mater. **36**(25), 2400140 (2024). https://doi.org/10.1002/adma.202400140
28. S. Yang, X. Liu, S. Li, W. Yuan, L. Yang et al., The mechanism of water oxidation using transition metal-based heterogeneous electrocatalysts. Chem. Soc. Rev. **53**(11), 5593–5625 (2024). https://doi.org/10.1039/d3cs01031g
29. Z. Jiang, X. Yang, J. Zhang, J. Yang, B. Sun et al., From conventional two-electron to emerging multi-electron zinc-iodine batteries: advantages, challenges, and future perspectives. Adv. Funct. Mater. **35**(50), e11754 (2025). https://doi.org/10.1002/adfm.202511754
30. H. Zhang, H.-C. Chen, S. Feizpoor, L. Li, X. Zhang et al., Tailoring oxygen reduction reaction kinetics of Fe-N-C catalyst *via* spin manipulation for efficient zinc-air batteries. Adv. Mater. **36**(25), e2400523 (2024). https://doi.org/10.1002/adma.202400523
31. H. Tian, Y. Lei, B. Sun, C.-C. Yang, C.-L. Chen et al.,P-d orbital hybridization induced by transition metal atom sites for room temperature sodium sulfur batteries. Natl. Sci. Rev. **12**(7), nwaf241 (2025). https://doi.org/10.1093/nsr/nwaf241
32. Z. Ma, A. Song, Z. Liu, Y. Guo, X. Yang et al., Nanoconfined expansion behavior of hollow MnS@Carbon anode with extended lithiation cyclic stability. Adv. Funct. Mater. **33**(28), 2301112 (2023). https://doi.org/10.1002/adfm.202301112
33. S. Zhao, Y. Yang, Z. Tang, Insight into structural evolution, active sites, and stability of heterogeneous electrocatalysts. Angew. Chem. Int. Ed. **61**(11), e202110186 (2022). https://doi.org/10.1002/anie.202110186
34. X. Zhao, Z.H. Levell, S. Yu, Y. Liu, Atomistic understanding of two-dimensional electrocatalysts from first principles. Chem. Rev. **122**(12), 10675–10709 (2022). https://doi.org/10.1021/acs.chemrev.1c00981
35. J. Zheng, D. Meng, J. Guo, X. Liu, L. Zhou et al., Defect engineering for enhanced electrocatalytic oxygen reaction on transition metal oxides: the role of metal defects. Adv. Mater. **36**(28), 2405129 (2024). https://doi.org/10.1002/adma.202405129
36. H.-X. Zhong, Y. Zhang, X.-B. Zhang, Superior oxygen reduction electrocatalyst: hollow porous spinel microsphere. Chem **4**(2), 196–198 (2018). https://doi.org/10.1016/j.chempr.2018.01.015
37. B. Zhou, N. Xu, T. Lu, Y. Wang, S. Lou et al., Dual-carbon assisted oxygen vacancy engineering for optimizing Mn(III) sites to enhance Zn–air battery performances. Adv. Funct. Mater. **35**(4), 2414269 (2025). https://doi.org/10.1002/adfm.202414269
38. H. Zhou, H. Liu, Y. Sun, L. Jiang, J. Xiao et al., Synergistic effect of single atomic Ce sites and CeO_2 nanoparticles for boosting oxygen reduction reaction. Adv. Energy Mater. **15**(14), 2404689 (2025). https://doi.org/10.1002/aenm.202404689
39. M. Zhou, J. Guo, R. Lu, J. Li, S. Lee et al., Amorphous metal metaphosphate for oxygen reduction. Interdiscip. Mater. **4**(2), 309–320 (2025). https://doi.org/10.1002/idm2.12228
40. X. Zou, Q. Lu, J. Wu, K. Zhang, M. Tang et al., Screening spinel oxide supports for RuO_2 to boost bifunctional electrocatalysts for advanced Zn–air batteries. Adv. Funct. Mater. **34**(36), 2401134 (2024). https://doi.org/10.1002/adfm.202401134
41. G. Gao, Z. Sun, X. Chen, Z. Guang, B. Sun et al., Recent advances in hydrogen production coupled with alternative oxidation reactions. Coord. Chem. Rev. **509**, 215777 (2024). https://doi.org/10.1016/j.ccr.2024.215777
42. G. Gao, C. Xiao, R. Zhang, W. Chen, C. Liu et al., ZIF-67 derivatives in electrocatalysis. Coord. Chem. Rev. **523**, 216296 (2025). https://doi.org/10.1016/j.ccr.2024.216296
43. G. Gao, G. Zhao, G. Zhu, B. Sun, Z. Sun et al., Recent advancements in noble-metal electrocatalysts for alkaline hydrogen evolution reaction. Chin. Chemical Lett. **36**(1), 109557 (2025). https://doi.org/10.1016/j.cclet.2024.109557
44. X. Zhang, J. Lu, J. Liu, M. Sun, G. Zhang et al., Curvature geometry-spin electronics-catalytic dynamics coupling in emerging catalytic engineering. Chem. Soc. Rev. **55**(5), 2691–2730 (2026). https://doi.org/10.1039/d5cs01114k
45. Q. Huang, F. Wang, Z. Sun, B. Zhang, W. Li et al., *In situ* growth and dynamic transformation of nickel chelate nanoarrays into reactive surface reconstituted heterostructure for overall water splitting. Adv. Funct. Mater. **34**(46), 2407407 (2024). https://doi.org/10.1002/adfm.202407407
46. L. Shang, Y. Ni, Y. Wang, W. Yang, L. Wang et al., Single-nanometer spinel with precise cation distribution for enhanced oxygen reduction. Adv. Mater. **36**(50), e2413141 (2024). https://doi.org/10.1002/adma.202413141
47. H. Tian, H. Tian, S. Wang, S. Chen, F. Zhang et al., High-power lithium-selenium batteries enabled by atomic cobalt electrocatalyst in hollow carbon cathode. Nat. Commun. **11**(1), 5025 (2020). https://doi.org/10.1038/s41467-020-18820-y
48. X. Zhang, Z. Song, B. Liu, B. Liu, J. Liu et al., The interfacial charge change enhanced by $Pr_{0.6}$ $Sm_{0.4}$ $Co_{0.8}$ $Mn_{0.2}O_3$ activated peroxymonosulfate was used for the efficient degradation of tetracycline under the nanoscale domain limiting and distance effect. Mater. Today Sustain. **28**, 101044 (2024). https://doi.org/10.1016/j.mtsust.2024.101044
49. X. Zhang, Z. Song, B. Liu, J. Liu, Y. Huang et al., Ni/Fe bimetallic atom cluster activate PMS to promote $^1O_2$ production to

 https://doi.org/10.1007/s40820-026-02197-6

efficiently remove BPA. ChemistrySelect **9**(8), e202303088 (2024). https://doi.org/10.1002/slct.202303088

50. Y. Yan, M. Wu, L. Zhou, W. Chen, L. Han et al., Enhancing electrocatalytic activity through targeted local electrolyte micro-environment. Adv. Funct. Mater. **35**(19), 2419328 (2025). https://doi.org/10.1002/adfm.202419328
51. S. Kong, J. Liu, X. Zhang, J. He, G. Zhang et al., Bridging organic and inorganic domains: advances and applications of hybrid materials in electrocatalysis. Adv. Energy Mater. **16**(5), e05010 (2026). https://doi.org/10.1002/aenm.202505010
52. Z. Song, X. Zhang, B. Liu, J. Liu, Y. Huang et al., Highly active Ni atomic clusters loaded with coal gasification slag derivatives effectively remove tetracycline by activating persulfate to enhance electron transfer ability. J. Water Process Eng. **66**, 105982 (2024). https://doi.org/10.1016/j.jwpe.2024.105982
53. X. Shi, Y. Jiang, B. Zeng, Z. Sun, M. Yun et al., *In situ* electrochemical production of solid peroxide from urine. Nat. Catal. **8**(1), 67–78 (2025). https://doi.org/10.1038/s41929-024-01277-3
54. J. Liu, Z. Song, B. Liu, X. Zhang, Y. Huang et al., Bimetallic Ni/Fe atom cluster catalysts enhance non-free radical degradation of organic pollutant phenol. Catal. Lett. **154**(5), 2182–2196 (2024). https://doi.org/10.1007/s10562-023-04472-2
55. J. Liu, Y. Huang, X. Song, Z. Song, X. Zhang et al., Ni-Co synergistic regulation of catalyst surface charge density for efficient DNA base degradation in water. J. Water Process. Eng. **71**, 107313 (2025). https://doi.org/10.1016/j.jwpe.2025.107313
56. G. Zhang, X. Zhang, J. Liu, J. He, W. Ge et al., Transition metal-based electrocatalysts for CO_2 reduction towards ethanol. Coord. Chem. Rev. **550**, 217403 (2026). https://doi.org/10.1016/j.ccr.2025.217403
57. C. Li, Y. Yang, J. Lu, L. Ren, X. Zhang et al., Micro-Cu doped Co_3O_4 as an effective oxygen reduction nano-flower-like catalyst to enhance the power output of air cathode microbial fuel cell. Catal. Lett. **154**(11), 6080–6093 (2024). https://doi.org/10.1007/s10562-024-04779-8
58. Y. Huang, Z. Song, B. Liu, X. Zhang, J. Liu et al., Highly active Co is injected into the $PrSmMnO_3$ parent structure to promote the $^1O_2$ pathway to efficiently degrade residual chloroquine phosphate in wastewater. Catal. Lett. **155**(1), 3 (2024). https://doi.org/10.1007/s10562-024-04844-2
59. M. Du, B. Chu, Q. Wang, C. Li, Y. Lu et al., Dual Fe/I single-atom electrocatalyst for high-performance oxygen reduction and wide-temperature quasi-solid-state Zn-air batteries. Adv. Mater. **36**(47), 2412978 (2024). https://doi.org/10.1002/adma.202412978
60. J. Zhang, Y. Mou, W. Suo, S. Yang, J. Shen et al., Single-atomic Co-N-C sites anchored on helical carbonaceous nanotubes for the oxygen reduction reaction. Adv. Funct. Mater. **35**(12), 2417621 (2025). https://doi.org/10.1002/adfm.202417621
61. C. Brea, G. Hu, Dual-atom catalysts for the oxygen reduction reaction: unraveling atomic structures under reaction conditions. J. Am. Chem. Soc. **147**(22), 19210–19216 (2025). https://doi.org/10.1021/jacs.5c04776
62. Y. Cao, Y. Liu, X. Zheng, J. Yang, H. Wang et al., Quantifying asymmetric coordination to correlate with oxygen reduction activity in Fe-based single-atom catalysts. Angew. Chem. Int. Ed. **64**(14), e202423556 (2025). https://doi.org/10.1002/anie.202423556
63. X. Cui, R. Jin, L. Gao, M. Wu, Y. Liu et al., High-loading single atoms *via* hierarchically porous nanospheres for oxygen reduction reaction with superior activity and durability. Adv. Funct. Mater. **35**(39), 2510108 (2025). https://doi.org/10.1002/adfm.202510108
64. M. Dan, X. Zhang, C. Du, Z. Guo, J. Zhang et al., Atomically dispersed Fe confined into MnO nanoclusters enhances alkaline oxygen reduction activity and stability. Angew. Chem. Int. Ed. **64**(29), e202501531 (2025). https://doi.org/10.1002/anie.202501531
65. M. Deng, D. Wang, Y. Li, General design concept of high-performance single-atom-site catalysts for H_2O_2 electrosynthesis. Adv. Mater. **36**(24), e2314340 (2024). https://doi.org/10.1002/adma.202314340
66. H. Huang, M. Sun, K. Chen, Y. Che, X. Tang et al., Unlocking the potential of Mn-based catalyst for durable two-electron oxygen reduction in acid at high current densities. Angew. Chem. Int. Ed. **64**(33), e202511844 (2025). https://doi.org/10.1002/anie.202511844
67. S.-M. Jung, S. Kim, J. An, K.-S. Kim, M. Kim et al., Synergistic effects of Co–N_4 and Ni–N_4 sites in 2D conductive metal–organic framework electrocatalysts for enhanced oxygen reduction reaction performance. ACS Catal. **15**(7), 5568–5576 (2025). https://doi.org/10.1021/acscatal.4c05773
68. S. Lin, J. Wang, J. Chen, P. Lin, H. Wang et al., Electrochemical pilot H_2O_2 production by solid-state electrolyte reactor: insights from a hybrid catalyst for 2-electron oxygen reduction reaction. Angew. Chem. Int. Ed. **64**(19), e202502144 (2025). https://doi.org/10.1002/anie.202502144
69. C. Liu, W. Shi, Y. Yuan, K. Zhu, Q. Zhang et al., Cascade hydrogen peroxide reduction reaction endows Cu-Fe dual-atom catalyst with durable oxygen reduction performance. Adv. Funct. Mater. **35**(35), 2503079 (2025). https://doi.org/10.1002/adfm.202503079
70. C. Liu, R. Yang, J. Wang, B. Liu, X. Chang et al., Synergistic catalysts with Fe single atoms and Fe3C clusters for accelerated oxygen adsorption kinetics in oxygen reduction reaction. Angew. Chem. Int. Ed. **64**(21), e202501266 (2025). https://doi.org/10.1002/anie.202501266
71. L. Liu, F. Chen, H. Yang, X. Yan, J. Ren et al., Asymmetric coordination strategy of Cu single-atom catalyst for robust all-pH oxygen reduction reaction. Small **21**(32), e2503745 (2025). https://doi.org/10.1002/smll.202503745
72. M. Liu, Y. Li, L. Yang, P. Zhao, J. Li et al., Defect-triggered orbital hybridization in FeMn dual-atom catalysts toward Sabatier-optimized oxygen reduction. Angew. Chem. Int. Ed. **64**(28), e202505268 (2025). https://doi.org/10.1002/anie.202505268

73. S. Liu, Q. Meyer, D. Xu, Y. Cheng, L. Osmieri et al., Breaking the activity and stability trade-off of platinum-free catalysts for the oxygen reduction reaction in hydrogen fuel cells. ACS Nano **19**(21), 19524–19551 (2025). https://doi.org/10.1021/acsnano.5c03610
74. Y. Liu, Y. Yang, X. Lin, Y. Lin, Z. Zhuo et al., The geometric-electronic coupled design of diatomic catalyst towards oxygen reduction reaction. Nat. Commun. **16**(1), 5158 (2025). https://doi.org/10.1038/s41467-025-60170-0
75. X. Lu, F. Xiang, S. Li, W. Liu, Y. Zeng et al., Hydrogen-bond-assisted synthesis of single-atom and nanocluster synergistic sites for enhanced oxygen reduction reaction. Adv. Funct. Mater. **35**(40), 2506982 (2025). https://doi.org/10.1002/adfm.202506982
76. Q. Ma, Y. Liao, Q. Zhao, R. Gan, Y. Ran et al., Triggering synergistic electronic effect *via* electron-directed transfer within PtNPs-Fe/NC oxygen reduction catalyst for zinc-air batteries. Small **21**(14), 2500344 (2025). https://doi.org/10.1002/smll.202500344
77. D. Shen, F. Sun, Z. Liang, H. Fu, L. Wang, Axial-N induced square-pyramidal crystal filed of atomically iron sites for enhancing acidic oxygen reduction. Angew. Chem. Int. Ed. **64**(33), e202505937 (2025). https://doi.org/10.1002/anie.202505937
78. Z. Wan, Z. Ma, X. Deng, Y. Wu, J. Li et al., Weakening the dissociation barrier of hydroxyl in Fe–N–C catalysts *via* precisely manipulating d–p orbital hybridization behaviors for efficient oxygen reduction reaction. Adv. Energy Mater. **15**(31), 2501630 (2025). https://doi.org/10.1002/aenm.202501630
79. P. Wang, Y. Xu, Y. Li, P. Xie, H. Li et al., Engineering active CeO_2/Fe_3C interfacial sites to generate high-charge-density Fe for enhanced oxygen reduction reaction efficiency. Adv. Funct. Mater. **35**(43), 2503577 (2025). https://doi.org/10.1002/adfm.202503577
80. H. Tian, A. Song, P. Zhang, K. Sun, J. Wang et al., High durability of Fe–N–C single-atom catalysts with carbon vacancies toward the oxygen reduction reaction in alkaline media. Adv. Mater. **35**(14), 2210714 (2023). https://doi.org/10.1002/adma.202210714
81. B. Zhang, J. Dang, H. Li, J.-J. Wang, D. Xu et al., Orderly stacked "tile" architecture with single-atom iron boosts oxygen reduction in liquid and solid-state Zn–air batteries. Adv. Funct. Mater. **35**(34), 2502834 (2025). https://doi.org/10.1002/adfm.202502834
82. T. Zhang, W. Wang, W. Liu, Z. Guo, J. Liu, Residual ligand-functionalized ultrathin $Ni(OH)_2$ *via* reconstruction for high-rate HO_2^- electrosynthesis. Nat. Commun. **16**(1), 5240 (2025). https://doi.org/10.1038/s41467-025-60467-0
83. Z. Zhang, Z. Zheng, N. Ma, E. Picheau, N. Sakai et al., Composition tuning and heterostructure construction of Fe-doped Co-Ni hydroxide nanosheets for boosting oxygen electrocatalysis in rechargeable Zn-air batteries. Chem. Eng. J. **509**, 161248 (2025). https://doi.org/10.1016/j.cej.2025.161248
84. Y. Zhao, Z. Gao, S. Zhang, X. Guan, W. Xu et al., Asymmetric-charge-distributed Co-Mn diatomic catalyst enables efficient oxygen reduction reaction. Adv. Funct. Mater. **35**(37), 2504260 (2025). https://doi.org/10.1002/adfm.202504260
85. J. Zou, L. Bao, Q. Sun, C. Bao, H. Chen et al., Oxygen reduction reaction catalysts for zinc-air batteries featuring single cobalt atoms in a nitrogen-doped 3D-interconnected porous graphene framework. Small **21**(8), 2409506 (2025). https://doi.org/10.1002/smll.202409506
86. C. Brea, G. Hu, Mechanistic insight into dual-metal-site catalysts for the oxygen reduction reaction. ACS Catal. **13**(7), 4992–4999 (2023). https://doi.org/10.1021/acscatal.3c00090
87. X. Cao, H. Guo, Y. Han, M. Li, C. Shang et al., Sandwiching intermetallic Pt_3Fe and ionomer with porous N-doped carbon layers for oxygen reduction reaction. Nat. Commun. **16**(1), 2851 (2025). https://doi.org/10.1038/s41467-025-58116-7
88. T. He, Y. Chen, Q. Liu, B. Lu, X. Song et al., Theory-guided regulation of FeN_4 spin state by neighboring Cu atoms for enhanced oxygen reduction electrocatalysis in flexible metal–air batteries. Angew. Chem. Int. Ed. **61**(27), e202201007 (2022). https://doi.org/10.1002/anie.202201007
89. J. Huang, C. Yu, J. Li, W. Xiao, J.B. Zhong et al., Rare-earth lanthanum-nitrogen-carbon enhanced by abundant microspores for efficient oxygen reduction reaction. J. Energy Chem. **106**, 812–822 (2025). https://doi.org/10.1016/j.jechem.2025.02.021
90. M. Tong, F. Sun, Y. Xie, Y. Wang, Y. Yang et al., Operando cooperated catalytic mechanism of atomically dispersed $Cu-N_4$ and $Zn-N_4$ for promoting oxygen reduction reaction. Angew. Chem. Int. Ed. **60**(25), 14005–14012 (2021). https://doi.org/10.1002/anie.202102053
91. M. Zhang, H. Li, J. Chen, F.-X. Ma, L. Zhen et al., Transition metal (Co, Ni, Fe, Cu) single-atom catalysts anchored on 3D nitrogen-doped porous carbon nanosheets as efficient oxygen reduction electrocatalysts for Zn-air battery. Small **18**(34), e2202476 (2022). https://doi.org/10.1002/smll.202202476
92. L. Zong, K. Fan, P. Li, F. Lu, B. Li et al., Promoting oxygen reduction reaction on atomically dispersed Fe sites *via* establishing hydrogen bonding with the neighboring P atoms. Adv. Energy Mater. **13**(5), 2203611 (2023). https://doi.org/10.1002/aenm.202203611
93. R. Jinnouchi, K. Kodama, T. Hatanaka, Y. Morimoto, First principles based mean field model for oxygen reduction reaction. Phys. Chem. Chem. Phys. **13**(47), 21070 (2011). https://doi.org/10.1039/c1cp21349k
94. V. Viswanathan, H.A. Hansen, J. Rossmeisl, J.K. Nørskov, Unifying the $2e^-$ and $4e^-$ reduction of oxygen on metal surfaces. J. Phys. Chem. Lett. **3**(20), 2948–2951 (2012). https://doi.org/10.1021/jz301476w
95. H. Chen, Z. Gao, N.T. Nguyen, Z. Li, R.-T. Gao et al., Bias-free photoelectrochemical water oxidation coupled with electrochemical oxygen reduction reaction *via* Fe-based electrodes with long-term operation. Adv. Funct. Mater. **35**(14), 2418670 (2025). https://doi.org/10.1002/adfm.202418670
96. H. Liu, J. Huang, K. Feng, R. Xiong, S. Ma et al., Reconstructing the coordination environment of Fe/Co dual-atom sites towards efficient oxygen electrocatalysis for Zn–air batteries.

 https://doi.org/10.1007/s40820-026-02197-6

Angew. Chem. Int. Ed. **64**(7), e202419595 (2025). https://doi.org/10.1002/anie.202419595

97. S. Bhattacharyya, D. Samanta, S. Roy, V.P. Haveri Radhakantha, T.K. Maji, *In situ* stabilization of Au and co nanoparticles in a redox-active conjugated microporous polymer matrix: facile heterogeneous catalysis and electrocatalytic oxygen reduction reaction activity. ACS Appl. Mater. Interfaces **11**(5), 5455–5461 (2019). https://doi.org/10.1021/acsami.8b20610
98. V. Beermann, M. Gocyla, E. Willinger, S. Rudi, M. Heggen et al., Rh-doped Pt–Ni octahedral nanoparticles: understanding the correlation between elemental distribution, oxygen reduction reaction, and shape stability. Nano Lett. **16**(3), 1719–1725 (2016). https://doi.org/10.1021/acs.nanolett.5b04636
99. Y. Chen, J. Xu, P. He, Y. Qiao, S. Guo et al., Metal-air batteries: progress and perspective. Sci. Bull. **67**(23), 2449–2486 (2022). https://doi.org/10.1016/j.scib.2022.11.027
100. J. Sun, T. Tang, S. Zhang, S. Chen, Y. Duan et al., A dual-atom La_2 catalyst for the oxygen reduction reaction. Angew. Chem. Int. Ed. **64**(34), e202509063 (2025). https://doi.org/10.1002/anie.202509063
101. Y. Wang, J. Wu, Q. Zhang, Y. Tan, J. Gao et al., Defect-induced Zn–Co pair active site for high-efficiency electrosynthesis of H_2O_2. Matter **8**(12), 102479 (2025). https://doi.org/10.1016/j.matt.2025.102479
102. P.H. van Langevelde, K. Ležaić, J.F.J. Coelho, D.G.H. Hetterscheid, F. De Bon, Interplay between the oxygen reduction reaction and atom transfer radical polymerization with molecular Cu-based catalysts in water. ACS Catal. **15**(16), 14548–14563 (2025). https://doi.org/10.1021/acscatal.5c04928
103. Y. Zhao, J. Wan, C. Ling, Y. Wang, H. He et al., Acidic oxygen reduction by single-atom Fe catalysts on curved supports. Nature **644**(8077), 668–675 (2025). https://doi.org/10.1038/s41586-025-09364-6
104. M. Sun, J. Chen, Z. Zhang, Y. Jing, M. Zhao et al., Ferromagnetic ordering outperforms coordination effects in governing oxygen reduction catalysis on high-index nickel single crystals. Angew. Chem. Int. Ed. **64**(31), e202504869 (2025). https://doi.org/10.1002/anie.202504869
105. Z. Lu, Z. Wang, Z. Yang, X. Jin, L. Tong et al., Engineering CoN_4 and FeN_4 dual sites with adjacent nanoclusters on flexible porous carbon fibers for enhanced electrocatalytic oxygen reduction and evolution. Adv. Funct. Mater. **35**(16), 2418489 (2025). https://doi.org/10.1002/adfm.202418489
106. M.L. Rigsby, D.J. Wasylenko, M.L. Pegis, J.M. Mayer, Medium effects are as important as catalyst design for selectivity in electrocatalytic oxygen reduction by iron–porphyrin complexes. J. Am. Chem. Soc. **137**(13), 4296–4299 (2015). https://doi.org/10.1021/jacs.5b00359
107. H. Wang, L. Cao, Y. Feng, J. Chen, W. Feng et al., Facile synthesis of defect-rich Fe-N-C hybrid from fullerene/ferrotetraphenylporphyrin as efficient oxygen reduction electrocatalyst for Zn-air battery. Chin. Chem. Lett. **34**(5), 107601 (2023). https://doi.org/10.1016/j.cclet.2022.06.024
108. Z. Wang, R. Xu, Q. Ye, X. Jin, Z. Lu et al., Tailoring first coordination sphere of dual-metal atom sites boosts oxygen reduction and evolution activities. Adv. Funct. Mater. **34**(28), 2315376 (2024). https://doi.org/10.1002/adfm.202315376
109. L. Wu, Y. Chen, C. Shao, L. Wang, B. Li, Engineering synergetic Fe-co atomic pairs anchored on porous carbon for enhanced oxygen reduction reaction. Adv. Funct. Mater. **34**(48), 2408257 (2024). https://doi.org/10.1002/adfm.202408257
110. P.-F. Xie, H. Zhong, L. Fang, Z. Lyu, W.-J. Yu et al., Molecular Fe-N_4 moieties coupled with atomic Co-N_4 sites toward improved oxygen reduction performance. Adv. Funct. Mater. **34**(32), 2314554 (2024). https://doi.org/10.1002/adfm.202314554
111. D. Xue, S. Zhao, B.-A. Lu, Y. Yu, Y. Wei et al., Disentangling the activity-stability trade-off of pyrrolic N-coordinated Fe-N_4 catalytic sites for long-life oxygen reduction reaction in acidic medium. Adv. Energy Mater. **14**(12), 2303733 (2024). https://doi.org/10.1002/aenm.202303733
112. H. Yang, H. Wang, S. Ji, V. Linkov, R. Wang, Synergy between isolated-Fe_3O_4 nanoparticles and CNx layers derived from lysine to improve the catalytic activity for oxygen reduction reaction. Int. J. Hydrog. Energy **39**(8), 3739–3745 (2014). https://doi.org/10.1016/j.ijhydene.2013.12.160
113. S. Yin, H. Yi, M. Liu, J. Yang, S. Yang et al., An *in situ* exploration of how Fe/N/C oxygen reduction catalysts evolve during synthesis under pyrolytic conditions. Nat. Commun. **15**, 6229 (2024). https://doi.org/10.1038/s41467-024-50629-x
114. P. Zhang, H.-C. Chen, H. Zhu, K. Chen, T. Li et al., Intersite structural heterogeneity induction of single atom Fe catalysts for robust oxygen reduction. Nat. Commun. **15**(1), 2062 (2024). https://doi.org/10.1038/s41467-024-46389-3
115. S. Ji, Y. Wang, H. Liu, X. Lu, C. Guo et al., Regulating the electronic synergy of asymmetric atomic Fe sites with adjacent defects for boosting activity and durability toward oxygen reduction. Adv. Funct. Mater. **34**(29), 2314621 (2024). https://doi.org/10.1002/adfm.202314621
116. P. Rao, Y. Liu, X. Shi, Y. Yu, Y. Zhou et al., Protection of Fe single-atoms by Fe clusters for chlorine-resistant oxygen reduction reaction. Adv. Funct. Mater. **34**(46), 2407121 (2024). https://doi.org/10.1002/adfm.202407121
117. J. Liu, Y. Liu, B. Nan, D. Wang, C. Allen et al., A two-in-one strategy to simultaneously boost the site density and turnover frequency of Fe−N−C oxygen reduction catalysts. Angew. Chem. Int. Ed. **64**(14), e202425196 (2025). https://doi.org/10.1002/anie.202425196
118. J. Qiao, C. Lu, L. Kong, J. Zhang, Q. Lin et al., Spin engineering of Fe-N-C by axial ligand modulation for enhanced bifunctional oxygen catalysis. Adv. Funct. Mater. **34**(51), 2409794 (2024). https://doi.org/10.1002/adfm.202409794
119. R. Sui, B. Liu, C. Chen, X. Tan, C. He et al., Constructing asymmetric Fe-Nb diatomic sites to enhance ORR activity and durability. J. Am. Chem. Soc. **146**(38), 26442–26453 (2024). https://doi.org/10.1021/jacs.4c09642
120. G. Yang, H. Cai, N. Zhang, B. Wang, C. Liang et al., Regulation of d-orbital electron in Fe-N_4 by high-entropy atomic

clusters for highly active and durable oxygen reduction reaction. Adv. Funct. Mater. **34**(46), 2407775 (2024). https://doi.org/10.1002/adfm.202407775

121. M. Yuan, Y. Liu, Y. Du, Z. Xiao, H. Li et al., Dual-shelled hollow leafy carbon support with atomically dispersed (N, S)-bridged hydroxy-coordinated asymmetric Fe sites for oxygen reduction. Adv. Funct. Mater. **34**(29), 2401484 (2024). https://doi.org/10.1002/adfm.202401484
122. Y. Zhu, B. Zhang, X. Liu, D.-W. Wang, D.S. Su, Unravelling the structure of electrocatalytically active Fe–N complexes in carbon for the oxygen reduction reaction. Angew. Chem. Int. Ed. **53**(40), 10673–10677 (2014). https://doi.org/10.1002/anie.201405314
123. X. Lin, D. Liu, L. Shi, F. Liu, F. Ye et al., Second-shell coordination environment modulation for MnN4 active sites by oxygen doping to boost oxygen reduction performance. Small 2407146 (2024). https://doi.org/10.1002/smll.202407146
124. Y. Qin, C. Guo, Z. Ou, C. Xu, Q. Lan et al., Regulating single-atom Mn sites by precisely axial pyridinic-nitrogen coordination to stabilize the oxygen reduction. J. Energy Chem. **80**, 542–552 (2023). https://doi.org/10.1016/j.jechem.2023.01.048
125. K. Kim, G. Kim, T. Jeong, W. Lee, Y. Yang et al., Activating the Mn single atomic center for an efficient actual active site of the oxygen reduction reaction by spin-state regulation. J. Am. Chem. Soc. **146**(49), 34033–34042 (2024). https://doi.org/10.1021/jacs.4c13137
126. Y. Song, C. Han, W. Li, X. Yi, Q. Liao et al., Engineering bimetallic cluster architectures: Harnessing unique "remote synergy effect" between Mn and Y for enhanced electrocatalytic oxygen reduction reaction. eScience **5**(3), 100332 (2025). https://doi.org/10.1016/j.esci.2024.100332
127. T. Stracensky, L. Jiao, Q. Sun, E. Liu, F. Yang et al., Bypassing formation of oxide intermediate *via* chemical vapor deposition for the synthesis of an Mn-N-C catalyst with improved ORR activity. ACS Catal. **13**(22), 14782–14791 (2023). https://doi.org/10.1021/acscatal.3c01982
128. Z. Luo, J. Xie, J. Cheng, F. Wei, S. Lyu et al., Spin-state manipulation of atomic manganese center by phosphide-support interactions for enhanced oxygen reduction. Adv. Mater. **37**(29), 2504585 (2025). https://doi.org/10.1002/adma.202504585
129. Y. Li, Z. Li, K. Shi, L. Luo, H. Jiang et al., Single-atom Mn catalysts *via* integration with Mn sub nano-clusters synergistically enhance oxygen reduction reaction. Small **20**(22), 2309727 (2024). https://doi.org/10.1002/smll.202309727
130. H. Tian, L. Zeng, Y. Huang, Z. Ma, G. Meng et al., *In situ* electrochemical Mn(III)/Mn(IV) generation of Mn(II)O electrocatalysts for high-performance oxygen reduction. Nano-Micro Lett. **12**(1), 161 (2020). https://doi.org/10.1007/s40820-020-00500-7
131. S. Ye, D. Zhang, Z. Ou, L. Zheng, W. Liu et al., Electron donor–acceptor activated single atomic sites for boosting oxygen reduction reaction. Adv. Funct. Mater. **34**(40), 2405884 (2024). https://doi.org/10.1002/adfm.202405884
132. C. Zhao, H. Li, W. Wang, J. Xu, B. Shao et al., Revealing the critical role of the lone pair electrons of Bi^{3+} in electrocatalytic oxygen reduction reaction on Mn-based $BiMn_2O_5$ mullite surface. Adv. Funct. Mater. **35**(9), 2416257 (2025). https://doi.org/10.1002/adfm.202416257
133. Y. Jing, Y. Cheng, L. Wang, Y. Liu, B. Yu et al., MOF-derived Co, Fe, and Ni Co-doped N-enriched hollow carbon as efficient electrocatalyst for oxygen reduction reaction. Chem. Eng. J. **397**, 125539 (2020). https://doi.org/10.1016/j.cej.2020.125539
134. B. Li, H. Nam, J. Zhao, J. Chang, N. Lingappan et al., Nanoreactor of nickel-containing carbon-shells as oxygen reduction catalyst. Adv. Mater. **29**(7), 1605083 (2017). https://doi.org/10.1002/adma.201605083
135. H. Li, S. Dai, Y. Wu, Q. Dong, J. Chen et al., Atomic scaled depth correlation to the oxygen reduction reaction performance of single atom Ni alloy to the NiO_2 supported Pd nanocrystal. Adv. Sci. **10**(11), 2207109 (2023). https://doi.org/10.1002/advs.202207109
136. M. Li, H. Zhu, Q. Yuan, T. Li, M. Wang et al., Proximity electronic effect of Ni/Co diatomic sites for synergistic promotion of electrocatalytic oxygen reduction and hydrogen evolution. Adv. Funct. Mater. **33**(4), 2210867 (2023). https://doi.org/10.1002/adfm.202210867
137. Y. Sun, K. Fan, J. Li, L. Wang, Y. Yang et al., Boosting electrochemical oxygen reduction to hydrogen peroxide coupled with organic oxidation. Nat. Commun. **15**(1), 6098 (2024). https://doi.org/10.1038/s41467-024-50446-2
138. Q. Zhang, Z. Zheng, R. Gao, X. Xiao, M. Jiao et al., Constructing bipolar dual-active sites through high-entropy-induced electric dipole transition for decoupling oxygen redox. Adv. Mater. **36**(26), 2401018 (2024). https://doi.org/10.1002/adma.202401018
139. W. Liu, R. Chen, Z. Sang, Z. Li, J. Nie et al., A generalized coordination engineering strategy for single-atom catalysts toward efficient hydrogen peroxide electrosynthesis. Adv. Mater. **36**(38), 2406403 (2024). https://doi.org/10.1002/adma.202406403
140. M. Liu, H. Su, X. Liu, X. He, P. Tan et al., Dynamic modulation of electron redistribution at the heterogeneous interface nickel hydroxides/platinum boosts acidic oxygen reduction reaction. Nat. Commun. **16**, 2826 (2025). https://doi.org/10.1038/s41467-025-58193-8
141. Z. Liu, W. Yuan, H. Yang, Z. Kang, M. Ma et al., Phase reconstruction-directed synthesis of oxalate-functionalized nickel hydroxide electrocatalyst for high-yield H_2O_2 generation at industrial currents. Adv. Funct. Mater. **35**(2), 2412198 (2025). https://doi.org/10.1002/adfm.202412198
142. H. Ze, X. Chen, X.-T. Wang, Y.-H. Wang, Q.-Q. Chen et al., Molecular insight of the critical role of Ni in Pt-based nanocatalysts for improving the oxygen reduction reaction probed using an *in situ* SERS borrowing strategy. J. Am. Chem. Soc. **143**(3), 1318–1322 (2021). https://doi.org/10.1021/jacs.0c12755
143. Q. Zhang, F. Luo, X. Long, X. Yu, K. Qu et al., N, P doped carbon nanotubes confined WN-Ni Mott-Schottky heterogeneous

 https://doi.org/10.1007/s40820-026-02197-6

electrocatalyst for water splitting and rechargeable zinc-air batteries. Appl. Catal. B Environ. **298**, 120511 (2021). https://doi.org/10.1016/j.apcatb.2021.120511

144. B. Cao, G.M. Veith, R.E. Diaz, J. Liu, E.A. Stach et al., Cobalt molybdenum oxynitrides: synthesis, structural characterization, and catalytic activity for the oxygen reduction reaction. Angew. Chem. Int. Ed. **52**(41), 10753–10757 (2013). https://doi.org/10.1002/anie.201303197
145. Y.-B. Chen, J.-J. Li, Y.-P. Zhu, J. Zou, H. Zhao et al., Vicinal Co atom-coordinated Fe–N–C catalysts to boost the oxygen reduction reaction. J. Mater. Chem. A **10**(18), 9886–9891 (2022). https://doi.org/10.1039/D2TA00884J
146. Y. Ha, B. Fei, X. Yan, H. Xu, Z. Chen et al., Atomically dispersed Co-pyridinic N-C for superior oxygen reduction reaction. Adv. Energy Mater. **10**(46), 2002592 (2020). https://doi.org/10.1002/aenm.202002592
147. L. Lin, Y. Ni, L. Shang, H. Sun, Q. Zhang et al., Atomic-level modulation-induced electron redistribution in Co coordination polymers elucidates the oxygen reduction mechanism. ACS Catal. **12**(13), 7531–7540 (2022). https://doi.org/10.1021/acscatal.2c01075
148. H. Shen, N. Qiu, L. Yang, X. Guo, K. Zhang et al., Boosting oxygen reduction for high-efficiency H_2O_2 electrosynthesis on oxygen-coordinated Co-N-C catalysts. Small **18**(17), 2200730 (2022). https://doi.org/10.1002/smll.202200730
149. J. Wang, H. Zhong, J. Yang, H. Li, P. Tang et al., Tuning the atomic configuration environment of MnN_4 sites by Co cooperation for efficient oxygen reduction. J. Energy Chem. **82**, 547–559 (2023). https://doi.org/10.1016/j.jechem.2023.04.010
150. Z. Yu, D. Zhang, Y. Wang, F. Liu, F. She et al., Spin manipulation of heterogeneous molecular electrocatalysts by an integrated magnetic field for efficient oxygen redox reactions. Adv. Mater. **36**(45), 2470360 (2024). https://doi.org/10.1002/adma.202470360
151. K. Sun, J. Dong, H. Sun, X. Wang, J. Fang et al., $Co(CN)_3$ catalysts with well-defined coordination structure for the oxygen reduction reaction. Nat. Catal. **6**(12), 1164–1173 (2023). https://doi.org/10.1038/s41929-023-01047-7
152. W. Xu, R. Zeng, M. Rebarchik, A. Posada-Borbón, H. Li et al., Atomically dispersed Zn/Co-N-C as ORR electrocatalysts for alkaline fuel cells. J. Am. Chem. Soc. **146**(4), 2593–2603 (2024). https://doi.org/10.1021/jacs.3c11355
153. Y. Yang, Y. Xiao, L. Zhang, H.-T. Wang, K.-H. Chen et al., Encaging Co nanoparticle in atomic CoN_4-dispersed graphite nanopocket evokes high oxygen reduction activity for flexible Zn-air battery. Appl. Catal. B Environ. Energy **347**, 123792 (2024). https://doi.org/10.1016/j.apcatb.2024.123792
154. M. Jiang, H. Wang, M. Zhu, X. Luo, Y. He et al., Review on strategies for improving the added value and expanding the scope of CO_2 electroreduction products. Chem. Soc. Rev. **53**(10), 5149–5189 (2024). https://doi.org/10.1039/D3CS00857F
155. D. Karapinar, C.E. Creissen, J.G. Rivera de la Cruz, M.W. Schreiber, M. Fontecave, Electrochemical CO_2 reduction to ethanol with copper-based catalysts. ACS Energy Lett. **6**(2), 694–706 (2021). https://doi.org/10.1021/acsenergylett.0c02610
156. Y. Lin, T. Wang, L. Zhang, G. Zhang, L. Li et al., Tunable CO_2 electroreduction to ethanol and ethylene with controllable interfacial wettability. Nat. Commun. **14**(1), 3575 (2023). https://doi.org/10.1038/s41467-023-39351-2
157. A. Shayesteh Zeraati, F. Li, T. Alkayyali, R. Dorakhan, E. Shirzadi et al., Carbon- and energy-efficient ethanol electrosynthesis *via* interfacial cation enrichment. Nat Synth **4**(1), 75–83 (2025). https://doi.org/10.1038/s44160-024-00662-x
158. Z. Jiang, W. Sun, H. Shang, W. Chen, T. Sun et al., Atomic interface effect of a single atom copper catalyst for enhanced oxygen reduction reactions. Energy Environ. Sci. **12**(12), 3508–3514 (2019). https://doi.org/10.1039/C9EE02974E
159. H. Li, Y. Wen, M. Jiang, Y. Yao, H. Zhou et al., Understanding of neighboring Fe-N_4-C and Co-N_4-C dual active centers for oxygen reduction reaction. Adv. Funct. Mater. **31**(22), 2011289 (2021). https://doi.org/10.1002/adfm.202011289
160. L. Zong, K. Fan, W. Wu, L. Cui, L. Zhang et al., Anchoring single copper atoms to microporous carbon spheres as high-performance electrocatalyst for oxygen reduction reaction. Adv. Funct. Mater. **31**(41), 2104864 (2021). https://doi.org/10.1002/adfm.202104864
161. W. Zhou, B. Li, X. Liu, J. Jiang, S. Bo et al., *In situ* tuning of platinum 5d valence states for four-electron oxygen reduction. Nat. Commun. **15**(1), 6650 (2024). https://doi.org/10.1038/s41467-024-51157-4
162. Q. Zhang, P. Kumar, X. Zhu, R. Daiyan, N.M. Bedford et al., Electronically modified atomic sites within a multicomponent Co/Cu composite for efficient oxygen electroreduction. Adv. Energy Mater. **11**(17), 2100303 (2021). https://doi.org/10.1002/aenm.202100303
163. Z. Liu, Z. Wang, D. Lv, H. Yang, Z. Kang et al., Efficient electrosynthesis of hydrogen peroxide enabled by a hierarchical hollow RE–P–O (RE = Sm, La, Gd) architecture with open channels. Adv. Mater. **37**(7), 2311997 (2025). https://doi.org/10.1002/adma.202311997
164. L. Yin, M. Sun, S. Zhang, Y. Huang, B. Huang et al., Chlorine axial coordination activated lanthanum single atoms for efficient oxygen electroreduction with maximum utilization. Adv. Mater. **37**(7), 2416387 (2025). https://doi.org/10.1002/adma.202416387
165. R. Cheng, X. He, M. Jiang, X. Shao, W. Tang et al., F-p-d gradient orbital coupling induced spin state enhancement of atomic Fe sites for efficient and stable oxygen reduction reaction. Adv. Funct. Mater. **35**(29), 2425138 (2025). https://doi.org/10.1002/adfm.202425138
166. X.-Z. Yue, Y.-C. Liu, B.-A. Lu, X. Du, W. Lei et al., Inherent anti-Fenton property of single-atom rhenium for the ultradurable oxygen reduction reaction. Energy Environ. Sci. **17**(16), 5892–5900 (2024). https://doi.org/10.1039/D4EE02375G
167. S. Ozkan, S.J. Kim, D.N. Miller, J.T.S. Irvine, A new approach to fuel cell electrodes: lanthanum aluminate yielding fine Pt nanoparticle exsolution for oxygen reduction reaction. Adv. Energy Mater. **14**(15), 2303025 (2024). https://doi.org/10.1002/aenm.202303025

168. X. Han, T. Zhang, W. Chen, B. Dong, G. Meng et al., Mn—N_4 oxygen reduction electrocatalyst: operando investigation of active sites and high performance in zinc–air battery. Adv. Energy Mater. **11**(6), 2002753 (2021). https://doi.org/10.1002/aenm.202002753
169. H. Li, G. Yan, H. Zhao, P.C. Howlett, X. Wang et al., Earthworm-inspired Co/Co_3O_4/CoF_2@NSC nanofibrous electrocatalyst with confined channels for enhanced ORR/OER performance. Adv. Mater. **36**(26), 2311272 (2024). https://doi.org/10.1002/adma.202311272
170. Z. Wang, H. Jin, T. Meng, K. Liao, W. Meng et al., Fe, Cu-coordinated ZIF-derived carbon framework for efficient oxygen reduction reaction and zinc–air batteries. Adv. Funct. Mater. **28**(39), 1802596 (2018). https://doi.org/10.1002/adfm.201802596
171. Z. Ji, C. Qiu, P. Li, Y. Li, J. Shi et al., Atomic modulation of FeN_4 sites on hollow carbon nanospheres by neighboring Mn atoms for ultra-stable Zn-air batteries. Chem. Eng. J. **500**, 157505 (2024). https://doi.org/10.1016/j.cej.2024.157505
172. L. Qiu, Z. Wu, Y. Liu, Z. Qin, Y. Liu et al., Mn doping at high-activity octahedral vacancies of γ-Fe_2O_3 for oxygen reduction reaction electrocatalysis in metal-air batteries. Angew. Chem. Int. Ed. **64**(12), e202421918 (2025). https://doi.org/10.1002/anie.202421918
173. Y. Li, A. Huang, L. Zhou, B. Li, M. Zheng et al., Main-group element-boosted oxygen electrocatalysis of Cu-N-C sites for zinc-air battery with cycling over 5000 h. Nat. Commun. **15**(1), 8365 (2024). https://doi.org/10.1038/s41467-024-52494-0
174. W. Zhang, B. Feng, L. Huang, Y. Liang, J. Chen et al., Fe/Cu diatomic sites dispersed on nitrogen-doped mesoporous carbon for the boosted oxygen reduction reaction in Mg-air and Zn-air batteries. Appl. Catal. B Environ. Energy **358**, 124450 (2024). https://doi.org/10.1016/j.apcatb.2024.124450
175. J. Xia, M. Zhou, H. Gao, F. He, Z. Du et al., Regulation of Ni/Co ratio and gas transport in high-order Ruddlesden–Popper perovskite air electrodes for protonic ceramic electrochemical cells. Adv. Funct. Mater. **34**(39), 2403493 (2024). https://doi.org/10.1002/adfm.202403493
176. Z. Yang, F. Lai, Q. Mao, C. Liu, S. Peng et al., Breaking the mutual-constraint of bifunctional oxygen electrocatalysis *via* direct O-O coupling on high-valence Ir single-atom on MnO_x. Adv. Mater. **37**(3), 2412950 (2025). https://doi.org/10.1002/adma.202412950
177. J. Li, M. Chen, D.A. Cullen, S. Hwang, M. Wang et al., Atomically dispersed manganese catalysts for oxygen reduction in proton-exchange membrane fuel cells. Nat. Catal. **1**(12), 935–945 (2018). https://doi.org/10.1038/s41929-018-0164-8
178. L. Zhang, Y. Dong, L. Li, Y. Shi, Y. Zhang et al., Concurrently boosting activity and stability of oxygen reduction reaction catalysts *via* judiciously crafting Fe-Mn dual atoms for fuel cells. Nano-Micro Lett. **17**(1), 88 (2024). https://doi.org/10.1007/s40820-024-01580-5
179. J. Bai, T. Zhao, M. Xu, B. Mei, L. Yang et al., Monosymmetric Fe-N_4 sites enabling durable proton exchange membrane fuel cell cathode by chemical vapor modification. Nat. Commun. **15**(1), 4219 (2024). https://doi.org/10.1038/s41467-024-47817-0
180. L. Shi, D. Liu, X. Lin, R. Cheng, F. Liu et al., Stable and high-performance flow H_2-O_2 fuel cells with coupled acidic oxygen reduction and alkaline hydrogen oxidation reactions. Adv. Mater. **36**(23), 2314077 (2024). https://doi.org/10.1002/adma.202314077
181. G. Chen, X. Qiu, S. Liu, Y. Cui, Y. Sun et al., Mn–N–C with high-density atomically dispersed Mn active sites for the oxygen reduction reaction. Angew. Chem. Int. Ed. **64**(26), e202503934 (2025). https://doi.org/10.1002/anie.202503934
182. J. Tian, Y. Song, X. Hao, X. Wang, Y. Shen et al., Greatly enhanced oxygen reduction reaction in anion exchange membrane fuel cell and Zn-air battery *via* hole inner edge reconstruction of 2D Pd nanomesh. Adv. Mater. **37**(1), e2412051 (2025). https://doi.org/10.1002/adma.202412051
183. Z. Sang, Y. Qiao, R. Chen, L. Yin, F. Hou et al., Internal hydrogen-bond enhanced two-electron oxygen reduction reaction for π-d conjugated metal-organic framework to H_2O_2 synthesis. Nat. Commun. **16**(1), 4050 (2025). https://doi.org/10.1038/s41467-025-58628-2
184. H. Huang, M. Sun, S. Li, S. Zhang, Y. Lee et al., Enhancing H_2O_2 electrosynthesis at industrial-relevant current in acidic media on diatomic cobalt sites. J. Am. Chem. Soc. **146**(13), 9434–9443 (2024). https://doi.org/10.1021/jacs.4c02031
185. F. Yang, C. Feng, S. Zuo, Q. Wang, F. Wei et al., Photocatalytic H_2O_2 production with >30% quantum efficiency *via* monovalent copper dynamics. J. Am. Chem. Soc. **147**(20), 17112–17120 (2025). https://doi.org/10.1021/jacs.5c02450
186. H. Gong, Z. Gong, J. Liu, G. Ye, H. Fei, General and ultrafast photothermal synthesis of atomic metal-nitrogen-carbon catalysts for H_2O_2 electrosynthesis. Adv. Funct. Mater. **34**(25), 2316438 (2024). https://doi.org/10.1002/adfm.202316438
187. K.-M. Zhao, D.-X. Wu, W.-K. Wu, J.-B. Nie, F.-S. Geng et al., Identifying high-spin hydroxyl-coordinated $Fe^{3+}N_4$ as the active centre for acidic oxygen reduction using molecular model catalysts. Nat. Catal. **8**(5), 422–435 (2025). https://doi.org/10.1038/s41929-025-01324-7

 https://doi.org/10.1007/s40820-026-02197-6